NATIONAL TRANSPORTATION SAFETY BOARD

Office of Research and Engineering
Washington, D.C. 20594

February 17, 2012

Aircraft Performance Study

by John O'Callaghan

ACCIDENT:

Location: Roswell, New Mexico
Date: April 2, 2011
Time: 09:34 Mountain Daylight Time (MDT)
Aircraft: Gulfstream Aerospace Corporation GVI (G650), registration N652GD
NTSB#: DCA11MA076

TABLE OF CONTENTS

NATIONAL TRANSPORTATION SAFETY BOARD

Office of Research and Engineering
Washington, D.C. 20594

February 17, 2012

Aircraft Performance Study

by John O'Callaghan

A. ACCIDENT

Location: Roswell, New Mexico
Date: April 2, 2011
Time: 09:34 Mountain Daylight Time (MDT)[1]
Aircraft: Gulfstream Aerospace Corporation GVI (G650), registration N652GD
NTSB#: DCA11MA076

B. GROUP

Chairman: John O'Callaghan
National Resource Specialist - Aircraft Performance
National Transportation Safety Board (NTSB)
490 L'Enfant Plaza E, SW
Washington, DC 20594

Members: Marie Moler
Mechanical Engineer
NTSB
490 L'Enfant Plaza E, SW
Washington, DC 20594

Bret Leonhardt
Technical Specialist III - Flight Dynamics
Gulfstream Aerospace Corporation (GAC)
500 Gulfstream Rd
Savannah, GA 31402

Steven Roell
Senior Flight Test Engineer
Federal Aviation Administration (FAA)
Wichita Aircraft Certification Office
1801 Airport Rd, Rm 100
Wichita, KS 67209

[1] Unless otherwise noted, all times in this *Study* are based on a 24-hour clock in MDT. MDT = Universal Coordinated Time (UTC) - 6 hours.

C. HISTORY OF FLIGHT

On April 2, 2011, about 0934 mountain daylight time, an experimental Gulfstream Aerospace Corporation (GAC) GVI (G650)[2], registration N652GD, serial number 6002, crashed during takeoff from runway 21 at Roswell International Air Center Airport (ROW), Roswell, New Mexico. The flight was being operated by the manufacturer as part of its G650 developmental field performance flight test program. The two pilots and the two flight test engineers were fatally injured, and the airplane was substantially damaged. The flight was being conducted under 14 *Code of Federal Regulations* Part 91, and visual meteorological conditions prevailed at the time of the accident.

At the time of the accident the aircraft was performing a simulated one-engine-inoperative (OEI) continued takeoff (CTO) with the flaps deflected to 10 degrees - an intermediate flap setting used for hot or high airfield operations. The purpose of this company testing was to validate takeoff reference speeds. Immediately prior to this incident the aircraft had completed a simulated single engine takeoff in this same configuration. However, during this earlier take-off, the aircraft exceeded the predicted takeoff safety speed (V_2) of 135 knots by about 10 knots. A repeat of this earlier test point was being undertaken at the time of the accident in an attempt to reduce the flight test derived V_2 speed to the predicted value.

The procedure for conducting the takeoff is specified in a "test card" for the OEI, CTO maneuver (see Reference 1). In this procedure, the airplane is aligned with the runway centerline and the brakes are applied. The engine power is set to the desired level, and then the brakes are released. At a specified speed[3] (105 knots in this case[4]), the right throttle is reduced to idle to simulate a failure of the right engine; the speed is selected so as to allow time for the engine power to reduce to idle by the rotation speed. At the rotation speed (127 knots in this case), the column is pulled with a specified force (60-65 lb. in this case[5]) to initiate rotation; the pull is then relaxed to "gradually capture [9°] pitch attitude."[6]

The procedure is then to "maintain target pitch attitude until V_2 [the takeoff safety speed] is achieved, then transition to speed." The landing gear is retracted after a positive rate-of-climb is established, and the pitch attitude is adjusted to maintain V_2 until the gear retraction is complete, or until the airplane climbs through 400 ft. above ground level (AGL) (whichever occurs first), at which point the maneuver is complete.

---

[2] Gulfstream uses the Roman numeral designation "GVI" for aircraft certification purposes and the designation "G650" for marketing purposes. These designations mean the same aircraft model for purposes of this *Study* and are used interchangeably.

[3] The speeds referenced in the test card are indicated airspeeds.

[4] This engine-failure speed (V_{EF}) is not specified on the test card, but was briefed by the flight test engineer (FTE) prior to the start of the previous takeoff, per the recorded cockpit video (the cockpit video is described in Section D-III). The FTE briefed V_{EF} as V_1 – 20 knots, where V_1 is the takeoff decision speed (see the full definition in the Glossary in Section G). V_1 for the accident takeoff was 125 knots.

[5] This force is not specified on the test card, but was briefed during pre-flight briefings (see Reference 1).

[6] The test card for the accident run specified a pitch target of 10°, but this target was reduced to 9° prior to the accident flight and was briefed during pre-flight briefings (see discussion in Reference 1).

The recorded data described in Section D-III, and ground scars and markings on the runway and airport property, indicate that shortly after takeoff rotation, N652GD's right wing dropped and contacted the runway. The airplane subsequently yawed to the right, departed the right side of the runway, traversed about 3000 ft. of airport property, and came to rest about 8404 ft. from the runway 21 threshold, and 1949 ft. to the right of the runway centerline.

The objective of this *Aircraft Performance Study* is to determine and analyze the motion of the airplane and the physical forces that produce that motion. In particular, the *Study* attempts to define the airplane's position and orientation throughout the flight, and determine the airplane's response to control inputs, external disturbances, and other factors that could affect its trajectory.

The data the *Study* uses to determine and analyze the airplane motion includes but is not limited to the following:

- Ground scars and markings.
- Recorded flight data.
- Weather information.
- Computational Fluid Dynamics (CFD) and flight simulation studies.

Because N652GD was being used for research and development flight tests, it was equipped with a flight test instrumentation system that recorded a wealth of high-quality data describing the airplane's motion and systems. Hence, the analysis of the airplane's motion is based primarily on this recorded data. The available data is described in Section D-III.

This *Study* describes the results of using the data listed above in defining the position of N652GD relative to the runway 21 threshold throughout the attempted takeoff. The *Study* introduces the airplane motion data collected during the investigation, describes the methods used to extract additional airplane motion information from the recorded data, and presents the results of these calculations. The *Study* also describes CFD and simulation work performed by GAC that indicates that during the attempted takeoff, the airplane's angle-of-attack (α) exceeded the stall α for the combination of flap setting, height above the ground, Mach number, and roll angle (ϕ) present at the time.

D. DETAILS OF THE INVESTIGATION

I. The GAC G650 Airplane

Figure 1 shows a 3-view image of the G650 airplane. Table 1 provides some characteristic dimensions of the airplane, as well as mass properties data estimated by GAC for the accident takeoff (aircraft 6002, Flight #153, Run 7A2[7]).

Item	Value
Reference dimensions:	
Wing area	1282.9 ft^2
Wing span	93.67 ft.
Mean Aerodynamic Chord (MAC)	15.60 ft.
Mass properties for Flight 153, Run 7A2:	
Weight	88000 pounds
Center of gravity (CG) position	23.3% MAC
Roll moment of inertia (I_{xx})	326242 slugs* ft^2
Pitch moment of inertia (I_{yy})	922988 slugs* ft^2
Yaw moment of inertia (I_{zz})	1172769 slugs* ft^2
Product of inertia (I_{xz})	71755 slugs* ft^2

Table 1. Dimensions of G650 airplane, and mass properties for Flight 153, Run 7A2[8].

II. Ground scars and markings

Surveys of the accident scene and survey coordinate systems

The recorded data described in Section D-III, and ground scars and markings on the runway and airport property, indicate that shortly after takeoff rotation, N652GD's right wing dropped and contacted the runway. The airplane subsequently yawed to the right, departed the right side of the runway, traversed about 3000 ft. of airport property, and came to rest about 8404 ft. from the runway 21 threshold, and 1949 ft. to the right of the runway centerline, about 300 ft. from the FAA control tower.

The NTSB requested assistance from the Federal Bureau of Investigation (FBI) with surveying the ground scars and markings left by the airplane, as well as the location of prominent wreckage items and airport property features. The FBI, in turn, requested the assistance of the New Mexico State Police (NMSP) and the Roswell Police Department (RPD) with this effort. Investigators from GAC and NTSB also surveyed the accident scene.

The NMSP surveyed the accident scene using a Nikon NPR-352 Total Station, as described in Reference 2. This survey resulted in tabulated coordinates of the surveyed items in a Cartesian coordinate system centered near the final location of N652GD. However, Reference 2 does not indicate the latitude and longitude of the origin of this coordinate system, or the orientation of the coordinates relative to true North.

[7] As described in Reference 1, GAC identifies flight test maneuvers performed with a particular airplane as "runs" conducted on given "flights." A "flight" is defined by an engine start-stop cycle, and can include multiple takeoffs and landings. "Runs" denote particular test maneuvers or procedures as defined on "test cards." Run 7A2 was a flaps 10, heavy weight, one-engine-inoperative (OEI) continued-takeoff (CTO) maneuver.

[8] Information provided by GAC to NTSB Aircraft Performance Group Chairman via email on 04/18/2011.

The GAC / NTSB survey did not include as many items as the NMSP survey, but was performed using Differential Global Positioning System (DGPS) equipment that recorded the latitude and longitude of the items surveyed.

The origin and orientation of the NMSP coordinate system can be computed by comparing the Cartesian coordinates of items surveyed by the NMSP using the Total Station with the latitude and longitude coordinates of identical items surveyed by GAC / NTSB investigators using DGPS. Once the origin and orientation of the NMSP coordinate system are known, the Cartesian coordinates surveyed by the NMSP can be transformed into latitude and longitude, and thence into another Cartesian coordinate system aligned with KROW runway 21 (see, for example, Reference 3). The origin of this runway coordinate system is at the runway threshold, with the x-axis extending from the threshold along the runway centerline, and with the y-axis extending to the right of the threshold, normal to the centerline (see Figures 2a and 2b). In this *Study*, the runway coordinate system will be used to describe the trajectory of the airplane and the location of surveyed items.

The latitude and longitude coordinates, and orientation relative to true North, of the NMSP survey coordinate system and the runway coordinate system used in this *Study* are listed in Table 2, and depicted in Figures 2a and 2b.

Item	NMSP survey coordinate system	KROW runway 21 coordinate system
Latitude of origin	N 33° 17’ 54.254”	N 33° 18’ 40.6635”
Longitude of origin	W 104° 31’ 49.397”	W 104° 30’ 24.3222”
Elevation of origin	3655 feet	3623.6 feet
Bearing of x-axis	107.1° (true)	225.14° (true runway heading)
Bearing of y-axis	17.1° (true)	315.14° (true)

Table 2. Origin and orientation of NMSP survey and KROW runway 21 coordinate systems.

Survey items of note

Selected items from the NMSP and GAC / NTSB surveys are presented in Table 3 and in Figures 2a and 2b. Figure 2a shows runway 21, the airplane trajectory recorded by the flight test instrumentation system, and ground scar evidence of the trajectory of the airplane in runway coordinates against a grid background. Figure 2b is identical, but presents the data against a *Google Earth* satellite image background. The times and content of selected comments recorded by the Cockpit Voice Recorder (CVR) are also presented in Figures 2a and 2b at the airplane positions corresponding to the times at which the comments were recorded (the CVR data is described further in Section D-III).

Item	Latitude	Longitude	x-runway coordinate (ft.)	y-runway coordinate (ft.)
Start of wing scrape	N 33° 18’ 05.15”	W 104° 31’ 07.99”	5160	71
Touchdown mark	N 33° 17’ 56.65”	W 104° 31’ 24.68”	6770	461
Telemetry trailer	N 33° 17’ 56.52”	W 104° 31’ 33.63”	7318	987
Service shaft	N 33° 17’ 55.38”	W 104° 31’ 35.30”	7500	1006
Weather station	N 33° 17’ 55.07”	W 104° 31’ 42.22”	7938	1398
End of recorded data	N 33° 17’ 55.11”	W 104° 31’ 44.36”	8064	1530
Final N652GD location	N 33° 17’ 55.68”	W 104° 31’ 50.69”	8404	1949

Table 3. Coordinates of selected items from the NMSP and GAC / NTSB accident site surveys.

The contact of the right wing with the runway produced a scrape mark on the runway starting about 5160 ft. from the threshold. When the airplane departed the paved surface about 5900 ft. from the threshold, this scrape became a "furrow" in the ground. The recorded data indicates that the main gear lifted off, though the ground scar evidence indicates that the right wingtip was still in contact with the ground at the time. The right wing ground furrow continues until a point where evidence indicates that the main gear touched down again; this is the "touchdown mark" listed in Table 3, about 6770 ft. from the runway threshold and 461 ft. to the right of the runway centerline.

After the main gear touched down, the airplane continued a right turn, generally tracking to the west. The ground track marks and debris field pass within about 150 feet of the GAC telemetry (TM) trailer, where GAC engineers were monitoring the flight. The airplane tracks pass over the locations of two substantial structures on the airport property: a concrete electrical service shaft, and a metal pole supporting weather instrumentation[9]. These objects are listed as the "service shaft" and "weather station," respectively, in Table 3.

The airplane position recorded in the flight test data stops updating at 09:34:09.0, about 8064 ft. from the runway threshold and 1530 ft. to the right of the runway centerline. However, the airplane slid for about another 540 ft., and came to rest 8404 ft. from the runway threshold and 1949 ft. to the right of centerline, about 300 ft. from the FAA control tower. The CVR recording ends at 09:34:10.3, and the flight test data recording ends at 09:34:23.4.

The x- and y- runway coordinates of the airplane are plotted as a function of time in Figure 3. Figure 3 also presents the content of selected CVR comments superimposed on vertical dash-dot lines, drawn at the times corresponding to the occurrence of the corresponding CVR comments.

The "N652GD ground track from accelerometer integration" lines in Figures 2a, 2b, and 3 are described below, in Section D-IV.

III. Recorded flight data

Flight Data Recorder (FDR) and Cockpit Voice Recorder (CVR)

The *Data Recorders Group Chairman's Factual Report* (Reference 4) describes the numerous flight data recording devices on board N652GD at the time of the accident. As noted in that document, GAC was operating N652GD under an experimental airworthiness certificate to perform flight testing to support the type certification of the G650. Consequently, at the time of the accident the aircraft and the Flight Data Recorder (FDR) and CVR systems had not yet been validated or certified. Reference 4 indicates that the FDR only recorded 10 seconds of the accident flight, and explains that

> Gulfstream reported that in late 2010 a wiring issue was identified that indicated power was not being applied to the FDR until the combined weight on wheels transitioned from ground to air. Therefore the FDR would only begin recording after the aircraft systems indicated "in air". At the time of the accident, this wiring issue had not been corrected in the N652GD aircraft, but had been identified as a deferred maintenance item.

[9] These structures were damaged by the airplane's impact; the cover of the service shaft was torn off, and the weather station pole was knocked down.

However, a great volume of flight data (of greater quality and quantity than that recorded by the FDR) was recorded by various elements of the airplane's Flight Test Instrumentation System (FTIS). These elements are described in detail in Reference 4, and briefly, as required, in the sections below. The analysis of the airplane's motion in this *Study* is based primarily on the FTIS data.

The *Cockpit Voice Recorder Group Chairman's Factual Report* (Reference 5) contains a description of the CVR and the official transcript of the CVR, as well as a description of the methods used to correlate the timing of the CVR recording with the recorded FTIS data. The CVR content and times cited in the *Study* are taken from Reference 5.

Many of the plots in this *Study* portray selected CVR content at positions corresponding to the occurrence of the content on the CVR. For example, plots of data vs. time include CVR content overlaid on vertical lines that intersect the x axis of the plot at the times that the CVR content was recorded. The CVR content portrayed on the plots is not the verbatim CVR transcript text, but rather a paraphrase or short-hand code for this text. The full CVR transcript text associated with each paraphrase or code is shown in Table 4.

Time	Text on plots	Full CVR transcript text
09:33:16.9	Brakes.	[HOT-1] okay thirty three seventeen is brake release.
09:33:22.2	Power.	[HOT-2] power set.
09:33:25.5	Airspeed.	[HOT-1] airspeed's alive I got the yoke.
09:33:32.3	80	[HOT-2] eighty knots.
09:33:37.8	Chop.	[HOT-2] chop.
09:33:45.7	Rotate.	[HOT-2] standby, rotate.
09:33:50.8	Expression 1.	[HOT-1] * (going on).
09:33:52.1	Expression 2.	[HOT-2] oh whoa whoa whoa whoa.
09:33:52.8	Expression 3.	[HOT-1] whoa whoa.
09:33:53.6	Bank angle.	[HOT] bank angle, bank angle [electronic voice].
09:33:54.3	Power.	[HOT-1] power power power.
09:33:57.4	Expression 4.	[HOT-2] no no no no. *.
09:33:58.5	Bank angle.	[HOT] bank angle, bank angle [electronic voice].
09:34:00.0	Expression 5.	[HOT-1] ah sorry guys.
09:34:02.4	Triple chime.	[HOT] [sound similar to triple chime alarm].
09:34:10.3	End of recording.	

Table 4. Full CVR transcript text corresponding to paraphrased / coded text on plots in this *Study*.

GAC Flight Test Instrumentation System (FTIS) Data

Reference 4 describes the relationship between various elements of the GAC FTIS as follows:

> … In addition to a standard Flight Data Recorder (FDR), the aircraft was outfitted with various devices that were parts of the Flight Test Instrumentation System (FTIS). The FTIS includes different recording devices and system instrumentation (e.g., pressure gauges). Data from the avionics standard communications bus (ASCB) is recorded by the Innovative Control Systems, Inc (ICS) Test Interface System (TIS). Data from various ARINC 429, intercom audio, analog and discrete sensors and selected ASCB parameters from the TIS are routed to a CAIS [Common Airborne Instrumentation System] Bus Data Acquisition Unit (CDAU) which is then routed to the Heim Flight Recorder (FR). The Heim FR can accept inputs from the TIS, multiple CDAU's and individual ARINC 429 data sources. Data from the CDAU was also routed to a telemetry system on the aircraft which allowed for select data to be broadcast to a dedicated ground station located in the vicinity of the testing. Data from the Heim FR was then routed to the Gulfstream Flight Test IADS data server. Data from a portable weather station was also transmitted from a ground based transmitter to the aircraft and acquired by the CDAU and recorded to the Heim FR. …

> … The aircraft was equipped with a NovAtel DL-V3 Global Navigation Satellite System (GNSS). High accuracy position data can be provided by the DL-V3 when coupled with real-time differential GPS (DGPS) service from OmniStar. GPS data from the DL-V3 system is routed to the CDAU for inclusion in the flight test data set sent to the Heim FR or TM station.

Reference 4 indicates that data from the flight was recorded by several elements of the FTIS, including the Heim FR, the IADS, and the TIS. Much of the same data is recorded on multiple devices (i.e., there is considerable data overlap); as described in Reference 4,

> …The availability of multiple recording devices (FDR, IADS, Heim, TIS, etc.) allows for individual parameters (e.g., Pitch, Roll, Heading, etc.) to be recorded by each device. The data recorded by the TIS recorder is limited to parameters from the ASCB-D data bus and subsets of these parameters are provided to both the CDAU and the Heim Flight Recorder. The data recorded by the Heim Flight Recorder consists of select ASCB-D bus data from the TIS, data transmitted by the CDAU's and select ARINC 429 data busses. The data recorded by the IADS server on the aircraft is a subset of parameters that are recorded by the Heim Flight Recorder. The data recorded by the IADS server in the TM Station includes all of the data acquired by the aircraft CDAU and received via the RF link from the aircraft. Data from the DGPS and the weather station is logged by their respective devices and also recorded in the FTIS.
>
> After reviewing all of the available flight test data sources available to the group and the limited data from the FDR, the determination was made to use the data recovered from the Heim Flight recorder and the TIS for the investigation.

In addition to the data recorded by these devices, extensive engine performance and thrust data was recorded by a Rolls Royce Deutschland Engine Monitoring System (EMS) installed in the airplane. The NTSB Data Recorders Group Chairman provided data sampled at 10 Hz from the Heim FR and the Rolls Royce Deutschland EMS to the NTSB Aircraft Performance Group Chairman for use in this Aircraft Performance *Study*.

Telemetry (TM) data

As mentioned in Reference 4, data sent by telemetry from N652GD to the TM Station (trailer) was recorded by the IADS server in the trailer. Since the TM data is a subset of the data recorded on the Heim FR and includes erroneous data "dropouts" that are not present in the Heim FR data, the TM data was not used for this *Study*.

Weather station data

As mentioned above, Reference 4 notes that "data from a portable weather station was also transmitted … to the aircraft and acquired by the CDAU and recorded to the Heim FR." The wind speed and direction data from this station is used in this *Study*.

Cockpit video

Video and audio information from a video camera installed in the cockpit of N652GD was recorded on the Epiphan model VGA Recorder PRO, as described in Reference 6. The video recording contained about 2.9 hours of information recorded on the day of the accident, up to and including the accident takeoff. However, the video recording ends at about 09:33:50.9, which is about 9 seconds after the co-pilot made the "rotate" call on the accident takeoff, 19.4 seconds before the end of the CVR, and 32.5 seconds before the end of the Heim FR data. Reference 6 indicates that the video recording ended sooner than the other recordings most likely due to the abnormal shutdown (sudden loss of power).

The video camera was located near the centerline of the airplane on the cockpit bulkhead behind the pilots, slightly above the top of the pilots' heads. The video images depicted a view looking forward, encompassing the throttle quadrant, the pilot and co-pilot instrument displays, the pilots, and the control column and wheel. Only a small portion of the windshield is visible in the images, and the external view from the windows cannot be discerned in the images.

The audio source recorded by the cockpit video is the airplane's intercom system, which contains signals picked up by the "hot microphones" on the pilots' and flight test engineers' headsets.

The CVR recording contains more audio information than the cockpit video recording, since the CVR recording ends several seconds *after* the end of the cockpit video recording.[10] In addition, the Heim FR data provides better definition of the cockpit control positions and flight parameters than the video images of the cockpit controls and flight instruments. For these reasons, the recorded cockpit video is not used in this *Study*, though the cockpit video was reviewed by the Airplane Performance Group Chairman to determine if it contained unique airplane performance information not available from other sources, and to confirm that the airplane performance information contained in the video was consistent with the information from other sources.

Time-alignment of recorded data

Reference 4 notes that

> The FTIS time source is synchronized to Coordinated Universal Time (UTC) via a built-in GPS receiver. The time source signal is provided to the Heim Flight Recorder, IADS Servers and the TIS recorder … The accident occurred in Roswell, NM which is in the Mountain Time zone. To reference the data … to Mountain Daylight Time (MDT), six hours need to be subtracted from the provided times.

In this *Study*, time is referenced to MDT.

The alignment of CVR time to the FTIS reference time is described in Reference 5.

IV. Additional performance parameters computed using FTIS data

Overview

The flight parameter data set recorded by the FTIS is quite comprehensive, and includes almost all airplane performance parameters of interest, including those parameters that are direct recordings of sensor signals (such as accelerometer and control position signals), and parameters that are the result of computations performed by either airplane systems or the FTIS using sensor signals (such as most of the air data parameters, including calibrated airspeed, true airspeed, Mach number, etc.). Nonetheless, additional computations using the recorded data are of interest for the accident investigation, for the following reasons:

[10] In addition, the CVR is designed to include an area microphone channel as well as the airplane intercom / hot microphone channels; however, the area microphone channel on N652GD was unusable (see Reference 5 for more information).

- To confirm the consistency between the air data parameters recorded by the FTIS.
- To correct accelerometer bias errors, and derive a kinematically consistent set of acceleration, velocity, and position parameters defining the trajectory of the center of gravity (CG) of the airplane.
- To correct α sensor data for body rotation rate effects, so as to compute the local α at the CG of the airplane and at various points along the wingspan.
- To compute the position of various parts of the airframe (tires, CG, wingtips) relative to the ground.
- To determine the forces and moments acting on the airplane as a function of time.

The computation of differential α along the wingspan and at the CG, and of the different heights of various *parts* of the airplane above the ground, are relevant in this case because the CFD work performed by GAC after the accident (described in Section D-VI) indicates that the reduction in the stall α due to the influence of the ground plane (ground effect) can be significant, and is in fact greater than what had been estimated by GAC prior to the accident. The CFD results also indicate that the ground effects decrease very rapidly with increasing height above the ground, so that height must be known precisely in order to accurately predict the stall α. Furthermore, since body-axis pitch and roll rates can introduce differential α at the α sensors, the CG, and at various stations along the wing, it is possible, at non-zero pitch and roll rates, for the local α at parts of one wing to be above stall, while the local α along the rest of the wing (and perhaps at the α sensors) are below stall.

The methods used to derive additional parameters from the FTIS data are described below, and the results of the calculations are presented and discussed at appropriate points throughout the *Study*.

Height of CG and other airplane components based on DGPS and terrain elevation data

The DGPS position data recorded by the FTIS is reportedly accurate to within 15 cm (0.5 ft.)[11] Using the known location of the DGPS antenna on the airplane (and the locations of other airplane components of interest relative to the DGPS antenna), the rigid body position of any part of the airplane can be computed. The position coordinate of interest in this *Study* is the height of the components above the ground, which is equal to their altitude above Mean Sea Level (MSL), minus the elevation of the terrain beneath the airplane.

The altitude above MSL of each component is equal to the altitude of the DGPS antenna, plus the altitude difference between the DGPS antenna and the component of interest. This altitude difference depends on the location of the component relative to the DGPS antenna (in an airplane-fixed coordinate system), and the orientation of the airplane coordinate system relative to the Earth. Let $\{\Delta x_b, \Delta y_b, \Delta z_b\}$ define the relative position of a component relative to the DGPS antenna; i.e.,

$$\begin{Bmatrix} \Delta x_b \\ \Delta y_b \\ \Delta z_b \end{Bmatrix} = \begin{Bmatrix} x_c - x_a \\ y_c - y_a \\ y_c - y_a \end{Bmatrix}_b \qquad [1]$$

[11] Per the OmniSTAR website (http://www.omnistar.com/services.html), "there are three levels of OmniSTAR service available - VBS (Virtual Base Station) for sub-meter operations, OmniSTAR XP - consistent decimeter service (< +/- 15 cms) worldwide, and OmniSTAR HP (High Performance) for horizontal accuracy of better than 10cms." GAC used the OmniSTAR XP service for the field performance testing at KROW.

where the subscript c denotes the airplane component of interest, the subscript a denotes the DGPS antenna, and the subscript b indicates that the coordinates are in the body-fixed axis system (see Figure 4).

The coordinates $\{\Delta x_b, \Delta y_b, \Delta z_b\}$ can be transformed into a coordinate system with two axes aligned with the North and East axes of the Earth, and the third axis normal to the Earth's surface (positive downwards), using the following transformation matrix:

$$\begin{Bmatrix}\Delta x_e\\ \Delta y_e\\ \Delta z_e\end{Bmatrix} = \begin{bmatrix} cos\theta cos\psi & sin\phi sin\theta cos\psi - cos\phi sin\psi & cos\phi sin\theta cos\psi + sin\phi sin\psi \\ cos\theta sin\psi & sin\phi sin\theta sin\psi + cos\phi cos\psi & cos\phi sin\theta sin\psi - sin\phi cos\psi \\ -sin\theta & sin\phi cos\theta & cos\phi cos\theta \end{bmatrix} \begin{Bmatrix}\Delta x_b\\ \Delta y_b\\ \Delta z_b\end{Bmatrix} \quad [2]$$

Where ψ, θ, and ϕ are the airplane's true heading, pitch, and roll angles, respectively. The resulting Δx_e is the distance of the airplane component North of the DGPS antenna, Δy_e is the distance of the component East of the DGPS antenna, and Δz_e is the distance of the component *below* the DGPS antenna. Hence, the altitude above MSL of an airplane component is given by

$$h_c = h_a - \Delta z_e = h_a + \Delta x_b sin\theta - \Delta y_b sin\phi cos\theta - \Delta z_b cos\phi cos\theta \quad [3]$$

The height of the component above the ground is therefore

$$h_{AGL,c} = h_c - h_{terrain} \quad [4]$$

Where $h_{terrain}$ is the elevation of the ground beneath the airplane.

In Figure 4, the body-fixed axis system is shown with its origin at the airplane CG, with the x_b axis pointing forward, the y_b axis pointing to the right, and the z_b axis pointing down. However, the coordinates of each component and of the DGPS antenna are most conveniently defined in the airplane's structural coordinate system, consisting of the Fuselage Station (FS) pointing rearwards, the Buttock Line (BL) pointing to the right, and the Water Line (WL) pointing upwards. The $\{x_c, y_c, z_c\}_b$ coordinates of each component (in CG-centered body axes) can be computed from its $\{FS_c, BL_c, WL_c\}_{STRUCT}$ coordinates (in structures axes) as follows:

$$\begin{Bmatrix}x_c\\ y_c\\ z_c\end{Bmatrix}_b = \begin{Bmatrix} -(FS_c - FS_{CG}) \\ BL_c - BL_{CG} \\ -(WL_c - WL_{CG}) \end{Bmatrix}_{STRUCT} \quad [5]$$

Where the CG subscript indicates the structures coordinates of the CG. Note that when computing the difference in body coordinates between a given airplane component and the DGPS antenna using Equations [1] and [5], the coordinates of the CG cancel out, and so are not needed for the calculation.

The structures coordinates of several airplane components of interest for this *Study* are listed in Table 5. These coordinates were either provided directly by GAC, or determined from technical drawings of the airplane.

Component	FS, inches	BL, inches	WL, inches
Average of lower and upper ADSP* locations	168.5	±36.2	88.9
Center of gravity (CG)	*668.2*†	*0.0*†	*77*†
Accelerometers	717.971	-24.183	73.447
DGPS antenna	660.0	0.0	151.0
Bottom of left main gear tire (full strut extension)	716.6	-86.0	-31.8
Bottom of left main gear tire (static @ max ramp weight)	728.7	-86.0	-12.7
Bottom of right main gear tire (full strut extension)	716.6	86.0	-31.8
Bottom of right main gear tire (static @ max ramp weight)	728.7	86.0	-12.7
Bottom of nose gear tire (full strut extension) (estimate)	180.44	0.0	-7
Cockpit (pilot station, at centerline)	239.6	0.	121.0
Left wingtip (static, no aerodynamic load)	939.4	-562.0	77.6
Right wingtip (static, no aerodynamic load)	939.4	562.0	77.6

Table 5. Structures coordinates of various airplane components of interest. *ADSP = Air Data SmartProbe. †These items are variable; values shown are those computed for the accident flight.

The terrain elevation $h_{terrain}$ required in Equation [4] was determined from the recorded DGPS latitude and longitude, and the Shuttle Radar Topography Mission (SRTM) elevation database maintained by the United States Geological Survey (USGS). The USGS provides SRTM digital elevation data with a resolution of 1 arc-second (about 100 ft.) for the United States and 3 arc-seconds (300 ft.) for global coverage[12]. A constant bias of -0.7 ft. was applied to the SRTM elevations so as to force Equation [4] to result in the height of the main gear above the terrain (with struts fully extended) to be zero at liftoff. The liftoff point is defined as the latest point at which the recorded wheel speed for any wheel starts to decay; in this case, the data shows that the left wheel lifted off at 09:33:48.8, followed by the right wheel at 09:33:50.3[13].

The results of the height calculations outlined above are presented as a function of the runway x-coordinate in Figure 5, and as a function of time in Figure 6. The calculations presented in these Figures cover the time period from 09:33:20 to 09:34:00 (40 seconds), starting at the point where the airplane accelerates through 13 knots on the takeoff roll, continuing through the rotation and liftoff, and ending at the point where the main gear touched down. Note that the surveyed locations of the start of the right wing scrape mark on the runway, and the touchdown location of the gear, agree well with the right wingtip and right main gear height calculations.

Small uncertainties or errors in the SRTM elevation data (on the order of ±2 feet) are evident in the computed heights of the fully-extended main gear shown in Figures 5 and 6. At maximum ramp weight, the gear compress about 1.6 feet from their fully extended positions. Hence, while rolling down the runway, one would expect the computed heights of the "fully extended" gear to be between -1.6 and 0 ft., i.e., *below* the runway. Figures 5 and 6 show that during the early part of the takeoff roll, these computed heights are actually *positive* in places, indicating that the terrain elevation at these points is erroneous. The computed height above the ground becomes very important during the rotation and liftoff, however, because of the

[12] See http://edcwww.cr.usgs.gov/#/Find_Data/Products_and_Data_Available/SRTM.

[13] GAC engineers indicated that the wheel speed signal defines the liftoff point more precisely than the "weight on wheels" (WOW) discretes recorded by the FTIS, which can lag slightly behind the actual liftoff. Liftoff is defined by the wheel speed break, which typically occurs before the landing gear strut fully extends. The left and right WOW discretes, however, signal liftoff much closer to the full (but not complete) strut extension. Consequently, the estimated liftoff times used in this *Study* are likely very precise, but the altitude data are in error by the difference between the full strut extension length and the actual strut extension length at liftoff. In this case, the altitude error is likely less than a foot, and has no substantive effect on the resulting analysis.

sensitivity of the stall angle of attack to the proximity of the ground. To obtain a more accurate calculation of heights in this critical area, the terrain elevation at liftoff is adjusted so that the extended gear height is zero at liftoff, as described above. Figures 5 and 6 indicate that the computed gear heights in the neighborhood of the rotation and liftoff appear reasonable.

The lines labeled "CG (accel. Integration)" in Figures 5 and 6 (and the lines labeled "N652GD groundtrack from accelerometer integration" in Figures 2a, 2b, and 3) are the results of computing the airplane position by integrating the load factor (accelerometer) data recorded on the FTIS. These calculations are described below, in sub-section "*Accelerometer data corrections and integration.*"

Figures 5 and 6 also present the content of selected CVR comments overlaid on vertical dash-dot lines, drawn at the runway x-coordinate (in Figure 5) or time (in Figure 6) corresponding to the occurrence of the corresponding CVR comment.

Air data calculations and consistency checks

The FTIS recorded both calibrated airspeed and true airspeed. The relationship between these parameters depends on the static temperature and pressure of the freestream air surrounding the airplane. The static pressure determines the pressure altitude, and static air temperature (SAT) and Mach number determine the total air temperature (TAT). Pressure altitude, SAT and TAT, and Mach number are all recorded by the FTIS. To confirm the consistency between these parameters and the recorded true and calibrated airspeeds, in this *Study* true airspeed, SAT, and Mach number are computed from other recorded parameters as described below, and compared with the recorded values of these parameters.

True airspeed equals the Mach number multiplied by the speed of sound, and the speed of sound is a function of SAT. SAT is obtained from TAT (recorded by the FTIS) and Mach number.

Mach number can be found from calibrated airspeed and static pressure. Calibrated airspeed is recorded directly by the FTIS, and the static pressure can be determined from the pressure altitude recorded by the FTIS.

In summary, the calibrated airspeed, pressure altitude, and TAT recorded by the FTIS are used to compute Mach number, SAT, and true airspeed. The computed results are then compared with the values of these parameters recorded by the FTIS to confirm the internal consistency of the air data recorded by the FTIS.

N652GD air data system

The G650 air data sensors consist of four Goodrich Aerospace "SmartProbes" mounted on the forward fuselage, forward of the cockpit windshield (two on each side of the airplane; see Figure 1). These sensors provide angle of attack (α), sideslip angle (β), airspeed, and altitude indications to the Flight Control System.[14] For the flight test program, TAT is sensed by a

[14] Reference 7, p. 4.

Rosemount TAT probe mounted on a window plug on the right side of the airplane.[15] Reference 7 describes the SmartProbes as follows:

> Four Goodrich Air Data SmartProbe (ADSP) modules are the basis of the GVI air data system. Each self-contained ADSP consists of a multi-function probe (MFP) mounted to a two-channel air data computer (ADC), which measures local total pressure, static pressure, and angle of attack. Compensation for sideslip errors and measurement of aircraft sideslip angle is accomplished through comparison of left and right side aircraft static source pressures. Each probe head includes four static source ports. The two aft are pneumatically manifolded for use in sideslip determination; the two forward are used in determination of static pressure and aircraft angle of attack. All communication between ADSP modules and other aircraft systems is done electronically and requires no pneumatic tubing. The four independent ADSP modules allow for multiple redundancies since each can function independently should one or more of the other ADSPs become inoperative [Reference 7, p. 5].

The FTIS recorded air data parameters from the airplane's four Air Data Systems (ADSs). Each ADS receives signals from two (of four total) ADSPs: one on the left side of the airplane, and the other on the right, as indicated in Table 6. ADS1 and ADS2 receive signals from the upper ADSPs, and ADS3 and ADS4 receive signals from the lower ADSPs.

ADS #	Left side ADSP (SmartProbe)	Right side ADSP (SmartProbe)
1	Upper, channel A (ADSP 1A)	Upper, channel A (ADSP 2A)
2	Upper, channel B (ADSP 1B)	Upper, channel B (ADSP 2B)
3	Lower, channel A (ADSP 3A)	Lower, channel A (ADSP 4A)
4	Lower, channel B (ADSP 3B)	Lower, channel B (ADSP 4B)

Table 6. G650 ADSP (Air Data SmartProbe) architecture (based on Figure 2 in Reference 7).

Figures 7a and 7b compare the calibrated airspeed, true airspeed, and Mach number parameters from the four ADSs. The true airspeed and Mach number computed from the recorded ADS3 parameters are also shown. Note that between 09:33:47 and 09:33:51 (as the airplane is rotating for takeoff), the data from ADS3 and ADS4 (using signals from the lower ADSPs) diverge (by as much as 4 knots) from the data from ADS1 and ADS2 (using signals from the upper ADSPs). The ground speed data from the airplane's inertial systems (see Figure10) is more consistent with the continuous acceleration apparent in the airspeed data from ADS1 and ADS2; hence, the "dip" or pause in airspeed recorded by ADS3 and ADS4 is likely the result of local flow effects over the lower ADSPs resulting from the pitch rate of the airplane, and does not reflect the actual airspeed behavior at that point.

The calculation of true airspeed and Mach number using the recorded ADS3 calibrated airspeed and FTIS TAT data results in a good match of the recorded ADS3 true airspeed and Mach number, providing a "spot check" confirmation that the ADS data is internally consistent.

The pressure altitude from the four ADSs is presented along with the FTIS TAT and SAT data in Figure 8. Here again the ADS3 and ADS4 data diverges from the ADS1 and ADS2 data during the takeoff rotation, and all four ADSs show unrealistic data behavior (including sharp jumps) in this area. In particular, ADS3 and ADS4 show an unrealistic 40 foot drop in pressure altitude during rotation, confirming that the airspeed artifacts in the same area are likely the result of rotation-induced local airflows about the lower ADSPs. The ADS1 and ADS2 pressure altitude artifacts are much smaller, but still indicate that the upper ADSPs are not immune from errors resulting from rotation-induced flow effects.

[15] Reference 7, p. 22. Reference 7 also indicates that "the production ADS [Air Data System] will use two Goodrich Aerospace dual-sensor Total Air Temperature (TAT) probes mounted below the cockpit on the left and right side of the aircraft" (p. 5).

The decrease in SAT with increasing airspeed shown in Figure 8 is likely an artifact resulting from inaccurate temperature sensing at low airspeed. As air flows past the TAT sensor with increasing speed, the measurement becomes more accurate; by 09:33:31, as the airplane accelerates through 80 knots, the SAT appears to have settled to a value of about 18.5° C (65.3° F). The SAT computed from the FTIS TAT and ADS3 speed and pressure data agrees well with the SAT recorded by the FTIS, providing another "spot check" of the internal consistency of the FTIS air data.

The bottom plot in Figure 8 presents the density altitude, as computed using the calculated SAT, and ADS3 pressure altitude data. The artifacts in temperature and pressure altitude described above are also apparent in the computed density altitude result.

Angle of attack (α) at the center-of-gravity (CG) and various wing stations

The angle of attack (α) is the angle between the longitudinal axis of the airplane and the projection of the velocity vector onto the plane defined by the longitudinal and vertical axes (see Figure 4). In steady, level flight, the velocity vectors of all parts of the airplane are the same, and so α is the same everywhere. When the airplane is rotating about its center of gravity, however, the rotation imparts additional velocities to different parts of the airplane according to their positions relative to the CG, and so each part can have a different velocity and angle of attack.[16]

The performance and controllability of the airplane depend strongly on the α of the wing, and so the values of α at different points along the wing are of interest. The α at the CG is also of interest, because since the CG is close to the aerodynamic center of the wing, the α there can generally be taken as representative of the wing α.

As described above, the ADSs compute α based on signals from the ADSPs on the forward fuselage. Because the ADSPs are located far (about 42 feet) from the CG, the α values computed by the ADSs are sensitive to pitch rate, which induces a vertical velocity component at the ADSPs and makes their local α differ from the α at the CG. However, if the pitch rate is known, its effects can be calculated and removed from the ADS α data to provide an estimate of α at the CG. Similarly, since the airplane roll and yaw rates are also known, the α induced at any point on the airplane can be determined.

Figure 4 illustrates the definitions of α and the sideslip angle β, along with the airplane axis systems and the velocity components in these systems. The *body axes* $\{x_b, y_b, z_b\}$, which were introduced above, are attached to the airplane. The *stability axes* $\{x_s, y_s, z_s\}$ are aligned with the body axes, but rotated about the y_b axis through the angle $-\alpha$. The sideslip angle β is the angle between the airplane velocity vector $\vec{V}$ and the x_s stability axis. $\{u, v, w\}$ are the components of $\vec{V}$ along the $\{x_b, y_b, z_b\}$ body axes. $\{P, Q, R\}$ are the components of the rotational velocity vector $\vec{\omega}$ in body axes (the roll rate, pitch rate, and yaw rate, respectively).

[16] During the takeoff rotation, the center of rotation is about the main gear tires (these remain at a constant height while other parts of the airplane rise or fall). This motion is kinematically equivalent to the superposition of a translation of the CG vertically, and a pure rotation about the CG. Consequently, the methods described here for computing α at various parts of the airplane can be applied in the takeoff rotation case.

It follows from Figure 4 that

$$u = V\cos(\beta)\,cos(\alpha) \quad [6]$$
$$v = V\sin(\beta) \quad [7]$$
$$w = V\cos(\beta)\sin(\alpha) \quad [8]$$

Consequently

$$\alpha = \tan^{-1}\left(\frac{w}{u}\right) \quad [9]$$

To determine α at a point, then, the velocity components of that point along the x_b and z_b axes must be known. The velocity of a point P on the airplane is given by

$$\vec{V}_P = \vec{V}_{CG} + \vec{\omega} \times \vec{r}_P \quad [10]$$

where $\vec{r}_P$ is the vector from the CG to the point P. The components of $\vec{r}_P$ and $\vec{\omega}$ in body axes are

$$\vec{r}_P = x_P\hat{\imath} + y_P\hat{\jmath} + z_P\hat{k} = \begin{Bmatrix} x_P \\ y_P \\ z_P \end{Bmatrix} \quad [11]$$

$$\vec{\omega} = P\hat{\imath} + Q\hat{\jmath} + R\hat{k} = \begin{Bmatrix} P \\ Q \\ R \end{Bmatrix} \quad [12]$$

where $\hat{\imath}, \hat{\jmath}, \hat{k}$ are unit vectors along the $\{x_b,\ y_b,\ z_b\}$ axes (throughout this *Study*, variables in matrix format represent the components of the vector in question in the body-axis system). Using the convention $dx/dt = \dot{x}$ to denote time derivatives, the angular rates $\{P, Q, R\}$ are:

$$\begin{Bmatrix} P \\ Q \\ R \end{Bmatrix} = \begin{bmatrix} -\sin\theta & 0 & 1 \\ \sin\phi\cos\theta & \cos\phi & 0 \\ \cos\phi\cos\theta & -\sin\phi & 0 \end{bmatrix} \begin{Bmatrix} \dot{\psi} \\ \dot{\theta} \\ \dot{\phi} \end{Bmatrix} \quad [13]$$

$\{P, Q, R\}$ are the body-axis roll rate, pitch rate, and yaw rate, respectively. The Euler angles (yaw (ψ), pitch (θ), and roll (ϕ)) are recorded by the FTIS[17]. Substituting Equations [11] and [12] into Equation [10], performing the cross product, and letting $\{u, v, w\}$ denote the velocity components of the CG gives

$$\vec{V}_P = \begin{Bmatrix} V_x \\ V_y \\ V_z \end{Bmatrix} = \begin{Bmatrix} u + (Qz_P - Ry_P) \\ v + (Rx_P - Pz_P) \\ w + (Py - Qx_P) \end{Bmatrix} \quad [14]$$

[17] The FTIS recorded data from the airplane's three inertial reference system (IRS) units, including the Euler angles and angular rates. The data from the three systems are in good agreement; for simplicity, only data from IRS2 is used in this *Study*.

The $\{V_x, V_y, V_z\}$ velocity components at the ADSPs can be calculated using Equations [6]-[8] and the ADS α and V values recorded by the FTIS.[18] Since $\{P, Q, R\}$ and $\{x_P, y_P, z_P\}$ are known, $\{V_x, V_y, V_z\}$ can be used with Equation [14] to compute the $\{u, v, w\}$ at the CG. α at the CG then follows from Equation [9]. Equations [14] and [9] can then be used to calculate α at any point on the airplane.

In this *Study*, the ADS3 α is corrected as outlined above to compute the α at the CG, and at the left and right wingtips. The structural coordinates of the CG, ADSP probes, and wingtips (from which the $\{x_b, y_b, z_b\}$ body-axis coordinates of these points can be computed) are presented in Table 5.

Figures 9a and 9b present the ADS α data, and the computed α at the CG and at each wingtip. The Figures also present the pitch angle recorded by the FTIS, as well as the α and flight path angle (γ)[19] computed by integrating the FTIS accelerometer data (as described below in sub-section "*Inertial α, β, and γ calculations*."

The effect of the pitch and roll rates on the α at the CG and wingtips can be seen clearly in the expanded-scales plots in Figure 9b. Between 09:33:47 and 09:33:49, where the pitch rate (Q) is highest, the vertical speed component induced at the ADSP locations make the ADSPs measure an α that is lower than the α at the CG by up to 1°. Similarly, vertical speed components induced at the left and right wingtips by the roll rate (P) decrease the α at the left wingtip, and increase the α at the right wingtip. This effect becomes quite noticeable in Figure 9 after 09:33:50, as the α difference between the wingtips grows to over 2°, and reaches a peak of about 4° at 09:33:52.5. P and Q recorded by the FTIS are presented in Figure 15.

The free-air (i.e., outside of ground-effect) stall α for the G650 is a function of Mach number, as determined by flight test (Reference 8). The free-air stall α for flaps 10 at the Mach numbers of the accident takeoff is shown in Figures 9a and 9b as the dashed purple line. At the time of the accident, GAC had estimated from minimum-unstick speed (V_{mu}) testing that ground effects would reduce the stall α from the free-air stall α by 1.6°[20]; the resulting α for stall in ground effect ($\alpha_{stall,IGE}$) is depicted in Figures 9a and 9b as the dashed blue line. Stall protection for the field performance flight test program consisted of a stick-shaker intended to alert the crew to a high-α condition and impending stall;[21] the α threshold for the stick-shaker activation for the conditions of the accident takeoff (α_{shaker}) are shown in Figures 9a and 9b as the dashed dark-yellow line.

Figures 9a and 9b show that the α on all parts of the airplane exceeded the estimated $\alpha_{stall,IGE}$ at about 09:33:54, and the free-air α_{stall} at 09:33:55.5. As α exceeds 16°, the α measurement by the ADSPs appears to break down; the α recorded by each of the four ADS systems diverge. α from ADS1 flat-lines at 25°, suggesting that 25° is the maximum

[18] Since the FTIS also records the ADS β, these β values can be used in Equations [6]-[8]. In this *Study*, however, for this calculation β was assumed to be small, so that $\cos(\beta) \approx 1$. This simplification has minimal effect on the resulting calculation of the α values at the CG and along the wingspan.

[19] While the airplane is on the ground, γ equals the runway slope.

[20] One of the flight test engineers on the accident flight computed this increment to α_{stall} based on an analysis of minimum-unstick speed takeoff (V_{mu}) tests performed previously on N652GD (References 9 and 10).

[21] Stall protection on the production G650 will consist of a fly-by-wire High Incidence Protection Function (HIPF), whereby the flight control system will prevent the pilot from pulling the airplane into a free-air stall. The HIPF was under development and therefore unavailable for field performance testing (References 7, 9, and 13).

α reportable by the ADS. The best estimate of α in this region is that based on the accelerometer integrations, which peaks at 22.7° at 09:33:57.7.

The data in Figures 9a and 9b make it clear that, at some point during the takeoff, the airplane stalled. A fundamental concern for the aircraft performance investigation is the timing of the stall relative to the right wing contact with the runway, and to α_{shaker} and the estimated $\alpha_{stall,IGE}$ prior to the accident. The effect of the stall on the lateral control of the airplane is also of fundamental interest. Consequently, it is important to identify the time at which the stall occurred. In this *Study*, "stall" will be defined to mean flow separation over any part of the wings that makes the airplane aerodynamic performance or handling characteristics observably different from that of the airplane free of flow separation.

To help identify the stall point thus defined, simulation and CFD work performed by GAC after the accident will be used to (1) compare the airplane's performance during the accident takeoff with the expected performance (as defined by GAC's engineering simulation), and (2) compare the angles of attack depicted in Figures 9a and 9b with updated estimates of $\alpha_{stall,IGE}$ based on detailed CFD predictions of the reduction in α_{stall} due to ground-effect. GAC's simulation work is described in Section D-V, and GAC's CFD work is described in Section D-VI. As will be seen and discussed further in these Sections, the aerodynamic rolling and yawing moments acting on the airplane during the accident takeoff start to differ from the moments predicted by the simulation *before* the airplane achieves either the $\alpha_{stall,IGE}$ estimated prior to the accident, or α_{shaker}. GAC's CFD analysis indicates that the reduction in α_{stall} due to ground effect (with the gear on the ground) is about 3°, about double the 1.6° that was estimated at the time of the accident. This information, together with a consideration of the height and α of the right wingtip, suggest that the stall likely occurred at about 09:33:50.5, as the airplane θ was increasing through 11.2°.

The remainder of this Section will describe additional parameters of interest that can be computed from the recorded FTIS data, including those that result from an integration of the recorded load factor data. In addition, parameters recorded by the FTIS that are relevant to the aircraft performance and control, such as flight control inputs and power settings, will also be presented.

Accelerometer data corrections and integration

As noted above, the FTIS record includes measurements of all the airplane state[22] parameters of interest, including linear load factors (accelerations) and speeds from the IRSs, angular rates and positions from the IRSs, air speeds from the ADCs, and airplane position from the DGPS. However, these measurements are not necessarily kinematically consistent; i.e., the mathematical relationships between acceleration, speed, and position do not necessarily hold perfectly between all the corresponding FTIS parameters. For example, the time-derivative of the DGPS position should yield a ground speed that matches the ground speed parameter provided by the IRSs. However, as shown in Figure 10, the ground speed derived from the DGPS signal is very noisy, and does not match (without smoothing, or filtering, or a similar correction) the IRS ground speed. Similarly, the airplane position

[22] The "state" parameters are those that define the airplane's angular and linear motion, including angular and linear accelerations, speeds, and positions.

obtained by integrating[23] the IRS ground speed and track parameters does not match the DGPS position perfectly.

A kinematically consistent calculation of the flight path of the airplane – which maintains the proper mathematical relationships between accelerations, speeds, and positions – can be obtained for relatively short intervals (about 30 to 60 seconds) by integrating the accelerations recorded at the CG of the airplane. An integration of the accelerations produces speeds, and an integration of speeds produces positions. The resulting state parameters can be used to confirm the general consistency (within measurement error) of the parameters recorded by the FTIS, and can also be used (along with recorded wind data) to compute inertial α and β angles for comparison with ADS data. In addition, the parameters resulting from integration provide the best estimate of some performance parameters of interest, such as rate of climb and flight path angle (γ).

However, the accelerometers that generate the load factor data recorded by the FTIS are not located exactly on the CG, and so the accelerations at the CG must be computed by adjusting the FTIS load factors for the effects of angular rates and accelerations.[24] Furthermore, accelerometers generally contain small offsets, or "biases," that produce large errors in speed and position if not removed prior to integration.[25] In addition, initial values of speed, rate of climb, and track angle are required during the integration process (these are essentially the "constants of integration" when integrating acceleration to get speeds). The constants of integration and the values of the accelerometer biases can be estimated by selecting them such that the aircraft position that results from the integration agrees with known positions determined from another source. In this *Study*, the "target" positions are those defined by an integration of the groundspeed and track angle data recorded by the FTIS, and the DGPS-based altitude of the CG shown in Figures 5 and 6. As described further below, the FTIS groundspeed and groundtrack are themselves corrected so that their integration produces positions that match the DGPS positions corresponding to the start and end of the integration period.

Accelerations at the CG

The accelerations at the CG can be computed from the load factors recorded by the FTIS as follows. The acceleration at any point P on the airplane, $\vec{a}_P$, is given by

$$\vec{a}_P = \begin{Bmatrix} \dot{u} + wQ - vR \\ \dot{v} + uR - wP \\ \dot{w} + vP - uQ \end{Bmatrix} + \begin{Bmatrix} Q(yP - xQ) + R(zP - xR) + (z\dot{Q} - y\dot{R}) \\ R(zQ - yR) + P(xQ - yP) + (x\dot{R} - z\dot{P}) \\ P(xR - zP) + Q(yR - zQ) + (y\dot{P} - x\dot{Q}) \end{Bmatrix} = \vec{a}_{CG} + \Delta\vec{a} \qquad [15]$$

where:

[23] Throughout this *Study*, "integrating" data refers to mathematical integration with respect to time, per the theorems of Calculus.

[24] In this case, the angular rates and accelerations are relatively small, and so the load factor corrections are also small. Hence, the FTIS load factor data are representative of the load factors at the CG.

[25] For details about the equations to be integrated and the bias correction technique described in this *Study*, see Appendix A of Reference 11.

$\{u, v, w\}$ = components of inertial velocity (not airspeed, as in Equation [14]) in the airplane body axes
$\{P, Q, R\}$ = components of angular velocity in the airplane body axes
$\{\dot{P}, \dot{Q}, \dot{R}\}$ = time derivatives of $\{P, Q, R\}$
$\{x, y, z\}$ = coordinates of point P in the airplane body axes

(see Figure 4). Since by definition $\{x, y, z\}$ at the CG = {0, 0, 0}, the first term in brackets in Equation [15] is the acceleration of the CG ($\vec{a}_{CG}$), and the second term is the increment in acceleration due to the point P being away from the CG ($\Delta\vec{a}$).

A three axis accelerometer at point P will measure load factors as follows:

$$\vec{n}_P = \frac{\vec{a}_P - \vec{g}}{g} = \frac{\vec{a}_{CG} + \Delta\vec{a} - \vec{g}}{g} = \vec{n}_{CG} + \frac{\Delta\vec{a}}{g} \quad [16]$$

Where $\vec{g}$ is the gravity vector, g is the acceleration due to gravity (32.17 ft/s^2), and Equation [15] has been used to substitute for $\vec{a}_P$. The components of $\vec{n}$ are $\{n_x, n_y, n_z\}$. The normal load factor (nlf) is

$$nlf = -n_z \quad [17]$$

The FTIS records n_x, n_y, and nlf from the three IRSs (data from IRS2 is used in this *Study*). The values of $\{n_x, n_y, n_z\}$ at the CG can be found using the FTIS data and Equations [17], [16], and [15], with $\{x\ y, z\}$ in [15] being the body-axis coordinates of the accelerometers (these can be determined from the structural coordinates of the accelerometers listed in Table 5).

$\{P, Q, R\}$ are recorded by the FTIS, and $\{\dot{P}, \dot{Q}, \dot{R}\}$ can be computed from the recorded $\{P, Q, R\}$. In addition, $\{P, Q, R\}$ can be computed from the θ, ϕ, and ψ angles recorded by the FTIS, using Equation [13]; this calculation provides a check of the consistency between the FTIS Euler angles and angular rates.

The angular rates and accelerations in this case are relatively small, and the accelerometers are relatively close to the CG. As a result, the $\Delta\vec{a}$ defined in Equation [15], while noticeable, is not large, and the $\{n_x, n_y, n_z\}$ recorded by the FTIS are good measures of the $\{n_x, n_y, n_z\}$ at the CG. However, these data must still be corrected for accelerometer bias.

Accelerometer bias calculations

In general, accelerometer biases are not constant throughout a flight, but drift over time. It is for this reason that integrating the accelerometer data works best over relatively short intervals, during which the accelerometer biases are approximately constant. In this case, the time period of interest spans 40 seconds (from 09:33:20 to 09:34:00), and so an acceptable result can be obtained using a single set of biases (as opposed to integrating multiple segments of the flight using different biases for each segment). For this case, the constants of integration and the accelerometer biases were chosen to minimize the difference between the trajectory resulting from the accelerometer data integration, and a "target" trajectory. The North and East components of the target trajectory are obtained from an integration of the FTIS groundspeed and track angle data. The altitude component of the target trajectory is the "CG (DGPS-based)" MSL altitude shown in Figures 5 and 6.

The constants of integration (the initial groundspeed, track angle, and rate of climb) are chosen to minimize the root-mean-square difference between the integrated flight path and the target flight path throughout the integration period. The accelerometer biases are chosen to minimize the error between the integration and the target at the end point of the integration; i.e., the biases are chosen so that the integrated flight path and target flight path coincide at the end of the period. The beginning and end times, constants of integration, and accelerometer biases used are listed in Table 7. The constants of integration are expressed as increments, or biases, on the initial groundspeed, track, and rate of climb that would be computed using the target trajectory.

The FTIS track angle, relative to true North, is computed as follows:

$$\psi_{GT} = \psi_T + \Delta\psi_{DRIFT} \quad [18]$$

Where ψ_T is the IRS magnetic heading recorded by the FTIS, and $\Delta\psi_{DRIFT}$ is the IRS drift angle recorded by the FTIS. The FTIS also recorded magnetic heading (ψ_M); thus, the magnetic variation at KROW can be computed as

$$\Delta\psi_{MAGVAR} = \psi_M - \psi_T = -8.18° \; (8.18° \; E) \quad [19]$$

ψ_{GT}, ψ_T, ψ_M, and $\Delta\psi_{DRIFT}$ are plotted in Figure 14, along with the true ground track angle resulting from the accelerometer data integration, and the true ground track angle computed from the DGPS data.

The integration of the FTIS groundspeed and track angle data, which serves as the "target" for the integration of the accelerometer data, requires some correction before the accelerometer data integration can proceed. This is because the track produced by integrating the FTIS groundspeed and track angle (without adjustment) differs slightly from the track recorded in the FTIS DGPS position data.[26]

To ensure that the integration of groundspeed and track angle match the DGPS track over the integration period, a time-weighted velocity vector is added to the North and East velocities defined by the FTIS groundspeed and track angle. This vector then forces the integration of the North and East velocities to match the DGPS position at a point near the end of the period. The vector can be thought of as a "wind," with a velocity and direction, that "blows" the airplane onto the DGPS position at the specified time.

The time-weighted "shape" of the velocity vector is shown in Figure 11. The magnitude of the vector is multiplied by the factor k in this Figure, which changes over the length of the integration. At the beginning and end of the integration, the value of k is 0.0, and so the corrected East and North velocities match those defined by the FDR groundspeed and drift angle data at these points. The k factor ramps up to 1.0 over the first third of the segment, remains at 1.0 over the second third, and ramps back to 0.0 over the last third.

[26] The DGPS provides a reliable measure of the absolute position of the airplane throughout the takeoff; however, speeds and track angles computed from the DGPS data are much more "noisy" than the inertial groundspeed and track angle recorded by the FTIS. To obtain a smooth "target" track for the accelerometer integration, the integrated groundspeed and track angle is preferred to the DGPS track. However, since the DGPS track, while noisier, provides a better measure of the "absolute" position of the airplane, the groundspeed / track angle integration must be adjusted to prevent it from diverging from the DGPS track over time.

The magnitude and direction of the corrective velocity vector used in this case is listed in Table 7.

Item	Value
Start time of integration	09:33:20
End time of integration	09:34:00
Speed bias, knots	-1.59
Track bias, degrees	2.21
Rate of climb bias, ft./min.	-19.69
n_x bias, G's	-0.0078433
n_y bias, G's	0.0088787
nlf bias, G's	0.0083784
Groundspeed / track correction vector magnitude, knots	2.42
Groundspeed / track correction vector direction, degrees true (from)	167.40

Table 7. Accelerometer biases and constants of integration for FTIS accelerometer data integration.

The runway x- and y- coordinates,[27] MSL altitude, and height above the ground of the CG resulting from the *accelerometer* data integrations (not the groundspeed/track angle integration) are shown in Figures 2a, 2b, 3, 5, and 6. The $\{n_x, n_y, nlf\}$ load factors recorded by the FTIS, and the corresponding load factors corrected for accelerometer location and bias, are plotted in Figure 12.

Inertial α, β, and γ calculations

A calculation of α and β that is completely independent of the ADS data recorded by the FTIS involves computing the airplane's airspeed components along each of the body coordinate axes, using the inertial speed components resulting from the accelerometer integration, and wind information from the GAC weather station described in Section III. This inertial α and β calculation serves as a consistency check on the ADS data and on the correction of α at the CG due to pitch rate effects on the ADSP α (described above).

Airspeed, groundspeed, and wind are related as follows:

$$\vec{V} = \vec{V}_G - \vec{V}_W \qquad [20]$$

Where $\vec{V}$ is the airspeed vector, $\vec{V}_G$ is the groundspeed vector and $\vec{V}_W$ is the wind vector. The components of $\vec{V}_G$ are the inertial $\{u, v, w\}$ velocities in the body-axis system, obtained through the integration of the accelerometer data. The weather station provides wind speed and direction relative to magnetic North (vertical wind is assumed to be zero). The wind speed and direction can be transformed into wind components in the body-axis system using the FTIS Euler angles. Once the body-axis components of $\vec{V}_G$ and $\vec{V}_W$ are defined, Equation [20] can be solved to obtain the $\{u, v, w\}$ components of $\vec{V}$ in the body-axis system. The inertial α and β can then be computed using Equations [9] and [7], respectively. Note that the total airspeed velocity V can also be computed from its $\{u, v, w\}$ components.

[27] The integrations are performed using the North-East coordinate system, and then the results are transformed into the runway coordinate system for presentation in this *Study*.

Figure 13 shows the weather station wind data recorded by the FTIS. Based on this data, a constant wind of 6 knots from 150° magnetic (the wind at the time of rotation) was used for the inertial α and β calculations. The resulting total airspeed V is plotted in Figure 10 as the magenta line, and matches the true airspeed recorded by the FTIS well. The resulting inertial α is shown in Figures 9a and 9b, and matches the computed α at the CG (i.e., ADS3 α corrected for pitch rate effects) very well. The resulting inertial β is shown in Figure 14, and is in general agreement with the β from the ADSs. The differences between the inertial and ADS β (as much as 2° at 09:33:44) may be the result of an erroneous wind direction assumed in the calculation; the winds seen by the airplane at the point of rotation may have been slightly different than those at the weather station.

The flight path angle is defined by

$$\gamma = \sin^{-1}\left(\frac{\dot{h}}{V}\right) \qquad [21]$$

where γ is the flight path angle, $\dot{h}$ is the rate of climb, and V is speed. Using airspeed gives γ relative to the airmass, and using groundspeed gives γ relative to the Earth. The inertial γ computed using Equation [21], with $\dot{h}$ and V from the integrated accelerometer data, is shown in Figures 9a and 9b. In this calculation, V is the total inertial speed relative to the Earth (not airspeed), so the inertial γ is also relative to the Earth.

Airplane attitude, flight controls, and power settings

The airplane attitude is described by the pitch, roll, and heading angles recorded by the FTIS, as presented in Figures 9a, 9b, and 14. The angular rates recorded by the FTIS (and those computed from the FTIS Euler angles, using Equation [13]) are presented in Figure 15. The flight controls and power settings are also recorded on the FTIS and do not require additional calculations or corrections. These data are presented as a function of time in Figures 16-19.

Figure 16 presents engine power parameters, including the throttle resolver angles (TRAs), engine N1 speeds, and the total net thrust of each engine, as computed by the Engine Monitor System (EMS) and recorded by the FTIS. Note that the TRA of the right engine was retarded at about 09:33:37, consistent with the procedure for a one-engine-inoperative continued-takeoff maneuver. The reduction in thrust is also apparent in the reduction in n_x shown in Figure 12, and the change in the slopes of the speed vs. time plots in Figure 10.

Figure 17 presents the longitudinal flight control parameters. Left and right control column positions and forces are shown in the top plot of the Figure; the resulting elevator positions are shown in the middle plot, and the recorded horizontal stabilizer position is shown in the bottom plot.

Figure 18 presents the lateral flight control parameters. Left and right control wheel positions and forces are shown in the top plot; the resulting aileron positions are shown in the middle plot, and the resulting spoiler positions are shown in the bottom plot.

Figure 19 presents the directional flight control parameters. Rudder pedal position[28] and left and right pedal forces are shown in the top plot; the resulting rudder position is shown in the middle plot, and the recorded nose wheel steering position is shown in the bottom plot.

Figures 17-19 indicate that the flight control surface movements are consistent with the cockpit control inputs. Reference 12 confirms that the flight control system response to the pilot inputs was as designed.

V. GAC simulation "residuals" analysis

GAC engineers used an engineering simulator to compute the expected aerodynamic forces and moments acting on N652GD during the takeoff, and to compare these expected forces and moments with the actual aerodynamic forces and moments required to produce the airplane motion recorded by the FTIS. The differences between the required and expected forces and moments are called simulation "residuals," and are a measure of phenomena affecting the real airplane that are not accounted for in the simulation. Since all simulation models are imperfect approximations of the real airplane, the residuals are not expected to be perfectly zero (i.e., no difference between the simulation and reality), even for cases that do not result in an accident. However, large residuals, or a sudden growth in the residuals, indicate the action of a relatively major, *non-modeled* (i.e., unexpected) phenomenon affecting the motion of the airplane. In the accident case, the sudden growth of residuals in the rolling and yawing moments can help identify the onset point of an (unexpected) stall on the right wing, that led to a loss of roll control and the impact of the right wingtip with the runway. Computational Fluid Dynamics (CFD) work performed by GAC engineers after the accident confirms that the onset of stall in ground effect occurs at a lower α than was predicted at the time of the accident (the CFD work is described in the next Section). The stall α predicted by the CFD results is in good agreement with the timing of the stall suggested by the simulation residual analysis, as will be described further below.

This section provides a brief description of simulators in general, and then describes the calculation of expected and actual aerodynamic forces and moments using the simulation models and the FTIS data. The differences between the actual and expected results are then presented as residual aerodynamic rolling and yawing moment coefficients.

Simulation overview

The simulation residual analysis described in this *Study* is a special application of the GAC G650 engineering simulator. The way this application works is best understood in terms of how it differs from a "standard" simulation, in which a human pilot seated at the controls of a simulator cab makes control inputs as he would in a real airplane, and the simulation calculates the appropriate response in the control forces, airplane motion, instrument displays, and visual scene.

Figure 20 is a flow chart describing the logic and data flow in a standard simulation. The boxes with bold lines and non-italicized text represent simulation models, that is, units of computer code and data that describe the behavior of a part of the airplane or its systems mathematically. The boxes with non-bold lines and italicized text represent physical quantities

[28] The FTIS record contains only one rudder pedal position parameter, though it contains separate parameters for left and right column and wheel positions.

or values computed by the simulation models. The arrows indicate which simulator models compute the various physical quantities, and how these quantities are in turn used as inputs by other models.

Starting with the box labeled “Human Pilot,” we see that by manipulating the simulator cab controls the pilot can generate inputs to the column, wheel, throttles, speedbrake handle, flaps, gear, and other cockpit controls duplicated in the cab. He can also provide inputs to the Flight Management Computer and Autopilot. In the case of desktop engineering simulations, which run on the computer without a cab, these “pilot” inputs are accomplished by computer code. For both desktop and cab-based simulations, the pilot inputs are eventually processed by the simulator flight controls model that calculates the appropriate response of the airplane control surfaces, and by the propulsion model that computes the response of the airplane’s engines and the resulting thrust forces and moments. The aerodynamic model then uses the control surface positions along with the motion state of the airplane (airspeed, altitude, etc.) to calculate aerodynamic forces and moments on the airplane. Ground reaction forces are computed by the gear model. The total forces and moments are used along with quantities calculated by the mass properties model in the solution of the equations of motion that determine the motion states, both angular and linear. Angular states are the airplane’s yaw, pitch and roll angles, and their time derivatives (angular rates and accelerations). Linear states are the components of the three dimensional position of the airplane in space and their time derivatives (velocities and accelerations). These states are also used as inputs in the various mathematical models that compute the quantities that eventually affect the forces and moments.

In the case of cab-based simulations, information about the airplane motion states and from the propulsion model are used to drive the visual displays and cockpit instruments in the cab. For simulator cabs on a motion base (such as Level-D training simulators), the motion information can be used to maneuver the base in an attempt to duplicate, within limits, the acceleration cues felt by the pilots.

Calculation of expected aerodynamic forces and moments

The aerodynamic forces and moments on an airplane depend on the airplane’s state (attitude, orientation, speed), configuration (flaps, landing gear), flight controls (column, wheel, pedal), and the environment (atmospheric properties, gravity). The simulation aerodynamic models use these quantities as inputs to determine aerodynamic forces and moments. In standard simulations, the airplane state must be continuously computed by the simulation itself, through a solution of the equations of motion. For the accident case, the airplane state (and other required inputs) are either recorded directly by the FTIS, or can be derived from the FTIS data, as described in Section D-IV. Consequently, there is no need for the simulation to solve the equations of motion in order to determine the aerodynamic forces and moments that the simulation models would *predict* would be acting on the airplane at every moment through the takeoff; the required state parameters can be provided to the models directly.

The six aerodynamic forces and moments are most conveniently expressed in the form of dimensionless aerodynamic coefficients. The three force coefficients are:

$$C_L = \frac{L}{\bar{q}S} \quad [22]$$

$$C_D = \frac{D}{\bar{q}S} \quad [23]$$

$$C_Y = \frac{Y}{\bar{q}S} \quad [24]$$

Where L, D, and Y are the lift, drag, and side forces, respectively; S is the wing reference area; and $\bar{q}$ is the dynamic pressure of the airstream:

$$\bar{q} = \frac{1}{2}\rho V^2 \quad [25]$$

Where ρ is the air density and V is the true airspeed.

The three aerodynamic moment coefficients are:

$$C_M = \frac{M}{\bar{q}S\hat{c}} \quad [26]$$

$$C_R = \frac{R}{\bar{q}Sb} \quad [27]$$

$$C_N = \frac{N}{\bar{q}Sb} \quad [28]$$

Where M, R, and N are the pitching, rolling, and yawing moments, respectively;[29] $\hat{c}$ is the wing mean aerodynamic chord (MAC); and b is the wingspan.

GAC computed the expected aerodynamic coefficients for the accident takeoff by querying the G650 simulation models using the airplane state and other required inputs determined from the FTIS record.

Calculation of actual aerodynamic forces and moments

The *total* forces and moments acting on the airplane are the sum of aerodynamic, propulsion, and ground reaction forces and moments. Consequently, the aerodynamic forces and moments can be computed if the total, propulsion, and ground reaction forces and moments are known or can be estimated:

$$\vec{F}_A = \vec{F}_T - \vec{F}_P - \vec{F}_G \quad [29]$$

$$\vec{M}_A = \vec{M}_T - \vec{M}_P - \vec{M}_G \quad [30]$$

[29] Textbooks in the United States commonly use a lower-case "L" (l) to denote the rolling moment, but in this *Study* an R is used to avoid potential confusion with C_L. Also note that in Europe, C_R and C_N are sometimes non-dimensionalized with the wing MAC ($\hat{c}$) instead of the wingspan (b).

Where the $\vec{F}$ denote forces, the $\vec{M}$ denote moments, and the subscripts A, P, G, and T denote aerodynamic, propulsion, ground reaction, and total forces (or moments), respectively. Note that the quantities in Equations [29] and [30] are vectors.

The *total* forces and moments acting on the airplane ($\vec{F}_T$ and $\vec{M}_T$) produce linear and angular accelerations in accordance with the equations of motion. For the accident case, since the linear and angular accelerations are included in or can be computed from the FTIS data, the $\vec{F}_T$ and $\vec{M}_T$ can be determined.

The FTIS record includes the net thrust of the engines as computed by the EMS, and so the $\vec{F}_P$ and $\vec{M}_P$ are also known or can be computed (to the degree that the EMS thrust calculations are correct). However, the FTIS does not measure or compute any parameters that can be used to determine $\vec{F}_G$ or $\vec{M}_G$. Instead, the simulation gear model can be used to estimate $\vec{F}_G$ and $\vec{M}_G$, using the airplane geometry (position and attitude) relative to the ground as input. This geometry can be determined from the FTIS data.

The $\vec{F}_T$ and $\vec{M}_T$ are computed from the linear and angular accelerations, and the airplane's mass properties, using Euler's equations of motion for a rigid body:

$$\vec{F}_T = \begin{Bmatrix} F_x \\ F_y \\ F_z \end{Bmatrix}_T = m\left[\begin{Bmatrix} \dot{u} + wQ - vR \\ \dot{v} + uR - wP \\ \dot{w} + vP - uQ \end{Bmatrix} - g\begin{Bmatrix} -\sin\theta \\ \sin\phi\cos\theta \\ \cos\phi\cos\theta \end{Bmatrix}\right] \quad [31]$$

$$\vec{M}_T = \begin{Bmatrix} M_x \\ M_y \\ M_z \end{Bmatrix}_T = \begin{Bmatrix} I_{xx}\dot{P} + (I_{zz} - I_{yy})QR + I_{xy}(PR - \dot{Q}) + I_{yz}(R^2 - Q^2) - I_{xz}(PQ + \dot{R}) \\ I_{yy}\dot{Q} + (I_{xx} - I_{zz})PR + I_{yz}(PQ - \dot{R}) + I_{xz}(P^2 - R^2) - I_{xy}(QR + \dot{P}) \\ I_{zz}\dot{R} + (I_{yy} - I_{xx})PQ + I_{xz}(QR - \dot{P}) + I_{xy}(Q^2 - P^2) - I_{yz}(PR + \dot{Q}) \end{Bmatrix} \quad [32]$$

In these equations, m is the mass of the airplane (equal to the airplane weight (W) divided by g), I_{xx}, I_{yy}, and I_{zz} are the moments of inertia, and I_{xy}, I_{xz}, and I_{yz} are the products of inertia. The weight and inertias for the accident condition are listed in Table 1. Note that because of the symmetry about the x-z plane, I_{xy} and I_{yz} are assumed to be zero.

The $\vec{F}_T$ and $\vec{M}_T$ defined in Equations [31] and [32] are in body-axis coordinates. Hence, care must be taken when using these parameters to compute $\vec{F}_A$ and $\vec{M}_A$ using Equations [29] and [30] that the $\vec{F}_P$ and $\vec{M}_P$, and $\vec{F}_G$ and $\vec{M}_G$, used in the calculation are also in body-axis coordinates. The resulting $\vec{F}_A$ and $\vec{M}_A$ will of course also be in body-axis coordinates.

The aerodynamic force and moment coefficients used in the simulator are in stability axis coordinates, and so to compute the aerodynamic coefficient residuals, $\vec{F}_A$ and $\vec{M}_A$ must be transformed into stability axes:

$$\vec{F}_{A,stab} = \begin{Bmatrix} F_x \\ F_y \\ F_z \end{Bmatrix}_{A,stab} = \begin{Bmatrix} -D \\ Y \\ -L \end{Bmatrix} = \begin{bmatrix} \cos\alpha & 0 & \sin\alpha \\ 0 & 1 & 0 \\ -\sin\alpha & 0 & \cos\alpha \end{bmatrix}\begin{Bmatrix} F_x \\ F_y \\ F_z \end{Bmatrix}_A \quad [33]$$

$$\vec{M}_{A,stab} = \begin{Bmatrix} M_x \\ M_y \\ M_z \end{Bmatrix}_{A,stab} = \begin{Bmatrix} R \\ M \\ N \end{Bmatrix} = \begin{bmatrix} \cos\alpha & 0 & \sin\alpha \\ 0 & 1 & 0 \\ -\sin\alpha & 0 & \cos\alpha \end{bmatrix} \begin{Bmatrix} M_x \\ M_y \\ M_z \end{Bmatrix}_A \quad [34]$$

Equivalently, the aerodynamic coefficient residuals can be computed in body-axis coordinates;[30] in this case, the simulator stability-axis forces and moments must be transformed into body-axis coordinates using the inverses of Equations [33] and [34]:

$$\vec{F}_A = \begin{Bmatrix} F_x \\ F_y \\ F_z \end{Bmatrix}_A = \begin{bmatrix} \cos\alpha & 0 & -\sin\alpha \\ 0 & 1 & 0 \\ \sin\alpha & 0 & \cos\alpha \end{bmatrix} \begin{Bmatrix} F_x \\ F_y \\ F_z \end{Bmatrix}_{A,stab} = \begin{bmatrix} \cos\alpha & 0 & -\sin\alpha \\ 0 & 1 & 0 \\ \sin\alpha & 0 & \cos\alpha \end{bmatrix} \begin{Bmatrix} -D \\ Y \\ -L \end{Bmatrix} \quad [35]$$

$$\vec{M}_A = \begin{Bmatrix} M_x \\ M_y \\ M_z \end{Bmatrix}_A = \begin{bmatrix} \cos\alpha & 0 & -\sin\alpha \\ 0 & 1 & 0 \\ \sin\alpha & 0 & \cos\alpha \end{bmatrix} \begin{Bmatrix} M_x \\ M_y \\ M_z \end{Bmatrix}_{A,stab} = \begin{bmatrix} \cos\alpha & 0 & -\sin\alpha \\ 0 & 1 & 0 \\ \sin\alpha & 0 & \cos\alpha \end{bmatrix} \begin{Bmatrix} R \\ M \\ N \end{Bmatrix} \quad [36]$$

Calculation of aerodynamic coefficient residuals

Once the actual and expected $\vec{F}_{A,stab}$ and $\vec{M}_{A,stab}$ (or their body-axis equivalents) are computed, the non-dimensional aerodynamic coefficients can be computed using Equations [22]-[28]. Finally, the coefficient residuals can be computed as the difference between the actual coefficients and the coefficients predicted by the simulator:

$$\Delta C_x = C_{x,act} - C_{x,sim} \quad [37]$$

Where ΔC_x is the coefficient residual, the x subscript denotes any of the force or moment coefficients, the "act" subscript refers to the actual coefficients computed using Equations [33], [34], and [22]-[28], and the "sim" subscript refers to the coefficients predicted by the simulator for the flight conditions recorded by the FTIS.

The results of GAC's simulation residual analysis are shown in the middle plot of Figure 21. The top plot of the Figure shows the θ and α data from the FTIS, as well as the computed α at the CG, vs. time (similar to the data shown in Figure 9b). The middle plot presents the rolling moment and yawing moment coefficient residuals (ΔC_R and ΔC_N, respectively), in body axis coordinates, vs. time.[31] The bottom plot in Figure 21 plots ΔC_R and ΔC_N (in body axes) vs. the computed α at the CG. These plots make it clear that ΔC_R and ΔC_N start to grow dramatically as the θ and α at the CG pass through 11.2° at about 09:33:50.5. This indicates that at α = 11.2°, a large aerodynamic effect suddenly takes place on the real airplane that is not modeled in the simulator. This effect produces large yawing and rolling moments to the right, which account for the continued roll and yaw of the airplane to the right in spite of the increasing left wheel and rudder applied by the pilot at the time (see Figures 18 and 19).

The abruptness, magnitude, and character of the aerodynamic effect on ΔC_R and ΔC_N are compelling indications of flow separation on the right wing (i.e., an asymmetric stall of the

[30] The residuals computed by GAC engineers for the accident analysis are in fact in body-axis coordinates.
[31] The "bump" in ΔC_R between 09:33:52.5 and 09:33:53.2 shown in Figure 21 are likely the result of the left rolling moment produced by the right wingtip striking the runway.

airplane), even though the aerodynamic effect occurs below both the $\alpha_{stall,IGE}$ predicted prior to the accident, and the α_{shaker} threshold in place at the time. The conclusion that the onset of the large ΔC_R and ΔC_N residuals at α = 11.2° is the result of an asymmetric stall is substantiated by the results of a Computational Fluid Dynamics (CFD) analysis of the G650 in ground-effect conducted by GAC after the accident, as described in the next Section.

VI. GAC Computational Fluid Dynamics ground-effects analysis

After the accident, GAC engineers conducted an extensive CFD analysis of the effect of the proximity of the ground on the aerodynamics of the G650 (ground-effect), and in particular of the influence of the ground on the stall angle of attack (α_{stall}). The difference between α_{stall} in-ground-effect ($\alpha_{stall,IGE}$) and α_{stall} out-of-ground-effect or in "free air" ($\alpha_{stall,OGE}$) is the increment in α_{stall} due to ground effect:

$$\Delta\alpha_{stall,IGE} = \alpha_{stall,IGE} - \alpha_{stall,OGE} \quad [38]$$

Based on previous GAC airplane programs and on low-speed wind tunnel tests, prior to the accident GAC engineers expected $\Delta\alpha_{stall,IGE}$ to be about -2° (Reference 14, p. 15). At a previous point in the flight test program, one of the flight test engineers on the accident flight adjusted this increment to -1.6° based on an analysis of minimum-unstick speed takeoff (V_{mu}) tests (References 9 and 10; Reference 14, p. 15).

During previous flight tests of the G650, $\alpha_{stall,OGE}$ was determined to be a function of flap setting and Mach number. The flaps 10 $\alpha_{stall,OGE}$ corresponding to the accident takeoff is plotted in Figures 9a and 9b; the decrease in $\alpha_{stall,OGE}$ with time as Mach number increases is apparent in the Figures. Figures 9a and 9b also show the $\alpha_{stall,IGE}$ corresponding to the pre-accident $\Delta\alpha_{stall,IGE}$ = -1.6° estimate. As described in Section D-V, the ΔC_R and ΔC_N residuals grow abruptly as α passes through 11.2° at 09:33:50.5, i.e., *before* α exceeds the pre-accident prediction for $\alpha_{stall,IGE}$. This observation, together with the nature of the accident (a loss of roll control leading to a wing-tip strike on takeoff rotation) indicate the necessity of an in-depth analysis of ground-effect on the G650, and on the magnitude and behavior of $\Delta\alpha_{stall,IGE}$ in particular.

Overview of ground effect

The physical basis and *qualitative* effects of ground-effect on an airplane's aerodynamics are well understood (see, for example, References 15-17). The airflow around the airplane cannot have a vertical component at the ground plane (i.e., air cannot flow into or out of the ground), and so the streamlines around the airplane are altered from what they would be in free air. Specifically, the downwash produced by the wing trailing vortices is reduced by the proximity of the ground plane, which in turn reduces the induced angle of attack and induced drag, and increases the C_L at a given α. These effects are sketched in Figure 22, which is taken from Reference 15.

The sketch in Figure 22 illustrates that $\alpha_{stall,IGE}$ is lower than $\alpha_{stall,OGE}$, and the sketch also suggests that the maximum C_L achievable (C_{Lmax}) in- and out- of ground-effect are the same. Recent research mirrors the behavior depicted in Figure 22; for example, Reference 18 notes that

> It has been established that the stall of all types of aircraft occurs approximately 2 to 4 degrees (AOA) lower with the wheels of the aircraft on the ground. …
>
> … The aircraft in ground effect possesses a similar CLMAX as in-flight, but the absolute AOA for stall has reduced.

However, other researchers have documented that C_{Lmax} can decrease in ground-effect. For example, one of the conclusions of Reference 22 is that "with flaps deflected, a decrease in height of the wing above the ground resulted in decreases in maximum lift …" [p. 10].

Given this disparity of evidence, the *quantitative* effects of ground-effect are likely unique to every airplane configuration, and must be evaluated either by test or analysis for each configuration. The CFD analysis performed by GAC for the G650 indicates that the wings-level $\Delta\alpha_{stall,IGE}$, with the main wheels on the ground and fully compressed, is about -3°. Notably, the CFD results also indicate that the C_{Lmax} achievable in-ground-effect is *also* reduced compared to C_{Lmax} out-of-ground-effect, in contrast to the behavior depicted in Figure 22 and noted in Reference 18, but consistent with the conclusions of Reference 22.

Overview of CFD tools and methods

Computational Fluid Dynamics (CFD) is the science of solving the equations of motion of fluids numerically with digital computers, and visualizing the resulting solutions. The partial differential equations that comprise the fluid equations of motion are discretized into finite-difference equations at the intersection points of a grid or mesh that describes the solution space or volume, and that defines the geometry of the objects about which the flow solution is sought (e.g., an airplane). The finite-difference equations are then integrated forward in time until, after a sufficient number of iterations or time steps, the solution asymptotes towards a steady-state value at each grid point (Reference 19).

The CFD tools and methods used by GAC to analyze the G650 in- and out- of ground-effect (and the results of the analysis) are described in Reference 20. That document provides the following bullet-points regarding the CFD solver and solution method:

- NSU3D [the CFD solver used by GAC] developed by the University of Wyoming & Scientific Simulations LLC [See more information at http://www.scientific-sims.com/software/nsu3d].
- This code is an unstructured Reynolds Averaged Navier-Stokes solver, used at GAC since April 18th, 2011.
- Employs multi-gridding for solution convergence.
- Parallel implementation is employed to reduce run-times (solver uses 2n processors for multi-gridding strategy).
- Employs a Spalart-Allmaras Turbulence Model, which was not developed for this application but seems to do a good job anyway.
- Solution time averages 2-3 hours for 30x106 cell grid on 256 processors. However, much longer run times [are] required to obtain complete solution convergence at aerodynamic stall conditions.
- To-date logged 1,361,912 CPU hours using NSU3D on this study.
- IGE study requires one model for each angle of attack. Process is labor intensive - total of 80 models built for 2 flap settings (flap 10 and 20) for h/b study alone.
- Half plane model used to reduce compute times where viable. Full span model used for sideslip, aileron, spoiler, rudder and banked flight study.
- Domain grids ranged from 25 to 65 x 106 cells.
- Each grid requires 32MB RAM and takes 2-3 CPU hours to close.
- Ground plane modeled as an inviscid boundary (to simplify boundary layer growth and its interaction with aircraft).

The surface grid used to define the G650 at flaps 10 and β = 0° with the gear on the ground and fully compressed is shown in Figure 23, which is taken from Reference 20.

GAC validated the use of NSU3D for predicting $\Delta\alpha_{stall,IGE}$ by first using it to predict $\alpha_{stall,OGE}$ for the geometry and conditions of a half-span wind tunnel model of the G650 that was tested at high-Reynolds number in the European Transonic Wind Tunnel (ETW). The CFD solutions duplicated the lift curve, C_{Lmax}, and α_{stall} obtained in the ETW very well, providing confidence that NSU3D could be used to determine the increments to C_{Lmax} and α_{stall} due to ground-effect. Note that GAC used the CFD solutions to obtain *increments* to aerodynamic properties due to ground-effect; the *absolute values* of the properties in-ground-effect were determined by adding the CFD ground-effect increments to the free-air values obtained from flight test.

CFD results: stall α in ground effect at zero sideslip angle

The results of the CFD in-ground effect analysis for flaps 10 and β = 0°, at Mach = 0.190 (120 kts. calibrated airspeed), are shown in Figure 24, which is taken from Reference 20. The numerical values on the C_L scale are omitted in order to protect the proprietary nature of the data. Figure 24 indicates that:

- The behavior of the lift curve in-ground-effect is similar to that sketched in Figure 22; however,
- C_{Lmax} in-ground-effect is reduced compared to C_{Lmax} out-of-ground-effect.
- With the gear on the ground, the CFD solution predicts $\Delta\alpha_{stall,IGE}$ = -3.25°.
- The effect of ground effect on α_{stall} and C_{Lmax} decreases rapidly with increasing gear height.
- The stall is abrupt, occurring over an α range of less than 1°, with little "bending over" of the lift curve prior to stall (these characteristics are also evident in the ETW data).
- There is a significant drop in C_L at the stall; consequently, if stall occurs on one wing but not the other, a large rolling moment will develop. Similarly, the large drag increase on the stalled wing will create a large yawing moment. Reference 20 notes that "post stall roll-off is abrupt and will saturate lateral control power."

On the basis of a curve fit through the CFD $\Delta\alpha_{stall,IGE}$ results for all flap settings, GAC engineers modeled $\Delta\alpha_{stall,IGE}$ as a quadratic function of the inverse of the height of a reference point on the airplane above the ground. This function is intended as a means of computing $\alpha_{stall,IGE}$ for safety of flight monitoring[32] (Reference 21):

$$\Delta\alpha_{stall,IGE} = 50.7453\left(\frac{1}{h_{CFD}}\right)^2 - 25.6787\left(\frac{1}{h_{CFD}}\right); \quad h_{CFD} \geq 5.3792 \text{ ft.} \qquad [39]$$

h_{CFD} is the height of the CFD reference point on the airplane. This point is computed by adding 5.3792 feet to the height of the bottom of the main gear tires above the ground, assuming that the main gear struts are fully compressed; hence, the minimum value of h_{CFD} (with the main gear on the ground and fully compressed) is 5.3792 ft.. Consequently, the minimum possible value of $\Delta\alpha_{stall,IGE}$ from Equation [39] is -3.02°, even though the flaps 10

[32] For safety of flight monitoring, $\alpha_{stall,IGE}$ would be computed by adding the $\Delta\alpha_{stall,IGE}$ defined by Equation [39] to the $\alpha_{stall,OGE}$ for the conditions at the time, and be available for display on the flight test engineers' IADS screens. h_{CFD} for this calculation would be based on DGPS data.

$\Delta\alpha_{stall,IGE}$ result from the CFD analysis is -3.25°. This 0.23° difference is acceptable given its small magnitude, the uncertainties inherent in the CFD analysis, the observed trend of $\Delta\alpha_{stall,IGE}$ with h_{CFD}, and the intent of the curve fit for safety-of-flight monitoring.

The h_{CFD} for the accident takeoff is shown in the top plot of Figure 25. Also shown is the "right wingtip equivalent h_{CFD}," which is the h_{CFD} at zero roll angle that would result in the same actual height of the wingtip above the ground as that plotted in Figures 5 and 6. At the start of the takeoff roll, both these h_{CFD} curves are identical, but as the airplane rolls and the right wingtip nears the ground, the "right wingtip equivalent h_{CFD}" decreases below the actual h_{CFD}.

The middle plot of Figure 25 shows the $\alpha_{stall,IGE}$ for the accident takeoff computed by adding the $\Delta\alpha_{stall,IGE}$ from Equation [39] to $\alpha_{stall,OGE}$. The $\alpha_{stall,IGE}$ computed using $\Delta\alpha_{stall,IGE}$ evaluated at both the actual h_{CFD} and the "right wingtip equivalent h_{CFD}" are shown[33]. Note that the $\alpha_{stall,IGE}$ based on the CFD results lies below α_{shaker}. Also note that at 09:33:50.5 (the point at which the stall occurs, based on the simulation residual analysis described in the previous Section), the α at the CG is still below $\alpha_{stall,IGE}$ (which would suggest that α is still not high enough to produce a stall), but that the α at the right wingtip reaches the $\alpha_{stall,IGE}$ computed using the "right wingtip equivalent h_{CFD}." This result is consistent with a stall on the right wing occurring at this point.

The bottom plot of Figure 25 shows the stick shaker discretes recorded by the FTIS. These indicate that the stick shaker "active" signals are consistent with the times where $\alpha > \alpha_{shaker}$ per the middle plot of the Figure.

Additional CFD results

GAC used the NSU3D solver to evaluate the effect of other parameters on the aerodynamics of the G650 in-ground-effect, including:

- Sideslip angle (β)
- Aileron and spoiler deflection
- Rudder deflection
- Roll angle

Reference 20 lists the following conclusions regarding these evaluations:

- CFD predicts sideslip has no effect on wing aero. stall margin when $\beta \leq 5$ degrees. At higher sideslip angles CFD predicts stall margin is reduced, but wind tunnel and Flight Test data suggest this may be a conservative estimate.
- Aileron deflection has no effect on α_{Max} [α_{stall}] but will change C_{Lmax}.
- Spoiler deflection has no effect on α_{Max} but will reduce C_{Lmax}.
- Ground effect has no impact on rudder effectiveness.
- Bank [roll] angle in ground effect will reduce wing angle of attack margin to aerodynamic stall on down-going wing.

[33] In Equation [39], $\Delta\alpha_{stall,IGE} \rightarrow \infty$ as $h_{CFD} \rightarrow 0$. To avoid unreasonably large values of $\Delta\alpha_{stall,IGE}$ evaluated using the "right wingtip equivalent h_{CFD}" (which drops below the minimum h_{CFD} of 5.3792 ft. allowed in Equation [39]), $\Delta\alpha_{stall,IGE}$ is constrained to be $\geq$ -3.02° (the value from Equation [39] evaluated at 5.3792 ft.) even for "right wingtip equivalent h_{CFD}" values < 5.3792 ft.. Reference 20 indicates that at ϕ = 10° and β = -4°, $\Delta\alpha_{stall,IGE}$ may have an additional increment of about -1°. At 09:33:50.5 (the time of the stall), ϕ = 2.3°.

The CFD results do indicate that a non-zero β will cause the "downstream" wing to stall first; i.e., a negative β (wind from the left) will cause the flow to separate on the right wing first. This is the situation on the accident flight; Figure 14 shows that β at 09:33:50.4 is about -3.5°. A visualization of the CFD results of a "mirror image" of this situation (i.e., positive β, and flow separating first on the left wing) is presented in Reference 20 and included here as Figure 26. The dark coloring on the left wingtip in the Figure indicates areas of flow separation.

The result reported in Reference 20 that "bank angle in ground effect will reduce wing angle of attack margin to aerodynamic stall on down-going wing" is consistent with the analysis presented above that related the height of the right wingtip to a "right wingtip equivalent h_{CFD}," and compared the $\alpha_{stall,IGE}$ using this equivalent h_{CFD} to the α at the right wingtip resulting from the combination of the α at the CG and the airplane's roll rate.

E. CONCLUSIONS

The accident scene information, recorded flight test and CVR data, and post-accident simulation and CFD analyses performed by GAC indicate the following sequence of events during the accident, from just prior to brake release to the final location of the airplane about 300 feet from the FAA control tower:

Longitudinal control and response

At 09:33:17, the airplane was on the runway centerline and aligned with the runway heading, and the power was set for takeoff, as the brakes were released. At this weight, altitude and flap position, the aircraft decision speed (V_1) was 125 knots calibrated airspeed (KCAS), the target rotation speed (V_R) was 127 KCAS, and the target take-off safety speed (V_2) was 135 KCAS. The test card for this OEI CTO maneuver specified that a target θ of 9° was to be captured immediately following rotation and maintained until V_2, and then adjusted so as to maintain V_2. Between 09:33:35 and 09:33:36 the right throttle was retarded ("chopped"), consistent with the engine-failure speed (V_{EF}) of 105 KCAS briefed for the takeoff. As the thrust from the right engine decreased, the pilot input left rudder to maintain runway heading. At 09:33:45.7, as the airplane was accelerating through 123 KCAS, the co-pilot called "rotate."

Between 09:33:46.5 and 09:33:47, as the airplane accelerated through 125-127 KCAS, the pilot pulled the control column aft 6° with about 50 lb. of force, and the elevators moved trailing-edge-up consistent with this control input. The pitch rate responded promptly, reaching a peak of 6 deg./sec. at 09:33:48. At 09:33:48.5, the pilot relaxed the pull force on the column to about 10 lb., and then increased it again to about 25 lb. at 09:33:49.5. Between 09:33:49.5 and 09:33:52, the pilot maintained between 23 and 30 lb. of pull force on the column, corresponding to a column position between 2.5° and 3.5° aft. At 09:33:49, as θ was increasing through about 9°, the pitch rate relaxed to about 1 deg./sec. and remained there until about 09:33:52.5.

Based on wheel speed data recorded by the FTIS, the left main gear tire lifted off at about 09:33:50.1, and the right tire lifted off at about 09:33:50.6. The simulation aerodynamic coefficient residual analysis conducted by GAC indicates that at 09:33:50.5, as θ and α were increasing through 11.2°, large aerodynamic rolling and yawing moments to the right, which were not modeled in the simulator, were acting on the airplane.

The abruptness, magnitude, and character of the unexpected aerodynamic rolling and yawing moments are compelling indications of flow separation on the right wing (i.e., an asymmetric stall of the airplane), even though these aerodynamic moments appear below both the $\alpha_{stall,IGE}$ predicted prior to the accident, and the α_{shaker} threshold in place at the time.

The conclusion that the onset of the large moments at α = 11.2° is the result of an asymmetric stall is substantiated by the results of a CFD analysis of the G650 in ground effect conducted by GAC after the accident, which indicates that at flaps 10, the increment in stall angle of attack due to ground-effect ($\Delta\alpha_{stall,IGE}$) can be as much as -3.25°, or about twice the $\Delta\alpha_{stall,IGE}$ of -1.6° that had been estimated at the time of the accident. The CFD analysis also indicates that at non-zero sideslip, the downwind wing will stall first, consistent with the situation during the accident. The results of the CFD analysis, together with the nose-right sideslip angle, the reduced height of the right wingtip due to the right roll angle, and the increased α on the right wing due to the right roll rate, are consistent with a stall occurring on the right wing at about 09:33:50.5, as suggested by the simulation residual analysis.

At 09:33:52.3, the recorded α data reached 12.4°, the threshold for the stick-shaker stall warning corresponding to the Mach number and flap setting at the time, and the stick-shaker discretes recorded by the FTIS changed from “inactive” to “active.” Between 09:33:52.3 and 09:33:52.6, the pilot pushed the column forward abruptly, moving it from 2.5° aft (a 20 lb. pull) to -1.2° forward (a 12.3 lb. push). Between 09:33:52.5 and 09:33:53.3, θ decreased from 12.9° to 11.5°, and α decreased from about 12.7° to about 11.5°.

Between 09:33:52.6 and 09:33:53.1, the pilot pulled back again on the column with about 38 lb. of force, moving it to about 4° aft. He relaxed the column to about 1.5° aft (15 lb. pull) at 09:33:54, then pulled back again with over 60 lb, moving the column to about 7.5° aft. The column remained aft, with the pilot pulling between 60 and 110 lb. of force, until the airplane touched down again at 09:34:00. The θ and α responded to these inputs; θ reached 13.8° at 09:33:54.5, decreased to 12.4° at 09:33:55.5, and then climbed to 14.8° at 09:33:57.5, before decreasing to -0.2° at touchdown at 09:34:00. α reached 15° at 09:33:54.5, decreased to 14° at 09:33:55.3, and then climbed to 22.7°[34] at 09:33:57.7, before decreasing to 9.5° at touchdown.

Lateral control and response

As the airplane accelerated down the runway following brake release, the pilot maintained a wheel input of about -1° to -2° (left), and the airplane’s roll angle remained within 1° of level. As the pilot was pulling back on the column between 09:33:46.5 and 09:33:47, a 1 deg./sec. right yaw rate developed, which lasted until about 09:33:50. At about 09:33:48.5, a right roll rate started to develop, that grew to about 4.9 deg./sec. at 09:33:51. At 09:33:50, the sideslip angle was about -3°, as a result of the yaw and a slight (2.5 knot) left crosswind; the roll angle was 1.4°. The control wheel deflection increased from about 1.8° left to about 11.9° left between 09:33:47 and 09:33:50.

Between 09:33:50 and 09:33:51.1, the pilot moved the control wheel from 11.9° left to 22.6° left, but this did not reverse the roll rate to the right (the stall on the right wing likely occurred at 09:33:50.5). The increased wheel input did arrest the increase in the roll rate briefly; the roll rate remained at about 4.9 deg./sec. between 09:33:51.0 and 09:33:51.8, before increasing to

[34] Based on the inertial α calculation; the α data from the ADS is unreliable at these high values.

a peak of 9.6 deg./sec. at 09:33:52.5. Between 09:33:52.5 and 09:33:53.1, the roll rate reversed rapidly from 9.6 deg./sec. to the right to 1.3 deg./sec. to the left. This reversal likely resulted from the contact of the right wingtip with the runway, about 5160 feet from the runway threshold, at a roll angle of 13.4°. Between 09:33:52.4 and 09:33:52.7, or about 1 second before the right wingtip strike, the pilot moved the control wheel abruptly from 26.5° left to 60° left (full deflection), but this did not prevent the roll rate from increasing to the right. Instead, between 09:33:52.7 and 09:33:58.8, the roll angle progressively increased from 15.5° to 32° right-wing-down. After 09:33:58.8, the roll rate reversed, and the roll angle decreased to 17° right-wing-down at touchdown at 09:34:00.

Directional control and response

During the takeoff roll prior to the right throttle chop, the pilot maintained a rudder pedal deflection of about 0.5 inches to the right. Following the throttle chop, the pilot moved the rudder pedal to about 1.4 inches left, modulating the input as required to maintain runway heading. Between 09:33:50.4 and 09:33:51, the pilot increased the left pedal deflection from about 1.6 inches to about 2.8 inches, and maintained this deflection for about one second. Between 09:33:52 and 09:33:52.7, the pilot moved the rudder pedal from 2.8 inches left to 3.5 inches left (full deflection).

Between 09:33:51 and 09:33:56.3, the yaw rate to the right increased continuously (except for a brief reduction between 09:33:52.8 and 09:33:53.5), from -0.3 deg./sec. (left) to 9.5 deg./sec. (right). Between 09:33:53.5 and 09:33:53.8, the right TRA was advanced to match the left TRA. Following this advance, the right engine power started to increase.

The contact of the right wing with the runway produced a scrape mark starting about 5160 feet from the threshold. When the airplane departed the paved surface about 5900 feet from the threshold, this scrape became a “furrow” in the ground. Following liftoff, the right main gear tire reached a maximum height above the runway of about 12.6 feet at 09:33:58, as the roll angle continued to increase to a maximum of 32° at 09:33:58.7. Ground scar evidence and recorded data indicate that the right wingtip was close to or in contact with the ground throughout the time that the main gear were airborne; the right wing ground furrow continues to the point where the main gear touched down again, about 6770 feet from the runway threshold and 461 feet to the right of the runway centerline.

After the main gear touched down, the airplane continued a right turn, generally tracking to the west. The ground track marks and debris field pass within about 150 feet of the GAC telemetry (TM) trailer, where GAC engineers were monitoring the flight. The airplane tracks pass over the locations of two substantial structures on the airport property: a concrete electrical service shaft, and a metal pole supporting weather instrumentation.

The recorded flight test data ends at 09:34:09.0, 8064 ft. from the runway threshold and 1530 ft. to the right of the runway centerline. The CVR recording ends 1.3 seconds later. The airplane continued to slide for about another 540 ft., coming to rest 8404 ft. from the runway threshold and 1949 ft. to the right of centerline, about 300 feet from the FAA control tower.

_____

John O’Callaghan
National Resource Specialist – Aircraft Performance
Office of Research and Engineering

F. REFERENCES

1. National Transportation Safety Board, Office of Aviation Safety, *Operations Group Chairman's Factual Report*, *GAC G650, Roswell, New Mexico, April 2, 2011*, NTSB Accident Number DCA11MA076, Docket Item 2 (Washington, DC: NTSB, February 24, 2012). (Contact NTSB at pubinq@ntsb.gov).

2. New Mexico State Police, *State of New Mexico Incident Report, Assist FBI with Aircraft Crash,* Incident # 2011-7166, Case # 11-23-8-0028, ORI # NMNSP2113, prepared 04/12/2011 by Agent Lauren Milligan, approved 04/25/2011 by Sergeant Shayne Arthur.

3. Y. Zhou, H. Leung, & M. Blanchette, *Sensor alignment with Earth-centered Earth-fixed (ECEF) coordinate system*, IEEE Transactions on Aerospace and Electronic Systems, Vol. 35 issue 2, April 1999, pp. 410-418.

4. National Transportation Safety Board, Office of Research and Engineering, *Data Recorders Group Chairman's Factual Report, GAC G650, Roswell, New Mexico, April 2, 2011*, NTSB Accident Number DCA11MA076, Docket Item 48 (Washington, DC: NTSB, February 8, 2012). (Contact NTSB at pubinq@ntsb.gov).

5. National Transportation Safety Board, Office of Research and Engineering, *Cockpit Voice Recorder Group Chairman's Factual Report, GAC G650, Roswell, New Mexico, April 2, 2011*, NTSB Accident Number DCA11MA076, Docket Item 73 (Washington, DC: NTSB, March 5, 2012). (Contact NTSB at pubinq@ntsb.gov).

6. National Transportation Safety Board, Office of Research and Engineering, *On Board Video Recording Group Chairman's Factual Report, GAC G650, Roswell, New Mexico, April 2, 2011*, NTSB Accident Number DCA11MA076, Docket Item 72 (Washington, DC: NTSB, January 27, 2012). (Contact NTSB at pubinq@ntsb.gov).

7. Gulfstream Aerospace Corporation, *GVI Field Performance Certification Flight Test Plan Rev. A*, Document # GVI-FT-082, initial release 01/14/2010, Rev. A dated 10/07/2010. (GAC proprietary document).

8. Gulfstream Aerospace Corporation, *G650 Artificial Stall Barrier System Angle of Attack Schedule Definition*, Document # FS-AERO-10-033 Rev C, dated11/23/2011. (GAC proprietary document).

9. Gulfstream Aerospace Corporation, *Evolution of Stall Warning Settings for Takeoff Testing.* PowerPoint presentation given by GAC to NTSB, August 2, 2011. (GAC proprietary document).

10. Gulfstream Aerospace Corporation, *GVI Minimum Unstick Speed Company FTR (DRAFT),* Document # GVI-FTA-017. Initial date 01/06/2011. Draft document, not released. (GAC proprietary document).

11. National Transportation Safety Board, Office of Research and Engineering, *Group Chairman's Aircraft Performance Study, American Airlines Flight 587, Airbus A300B4-605R, Belle Harbor, New York, November 12, 2001,* NTSB Accident Number DCA02MA001, Docket Item 188 (Washington, DC: NTSB, October 10, 2002). (Contact NTSB at pubinq@ntsb.gov).

12. National Transportation Safety Board, Office of Aviation Safety, *Airworthiness Group Chairman's Factual Report of Investigation*, *GAC G650, Roswell, New Mexico, April 2, 2011*, NTSB Accident Number DCA11MA076, Docket Item 68 (Washington, DC: NTSB, January 25, 2012). (Contact NTSB at pubinq@ntsb.gov).

13. Gulfstream Aerospace Corporation, *G650 Stall Warning System Description.* PowerPoint presentation given by GAC to NTSB, August 2, 2011. (GAC proprietary document).

14. National Transportation Safety Board, *Interviews of Gulfstream Personnel (October 2011), Investigation of GAC G650, Roswell, New Mexico, April 2, 2011*, NTSB Accident Number DCA11MA076, Docket Item 20 (Washington, DC: NTSB, March 2, 2012). (Contact NTSB at pubinq@ntsb.gov).

15. Hurt, H. H. Jr., *Aerodynamics for Naval Aviators,* U. S. Naval Air Systems Command, NAVAIR Report # 00-80T-80, Revised January 1965.

16. Anderson, John D. Jr., *Introduction to Flight, Sixth Edition*, McGraw Hill, October 2007. ISBN-10: 0073529397, ISBN-13: 978-0073529394.

17. Kuethe, A., & Chow, C.-Y., *Foundations of Aerodynamics, Fifth Edition*, J. Wiley, December 1997. ISBN-10: 0471129194, ISBN-13: 978-0471129196.

18. Tanner, Clinton E., *The Effect of Wing Leading Edge Contamination on the Stall Characteristics of Aircraft*, SAE paper 2007-01-3286, presented at the SAE Aircraft & Engine Icing International Conference, Seville, Spain, September 24-27, 2007.

19. Anderson, Dale A., Tannehill, John C., & Pletcher, Richard H., *Computational Fluid Mechanics and Heat Transfer,* Hemisphere Publishing Corporation, 1984. ISBN 0-89116-471-5.

20. Gulfstream Aerospace Corporation, *G650 Aerodynamic Characteristics in Ground Effect Update.* PowerPoint presentation provided by GAC to NTSB, December 12, 2011. (GAC proprietary document).

21. Gulfstream Aerospace Corporation, *IADS IGE Stall Angle for Field Performance Safety of Flight Monitoring (DRAFT),* Document # FS-AERO-11-077. Initial date 12/22/2011. Draft document. (GAC proprietary document).

22. Carter, Arthur W., *Effects of Ground Proximity on the Longitudinal Aerodynamic Characteristics of an Unswept Aspect-Ratio-10 Wing.* NASA Technical Note TN D-5662, February 1970.

G. GLOSSARY OF SYMBOLS AND ACRONYMS

English characters

$\vec{a}$	Acceleration vector
ADC	Air Data Computer
ADS	Air Data System
ADSP	Air Data SmartProbe
AGL	Above Ground Level
ASCB	Avionics Standard Communication Bus
b	Wingspan
BL	Buttock Line
$\hat{c}$	Mean aerodynamic chord
CAIS	Common Airborne Instrumentation System
C_D	Drag coefficient
CDAU	CAIS Bus Data Acquisition Unit
CFD	Computational Fluid Dynamics
CG	Center of Gravity
C_L	Lift coefficient
C_M	Pitching moment coefficient
C_N	Yawing moment coefficient
C_R	Rolling moment coefficient
CVR	Cockpit Voice Recorder
C_Y	Side-force coefficient
D	Drag force
DGPS	Differential Global Positioning System
EMS	Rolls Royce Deutschland Engine Monitor System
$\vec{F}$	Force vector
FAA	Federal Aviation Administration
FBI	Federal Bureau of Investigation
FDR	Flight Data Recorder
FR	Heim Flight Recorder
FS	Fuselage Station
FTIS	Flight Test Instrumentation System
$\vec{g}$	Gravity vector
g	Acceleration due to gravity (32.17 ft/s^2)
GAC	Gulfstream Aerospace Corporation
GNSS	Global Navigation Satellite System
GPS	Global Positioning System
h	Altitude or height above the ground
HIPF	High Incidence Protection Function
$\hat{\imath}$	Unit vector along body x-axis
ICS	Innovative Control Systems, Inc.
IGE	In-ground-effect
IRS	Inertial Reference System
I_{xx}	Roll moment of inertia
I_{xz}	Product of inertia
I_{yy}	Pitch moment of inertia
I_{zz}	Yaw moment of inertia
$\hat{\jmath}$	Unit vector along body y-axis
$\hat{k}$	Unit vector along body z-axis
KCAS	Knots calibrated airspeed
KROW	Roswell International Air Center Airport
L	Lift force
m	Airplane mass = W/g
M	Pitching moment
$\vec{M}$	Moment vector
N	Yawing moment
OGE	Out-of-ground-effect

MAC	Mean Aerodynamic Chord
MDT	Mountain Daylight Time
MFP	Multi-function Probe
MSL	Mean Sea Level
$\vec{n}$	Load factor vector
nlf	Normal load factor = $-n_z$
NMSP	New Mexico State Police
NTSB	National Transportation Safety Board
P	Body-axis roll rate
$\bar{q}$	Dynamic pressure
Q	Body-axis pitch rate
$\vec{r}_P$	Vector from the CG to point P
R	Body-axis yaw rate or rolling moment (dependent on context)
RPD	Roswell Police Department
S	Wing area
SAT	Static Air Temperature
SRTM	Shuttle Radar Topography Mission
TAT	Total Air Temperature
TIS	Honeywell Test Interface System
TM	Telemetry
TRA	Throttle Resolver Angle
u	Velocity component along x-body axis
USGS	United States Geological Survey
UTC	Universal Coordinated Time
v	Velocity component along y-body axis
V	Total velocity (inertial speed or airspeed dependent on context)
$\vec{V}$	Velocity vector (inertial speed or airspeed dependent on context)
V_1	Takeoff decision speed. V_1 means the maximum speed in the takeoff at which the pilot must take the first action (e.g., apply brakes, reduce thrust, deploy speed brakes) to stop the airplane within the accelerate-stop distance. V_1 also means the minimum speed in the takeoff, following a failure of the critical engine at V_{EF}, at which the pilot can continue the takeoff and achieve the required height above the takeoff surface within the takeoff distance.
V_2	Takeoff safety speed
V_{EF}	Speed at which the critical engine is assumed to fail during takeoff
VFR	Visual Flight Rules
V_{mu}	Minimum unstick speed
V_R	Takeoff rotation speed
w	Velocity component along z-body axis
W	Airplane weight = mg
WL	Water Line
x	x-coordinate (axis system dependent on context)
y	y-coordinate (axis system dependent on context)
Y	Side-force
z	z-coordinate (axis system dependent on context)

Greek characters

α	Angle of attack
β	Sideslip angle
γ	Flight path angle
Δ	Increment or difference in the quantity following the Δ
θ	Pitch angle
ϕ	Roll angle
ψ	Heading or track angle (magnetic or true dependent on context)
$\vec{\omega}$	Rotational velocity vector
ρ	Air density

FIGURES

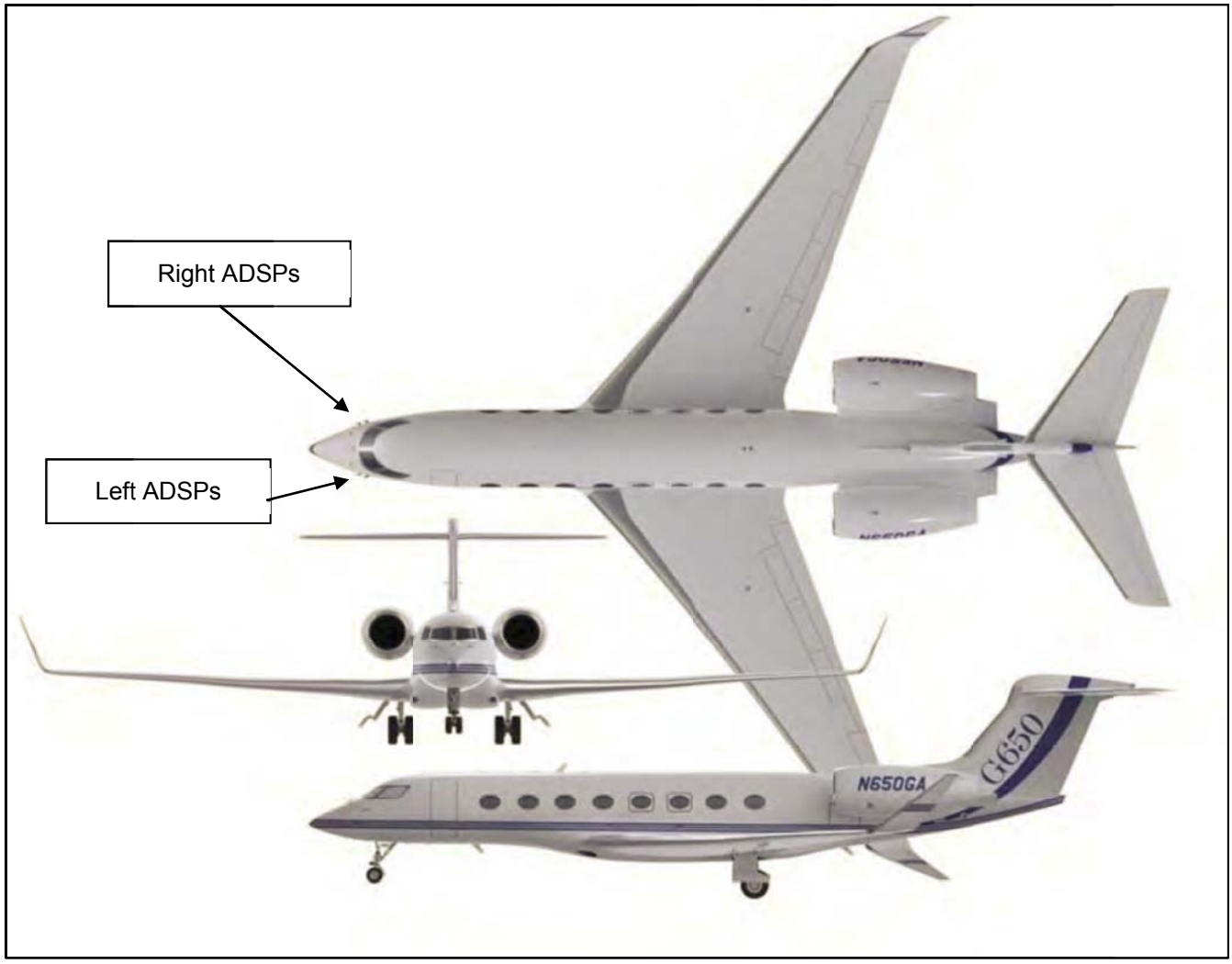

Figure 1. 3-view image of the Gulfstream G650 airplane (from Reference 7).

DCA11MA076: GAC G650, N652GD, Roswell, NM, 04/02/2011
Plan view of aircraft trajectory and accident scene

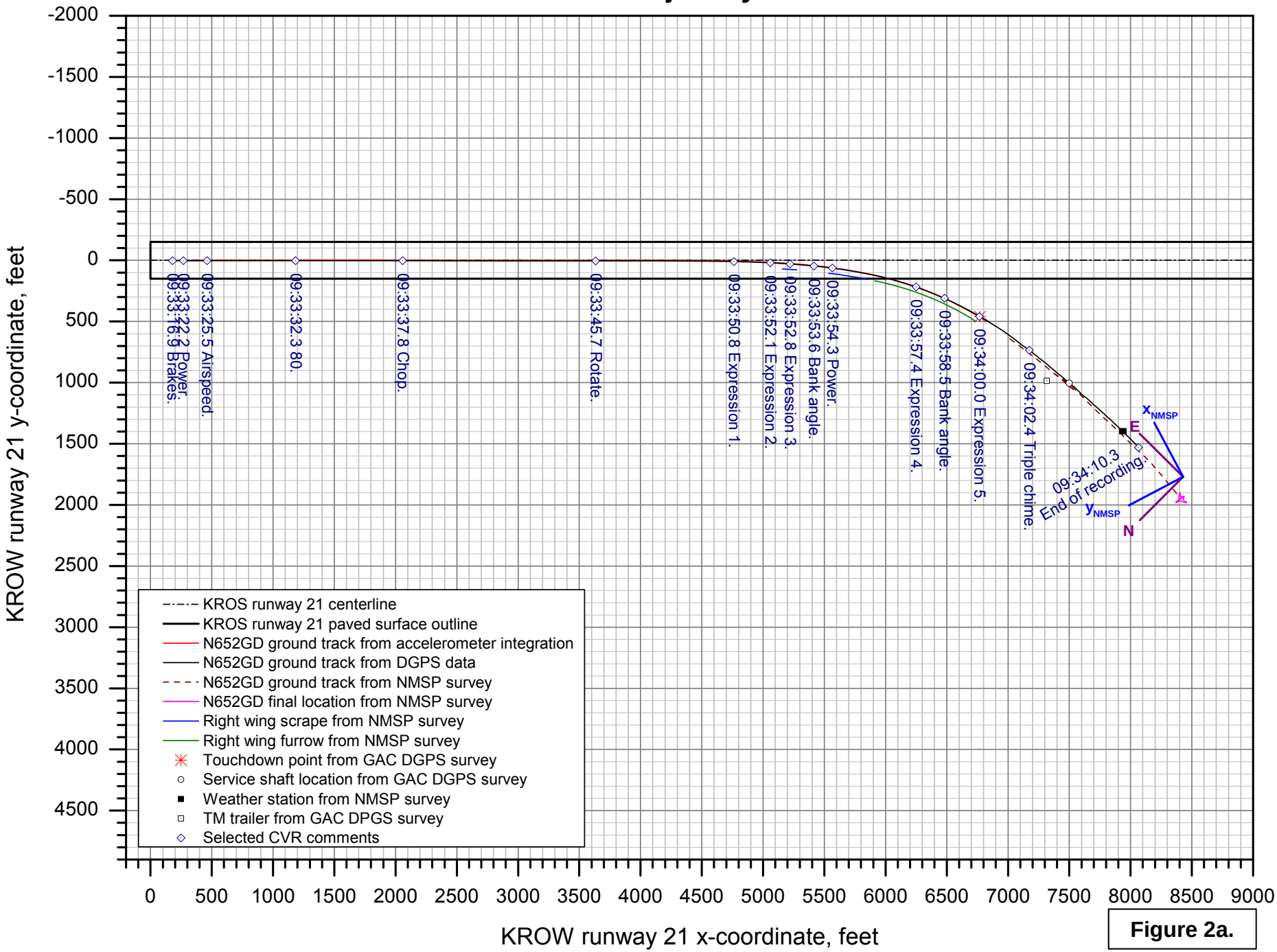

Figure 2a.

DCA11MA076: GAC G650, N652GD, Roswell, NM, 04/02/2011
Plan view of aircraft trajectory and accident scene

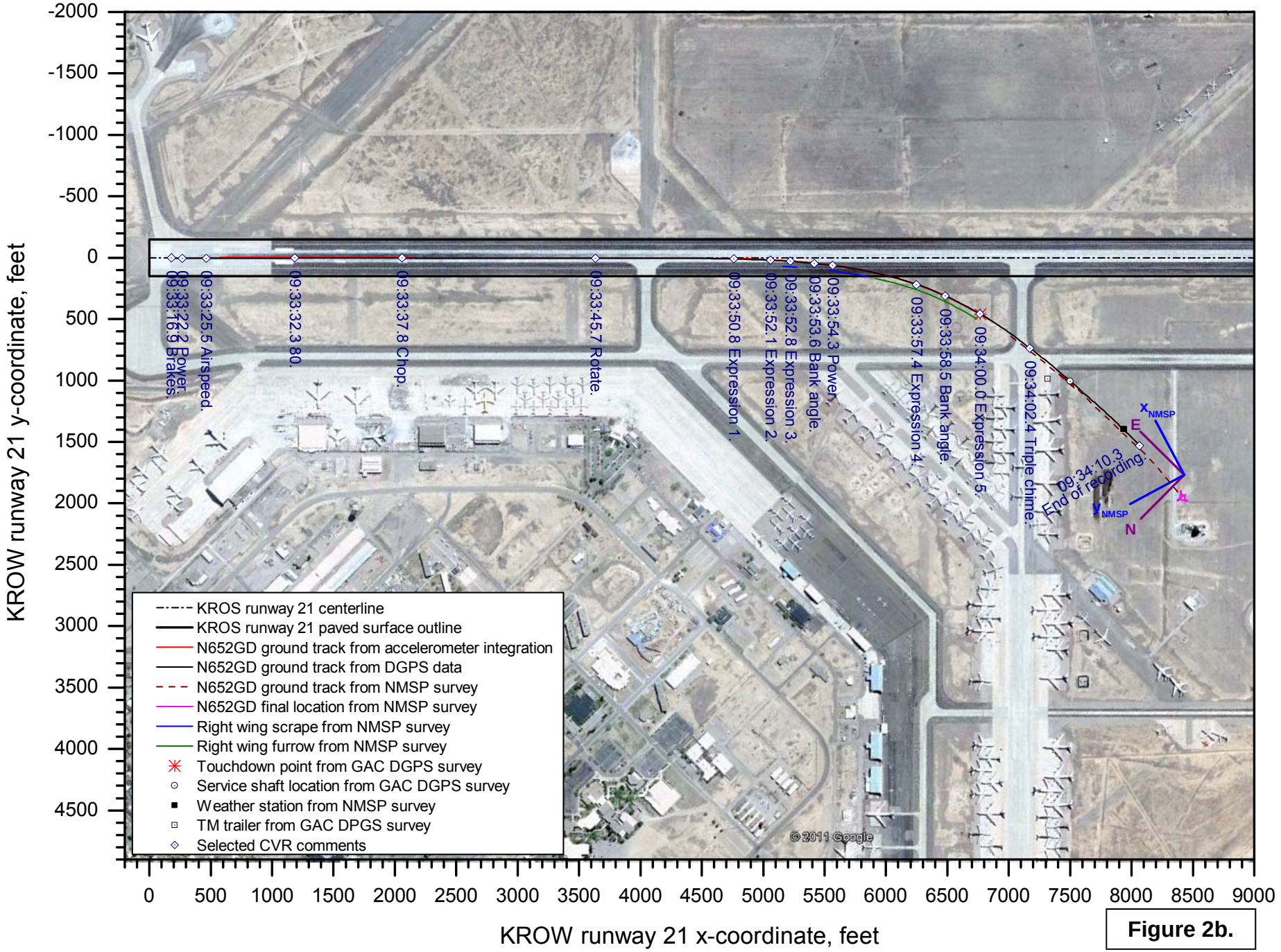

Figure 2b.

DCA11MA076: GAC G650, N652GD, Roswell, NM, 04/02/2011
Ground track vs. time

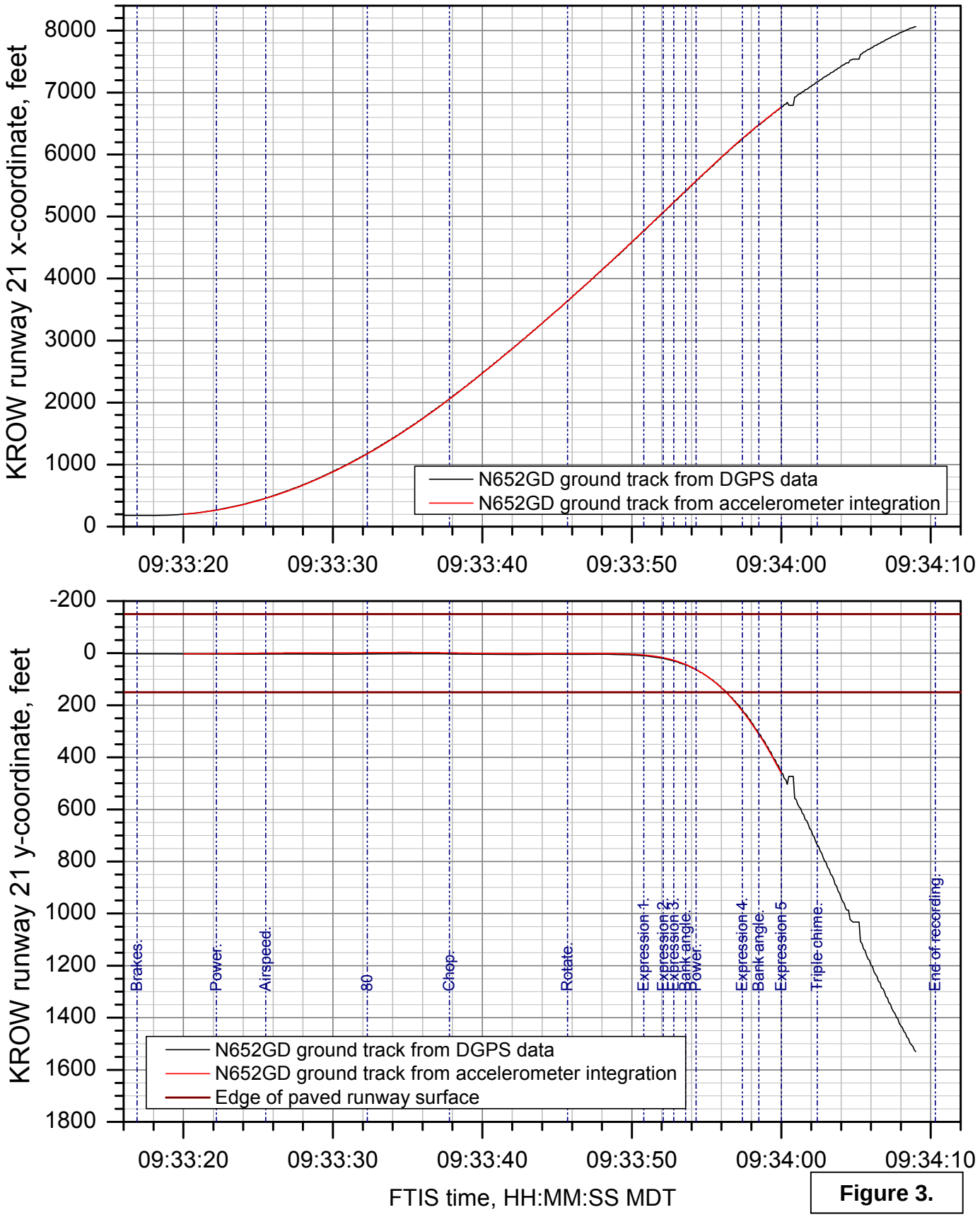

Figure 3.

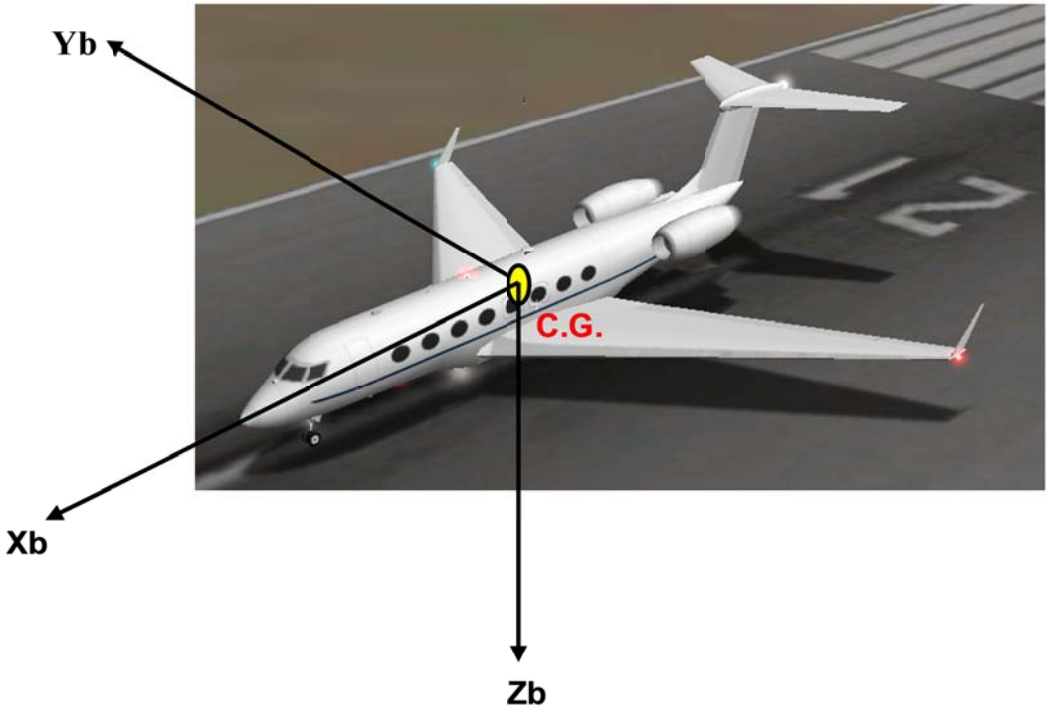

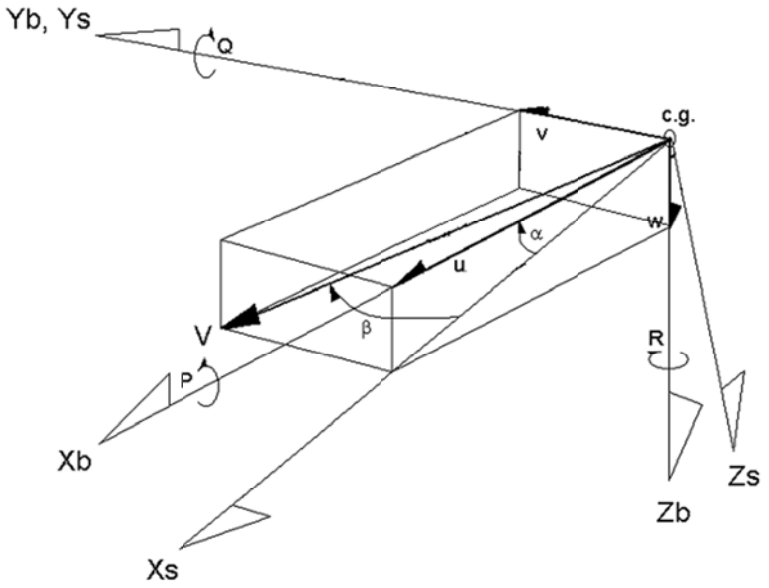

C.G. = center of gravity

{Xb, Yb, Zb} = body axis system

{Xs, Ys, Zs} = stability axis system

V = velocity vector

α = angle of attack

β = sideslip angle

P = body axis roll rate

Q = body axis pitch rate

R = body axis yaw rate

u = component of V along Xb

v = component of V along Yb

w = component of V along Zb

Figure 4.

DCA11MA076: GAC G650, N652GD, Roswell, NM, 04/02/2011
Profile view of aircraft trajectory

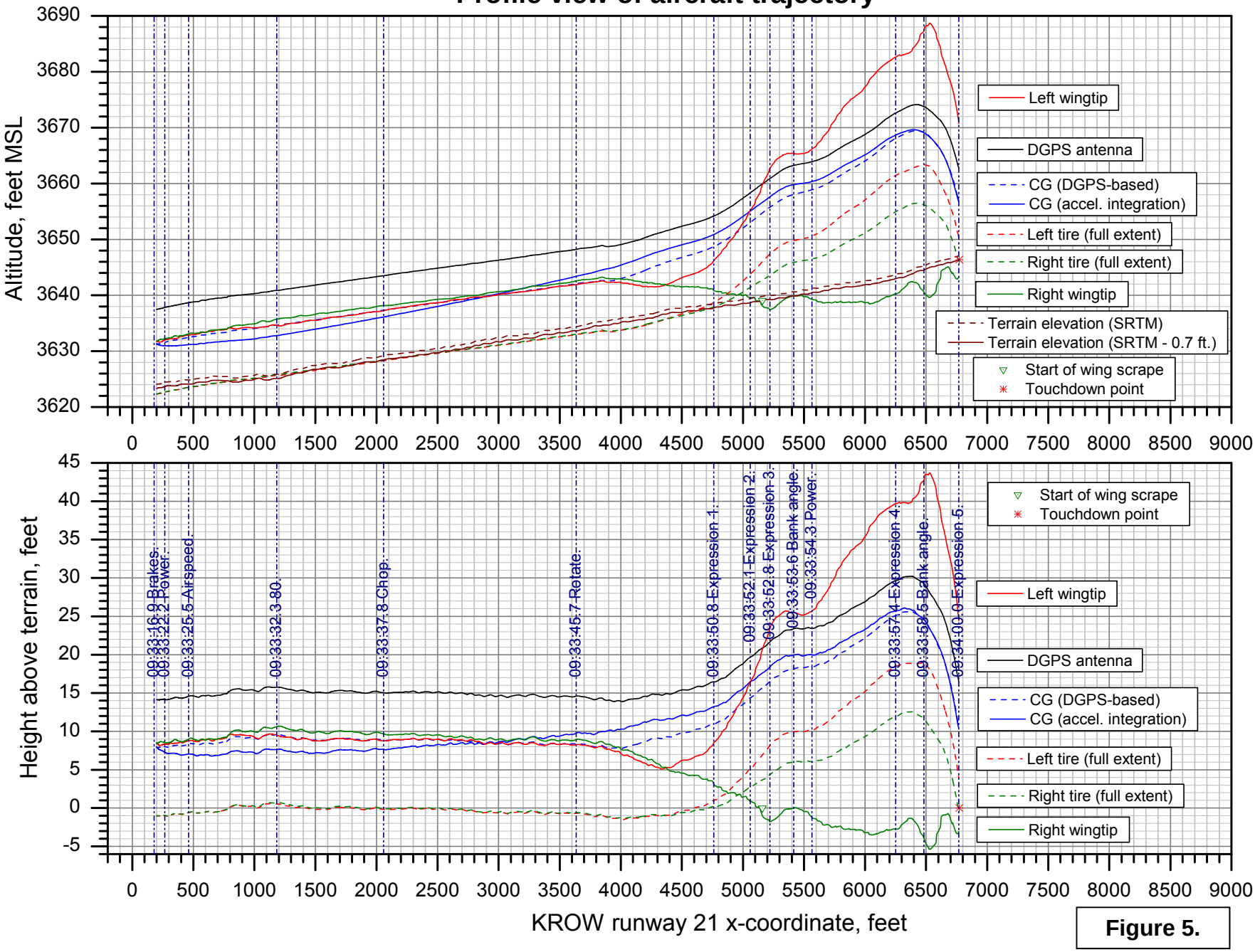

Figure 5.

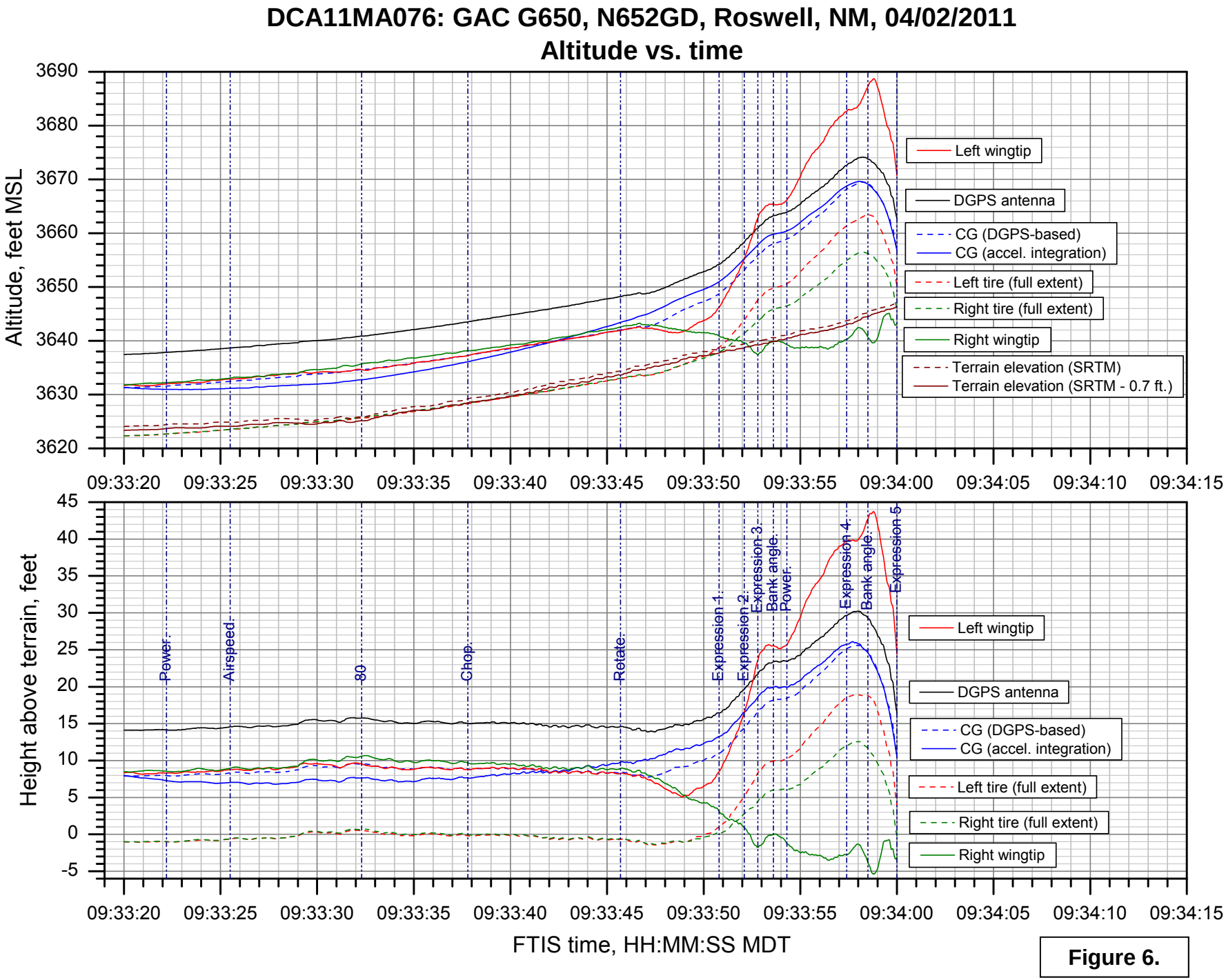
DCA11MA076: GAC G650, N652GD, Roswell, NM, 04/02/2011
Altitude vs. time
Altitude, feet MSL
3690
3680
3670
3660
3650
3640
3630
3620
Left wingtip
DGPS antenna
CG (DGPS-based)
CG (accel. integration)
Left tire (full extent)
Right tire (full extent)
Right wingtip
Terrain elevation (SRTM)
Terrain elevation (SRTM - 0.7 ft.)
09:33:20
09:33:25
09:33:30
09:33:35
09:33:40
09:33:45
09:33:50
09:33:55
09:34:00
09:34:05
09:34:10
09:34:15
Height above terrain, feet
45
40
35
30
25
20
15
10
5
0
-5
Power.
Airspeed.
80.
Chop.
Rotate.
Expression 1.
Expression 2.
Expression 3.
Bank angle.
Power.
Expression 4.
Bank angle.
Expression 5
Left wingtip
DGPS antenna
CG (DGPS-based)
CG (accel. integration)
Left tire (full extent)
Right tire (full extent)
Right wingtip
09:33:20
09:33:25
09:33:30
09:33:35
09:33:40
09:33:45
09:33:50
09:33:55
09:34:00
09:34:05
09:34:10
09:34:15
FTIS time, HH:MM:SS MDT

Figure 6.

DCA11MA076: GAC G650, N652GD, Roswell, NM, 04/02/2011
FTIS & computed airspeed and Mach number

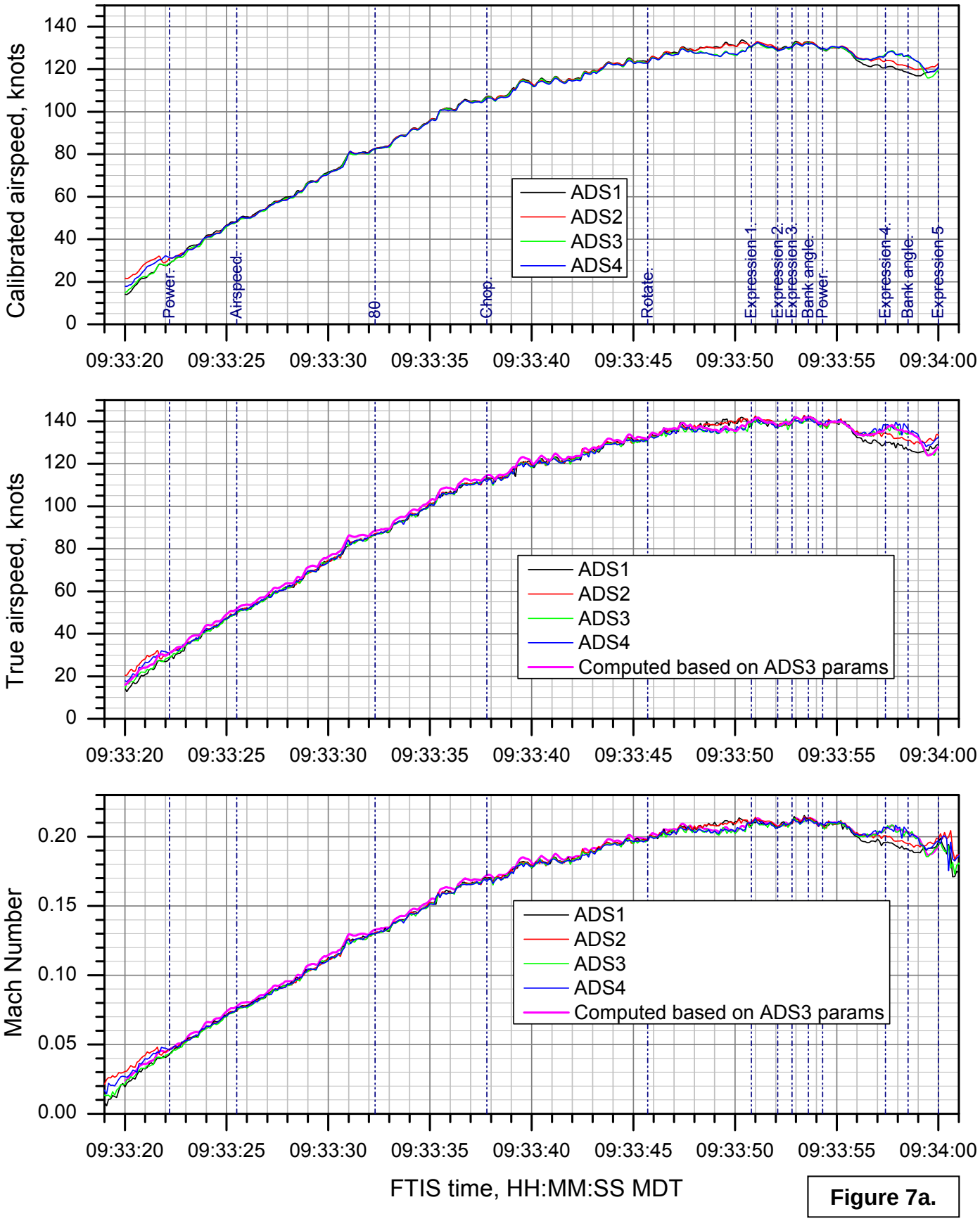

Figure 7a.

DCA11MA076: GAC G650, N652GD, Roswell, NM, 04/02/2011
FTIS & computed airspeed and Mach number (detail)

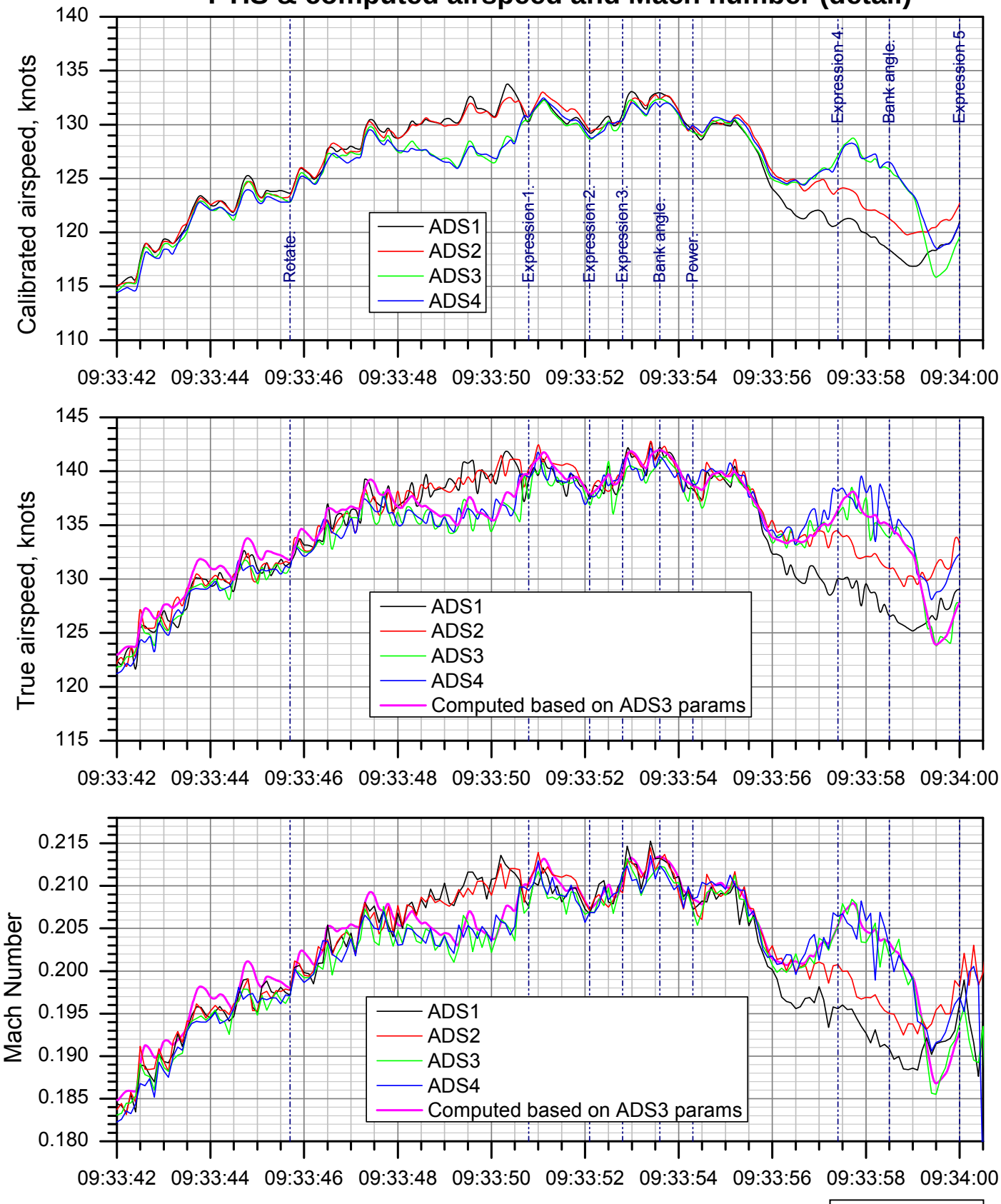

Figure 7b.

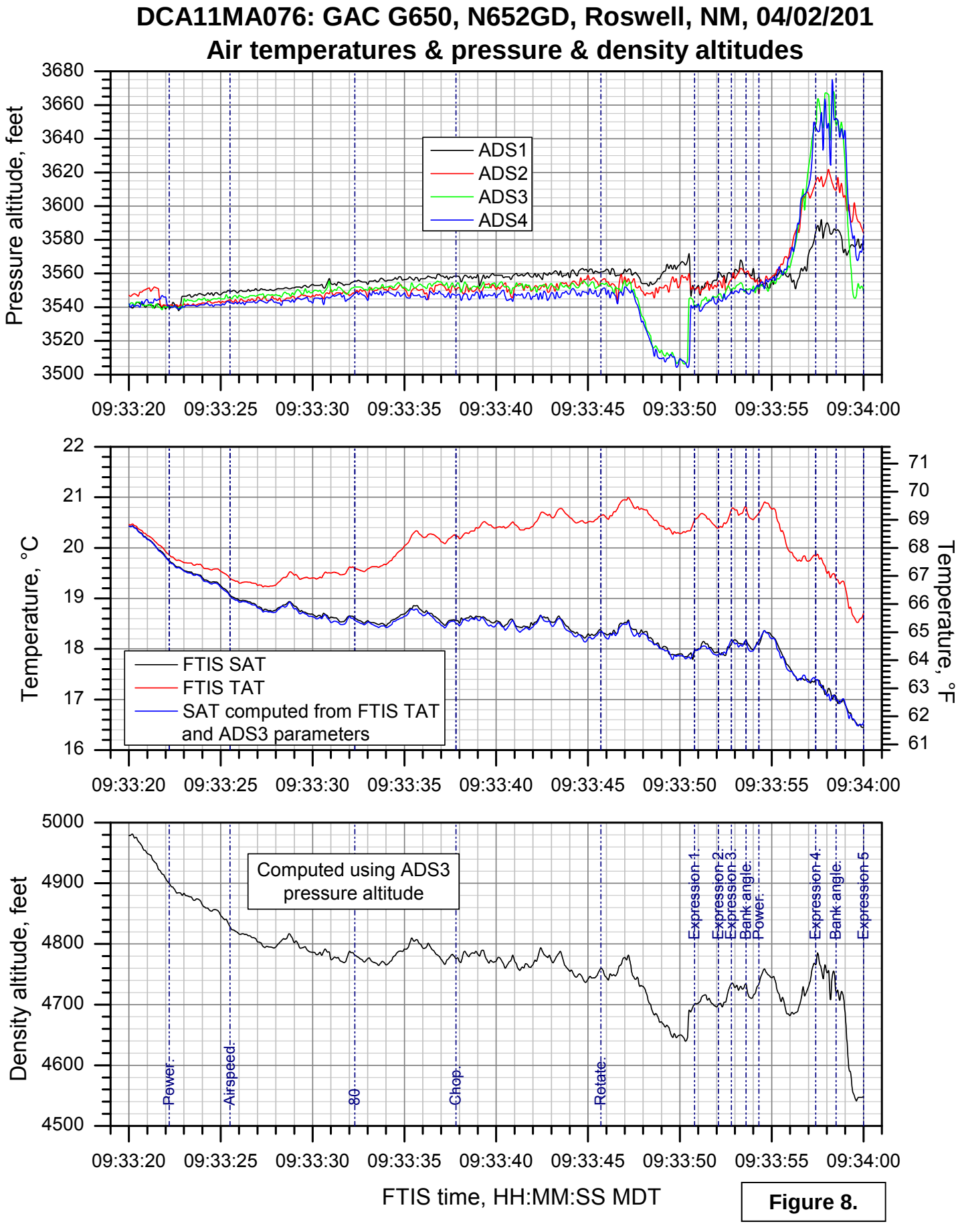
DCA11MA076: GAC G650, N652GD, Roswell, NM, 04/02/201
Air temperatures & pressure & density altitudes
Pressure altitude, feet
ADS1
ADS2
ADS3
ADS4
Temperature, °C
Temperature, °F
FTIS SAT
FTIS TAT
SAT computed from FTIS TAT and ADS3 parameters
Density altitude, feet
Computed using ADS3 pressure altitude
Power
Airspeed
80
Chop
Rotate
Expression 1
Expression 2
Expression 3
Bank angle
Power
Expression 4
Bank angle
Expression 5
FTIS time, HH:MM:SS MDT

Figure 8.

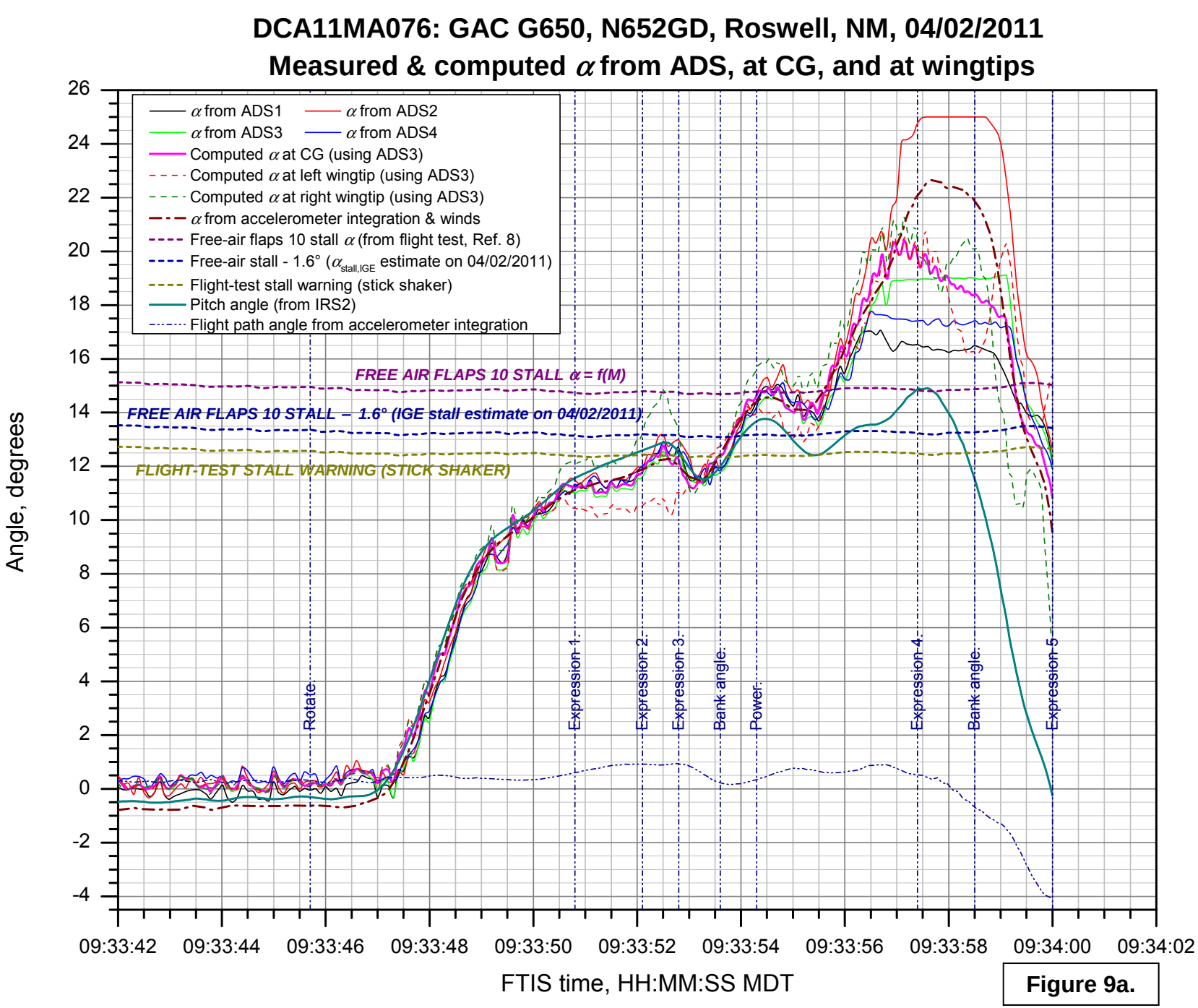
DCA11MA076: GAC G650, N652GD, Roswell, NM, 04/02/2011
Measured & computed α from ADS, at CG, and at wingtips
α from ADS1
α from ADS2
α from ADS3
α from ADS4
Computed α at CG (using ADS3)
Computed α at left wingtip (using ADS3)
Computed α at right wingtip (using ADS3)
α from accelerometer integration & winds
Free-air flaps 10 stall α (from flight test, Ref. 8)
Free-air stall - 1.6° (α stall,IGE estimate on 04/02/2011)
Flight-test stall warning (stick shaker)
Pitch angle (from IRS2)
Flight path angle from accelerometer integration
FREE AIR FLAPS 10 STALL α = f(M)
FREE AIR FLAPS 10 STALL – 1.6° (IGE stall estimate on 04/02/2011)
FLIGHT-TEST STALL WARNING (STICK SHAKER)
Rotate
Expression 1.
Expression 2.
Expression 3.
Bank angle.
Power.
Expression 4.
Bank angle.
Expression 5.
Angle, degrees
26
24
22
20
18
16
14
12
10
8
6
4
2
0
-2
-4
09:33:42
09:33:44
09:33:46
09:33:48
09:33:50
09:33:52
09:33:54
09:33:56
09:33:58
09:34:00
09:34:02
FTIS time, HH:MM:SS MDT

Figure 9a.

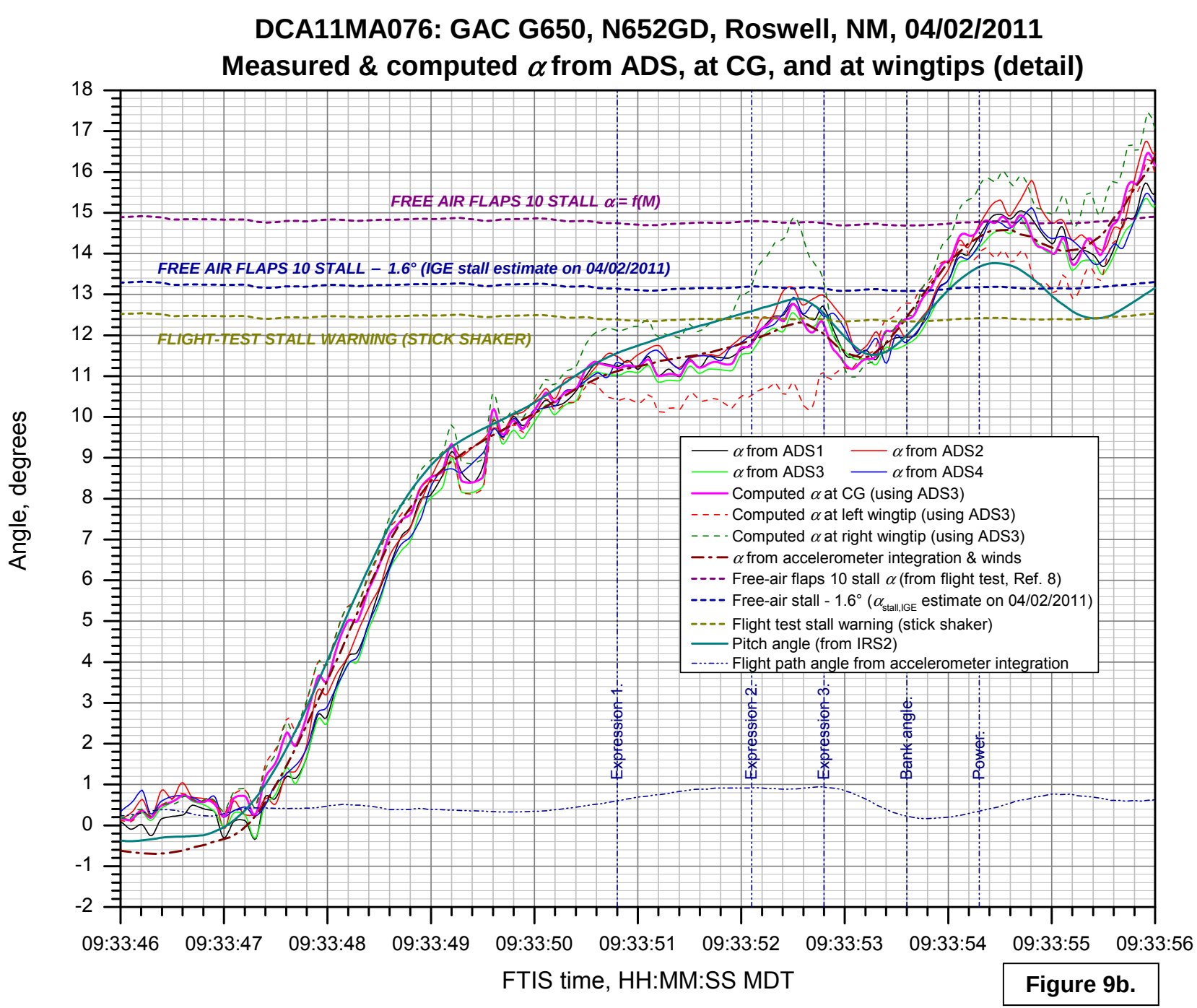
DCA11MA076: GAC G650, N652GD, Roswell, NM, 04/02/2011
Measured & computed α from ADS, at CG, and at wingtips (detail)
FREE AIR FLAPS 10 STALL α = f(M)
FREE AIR FLAPS 10 STALL – 1.6° (IGE stall estimate on 04/02/2011)
FLIGHT-TEST STALL WARNING (STICK SHAKER)
α from ADS1
α from ADS2
α from ADS3
α from ADS4
Computed α at CG (using ADS3)
Computed α at left wingtip (using ADS3)
Computed α at right wingtip (using ADS3)
α from accelerometer integration & winds
Free-air flaps 10 stall α (from flight test, Ref. 8)
Free-air stall - 1.6° (α stall,IGE estimate on 04/02/2011)
Flight test stall warning (stick shaker)
Pitch angle (from IRS2)
Flight path angle from accelerometer integration
Expression 1.
Expression 2.
Expression 3.
Bank angle.
Power.
Angle, degrees
18
17
16
15
14
13
12
11
10
9
8
7
6
5
4
3
2
1
0
-1
-2
09:33:46
09:33:47
09:33:48
09:33:49
09:33:50
09:33:51
09:33:52
09:33:53
09:33:54
09:33:55
09:33:56
FTIS time, HH:MM:SS MDT

Figure 9b.

DCA11MA076: GAC G650, N652GD, Roswell, NM, 04/02/2011
Ground speed and rate of climb

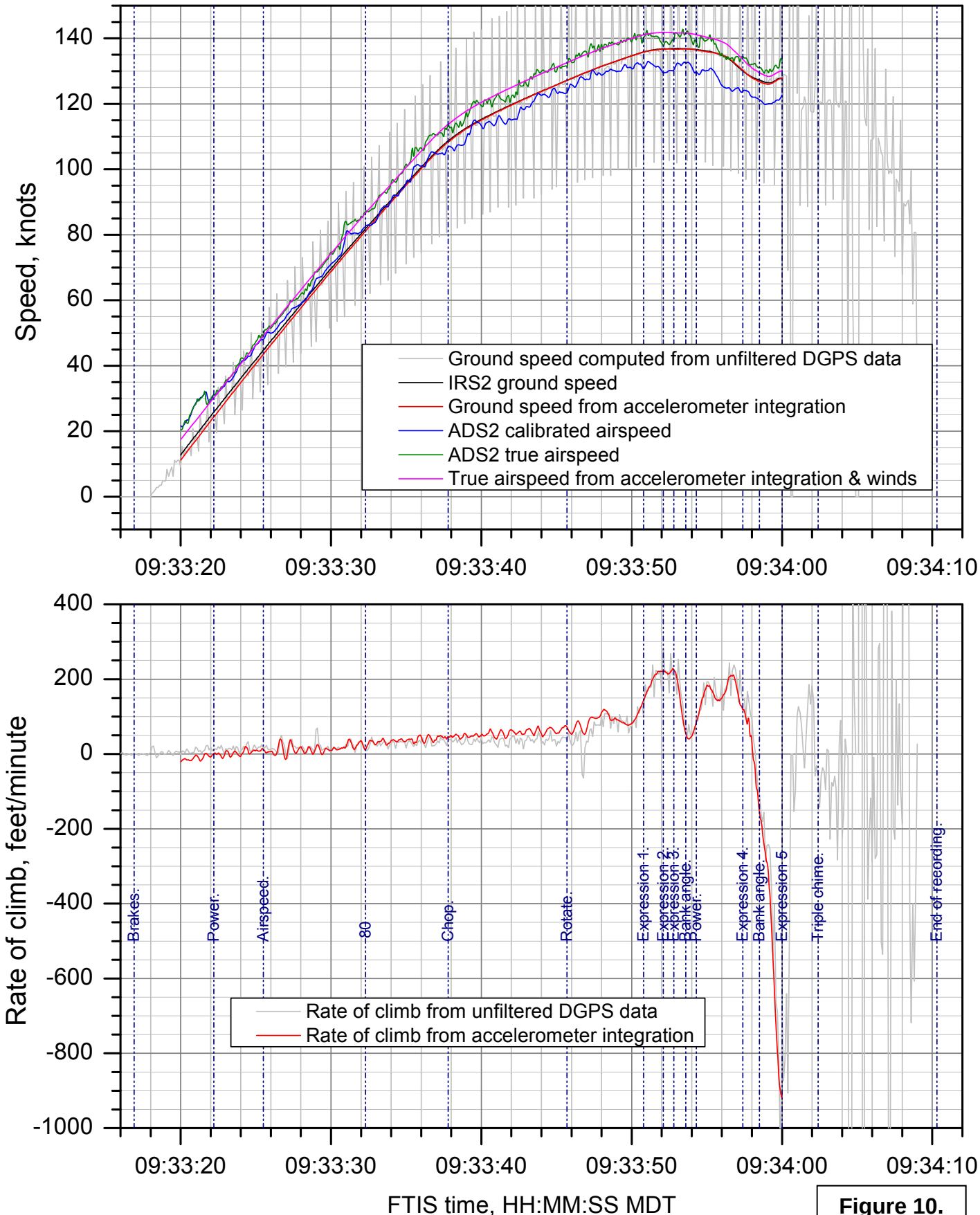

Figure 10.

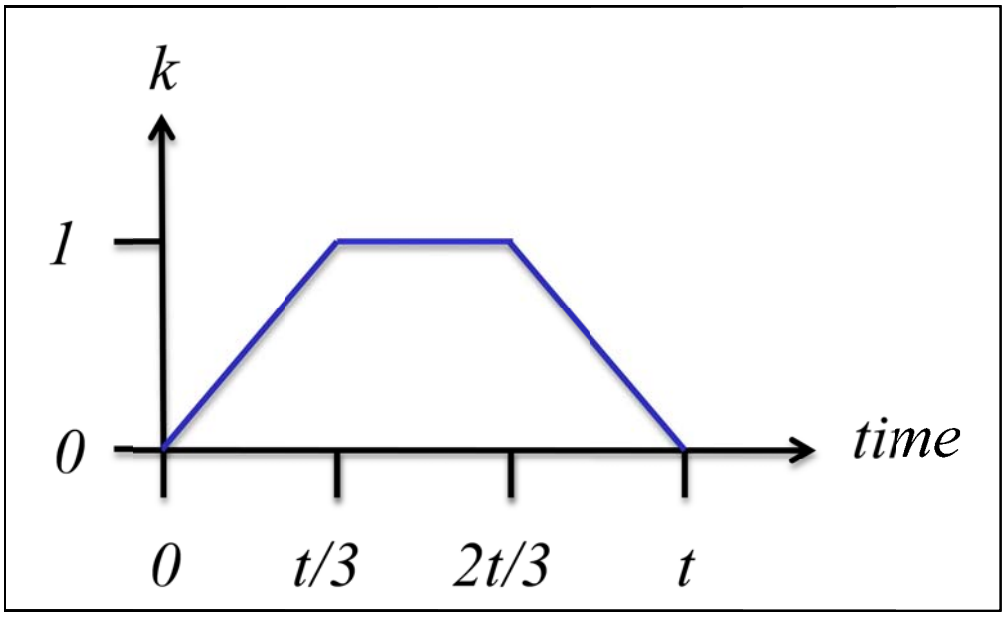

Figure 11. k – factor for velocity vector addition to velocity defined by FTIS groundspeed and track angle.

DCA11MA076: GAC G650, N652GD, Roswell, NM, 04/02/201
Load factors

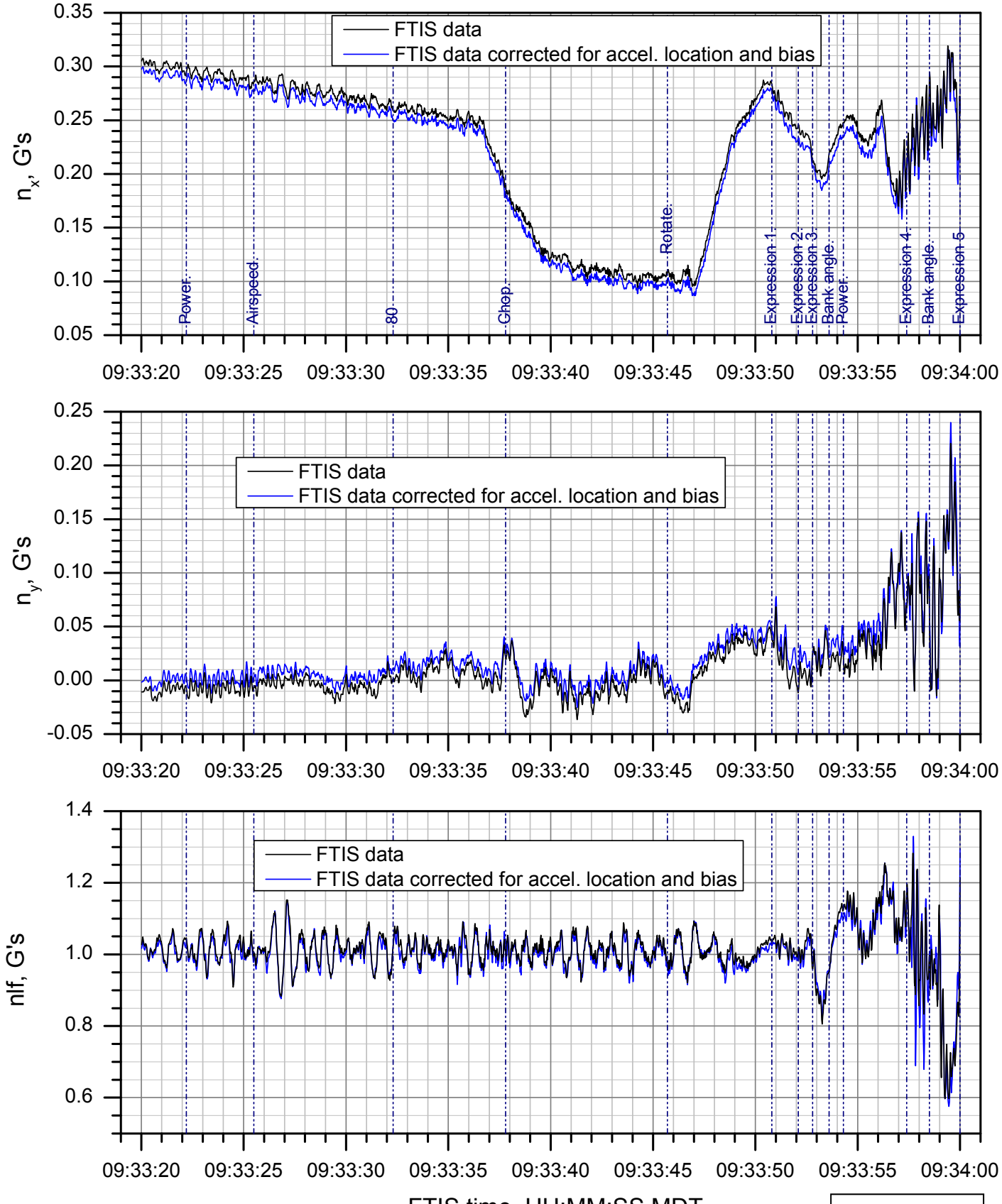

Figure 12.

DCA11MA076: GAC G650, N652GD, Roswell, NM, 04/02/2011
Wind data from GAC weather station

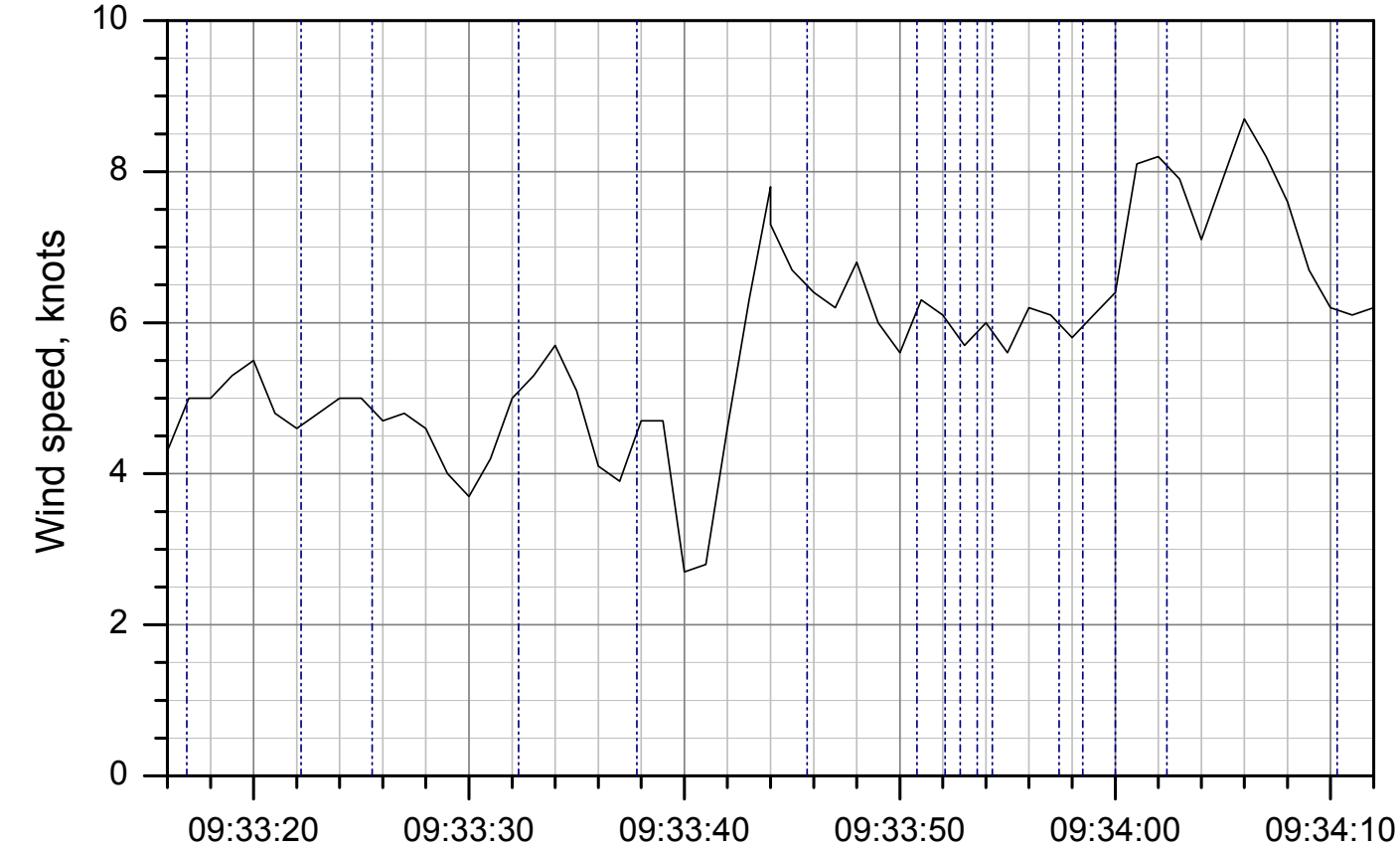

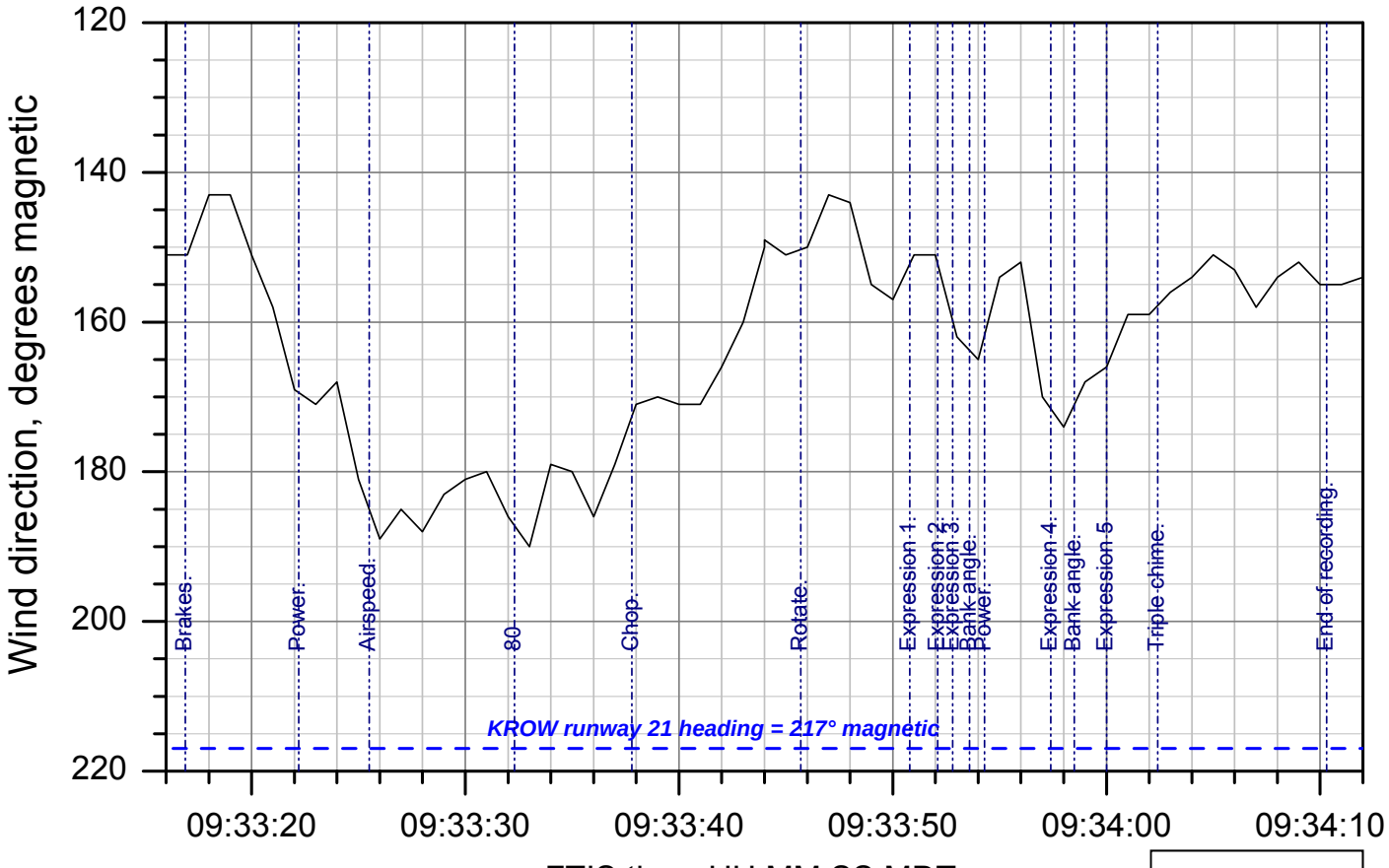

Figure 13.

DCA11MA076: GAC G650, N652GD, Roswell, NM, 04/02/2011
Lateral-directional angles

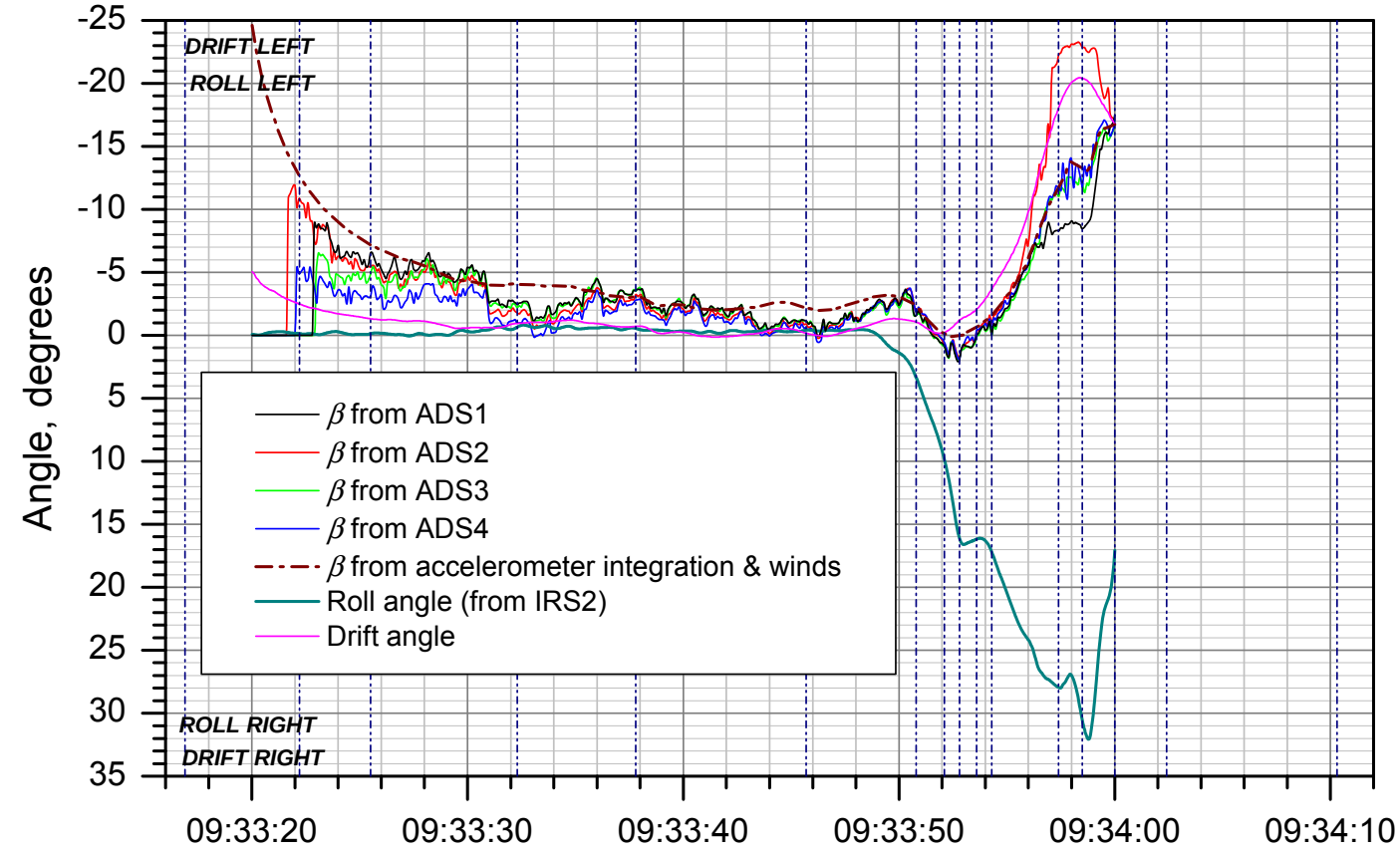

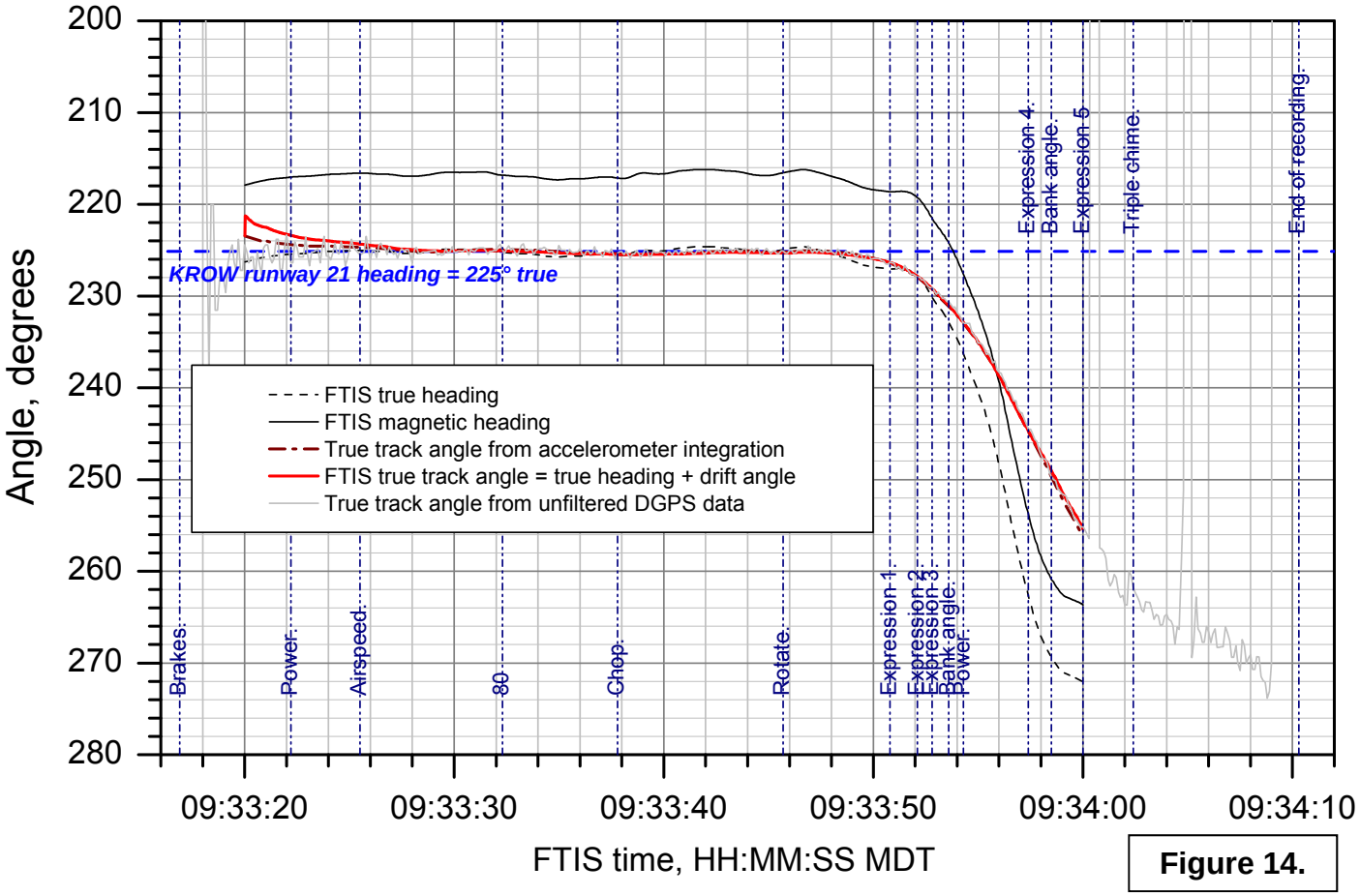

Figure 14.

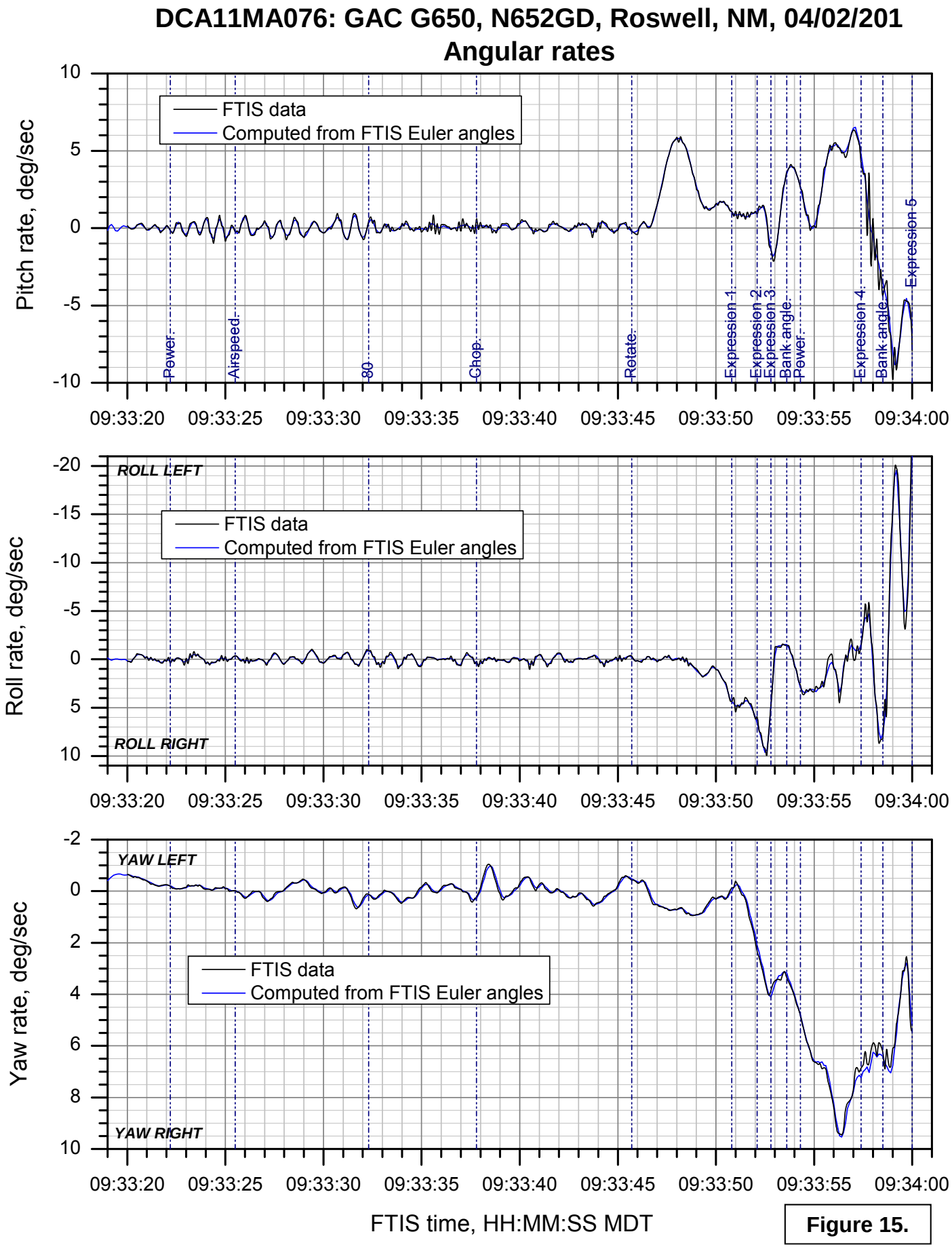
DCA11MA076: GAC G650, N652GD, Roswell, NM, 04/02/201
Angular rates
Pitch rate, deg/sec
Roll rate, deg/sec
Yaw rate, deg/sec
FTIS data
Computed from FTIS Euler angles
ROLL LEFT
ROLL RIGHT
YAW LEFT
YAW RIGHT
Power
Airspeed
80
Chop
Retate
Expression 1
Expression 2
Expression 3
Bank angle
Power
Expression 4
Bank angle
Expression 5
09:33:20
09:33:25
09:33:30
09:33:35
09:33:40
09:33:45
09:33:50
09:33:55
09:34:00
FTIS time, HH:MM:SS MDT

Figure 15.

DCA11MA076: GAC G650, N652GD, Roswell, NM, 04/02/201

Engine data

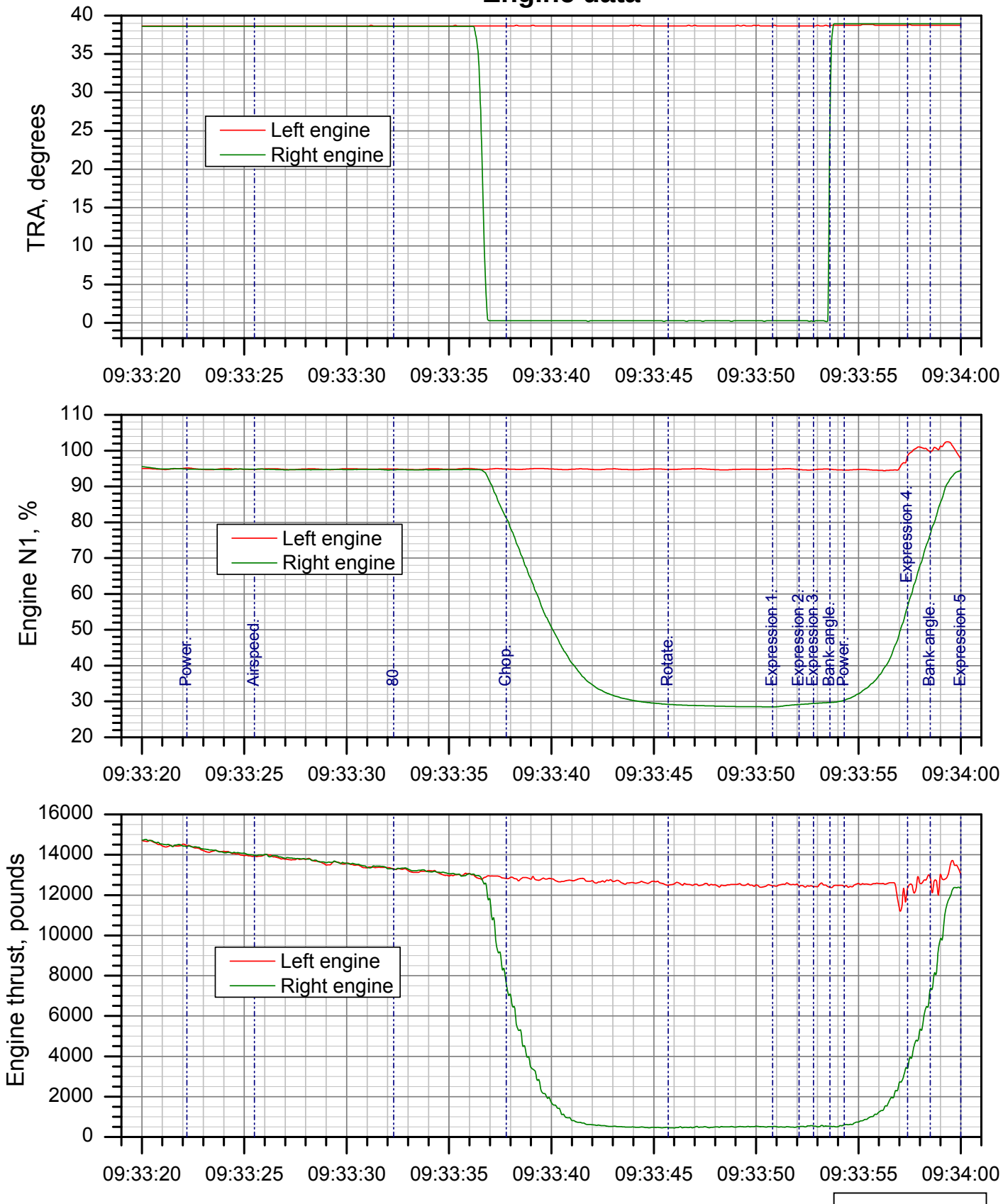

Figure 16.

DCA11MA076: GAC G650, N652GD, Roswell, NM, 04/02/201
Longitudinal controls

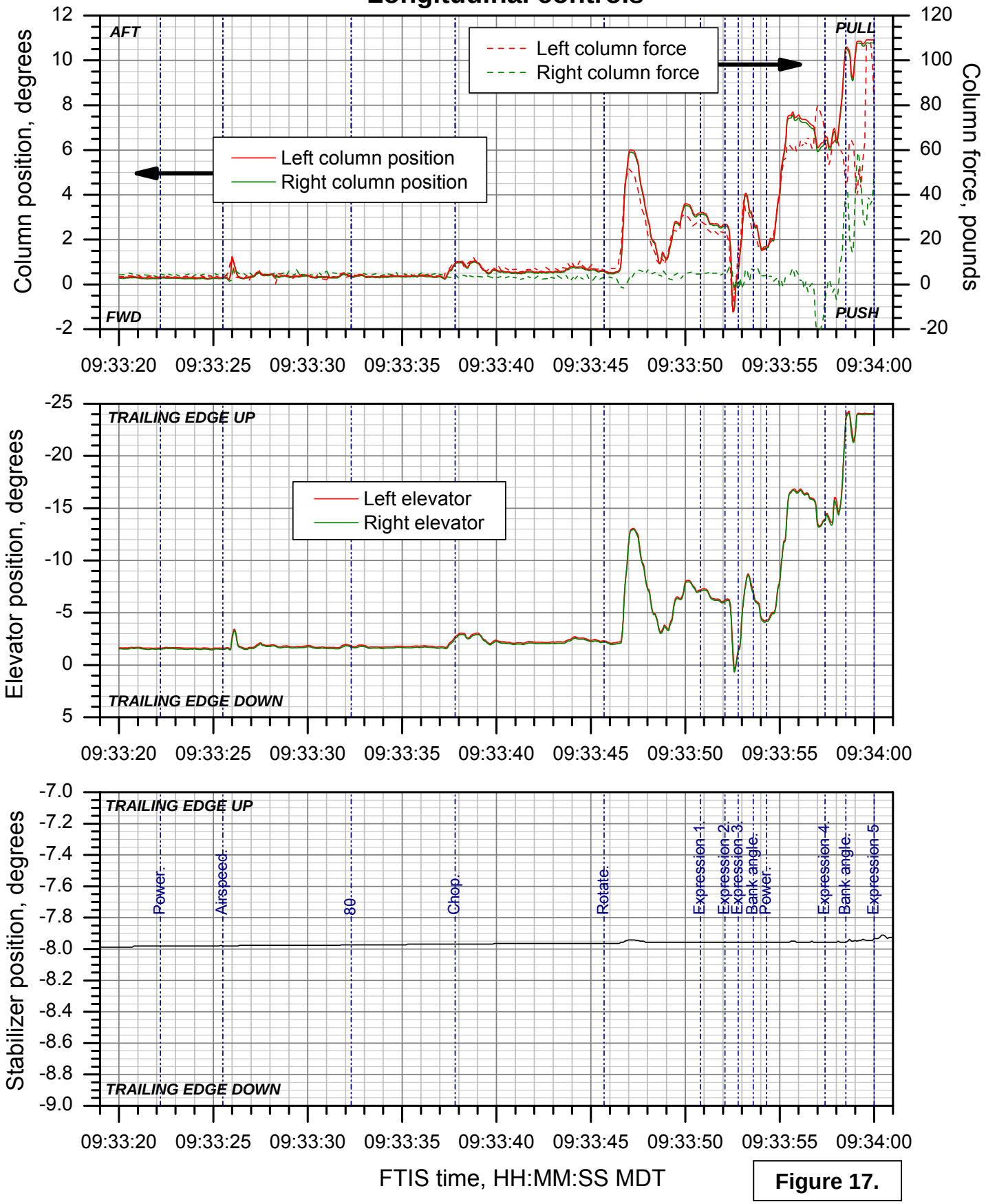

Figure 17.

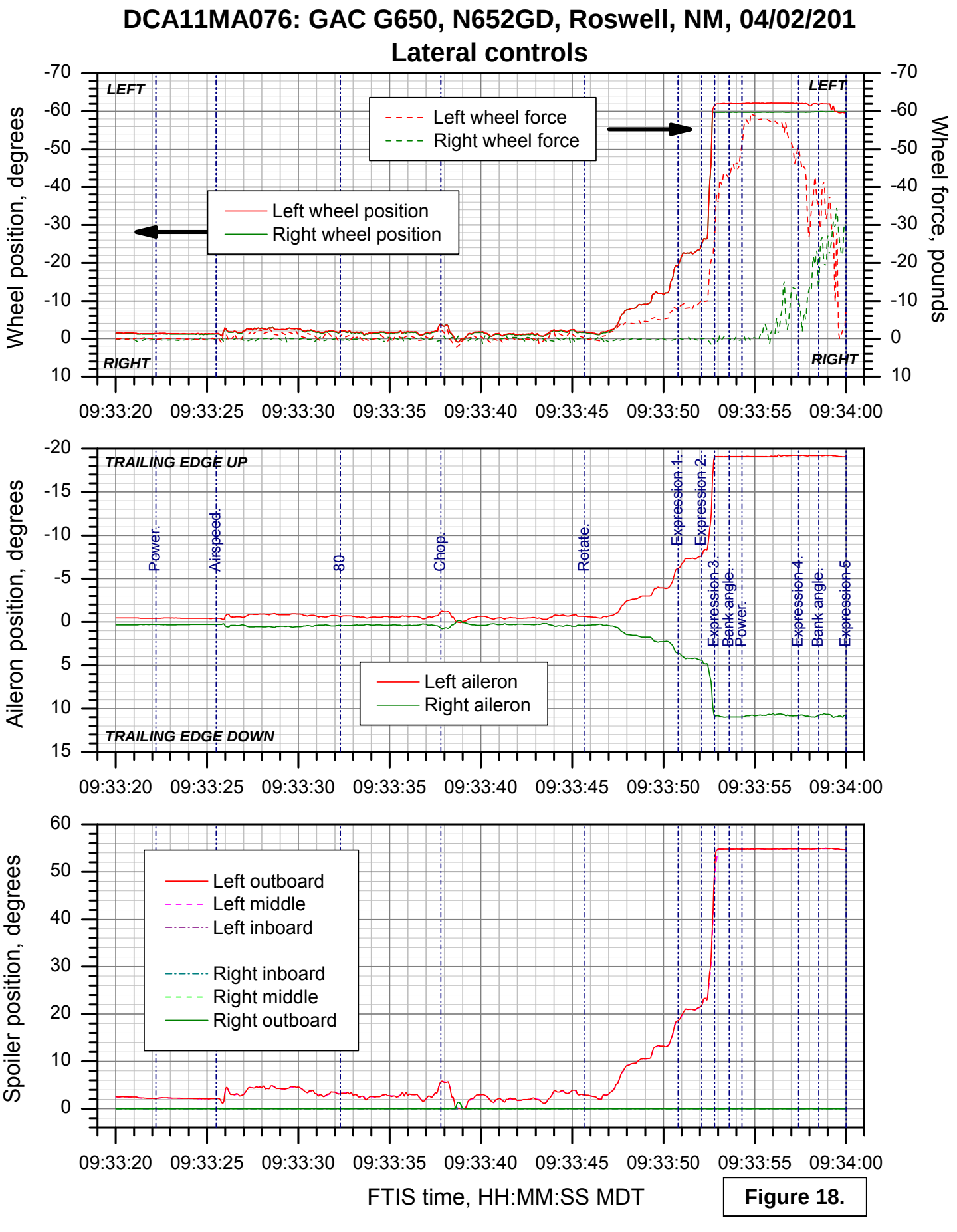
DCA11MA076: GAC G650, N652GD, Roswell, NM, 04/02/201
Lateral controls
Wheel position, degrees
Wheel force, pounds
LEFT
RIGHT
Left wheel force
Right wheel force
Left wheel position
Right wheel position
-70
-60
-50
-40
-30
-20
-10
0
10
09:33:20
09:33:25
09:33:30
09:33:35
09:33:40
09:33:45
09:33:50
09:33:55
09:34:00
Aileron position, degrees
TRAILING EDGE UP
TRAILING EDGE DOWN
Power.
Airspeed.
80.
Chop.
Rotate.
Expression 1.
Expression 2.
Expression 3.
Bank angle.
Power.
Expression 4.
Bank angle.
Expression 5.
Left aileron
Right aileron
-20
-15
-10
-5
0
5
10
15
Spoiler position, degrees
Left outboard
Left middle
Left inboard
Right inboard
Right middle
Right outboard
60
50
40
30
20
10
0
FTIS time, HH:MM:SS MDT

Figure 18.

DCA11MA076: GAC G650, N652GD, Roswell, NM, 04/02/201

Directional controls

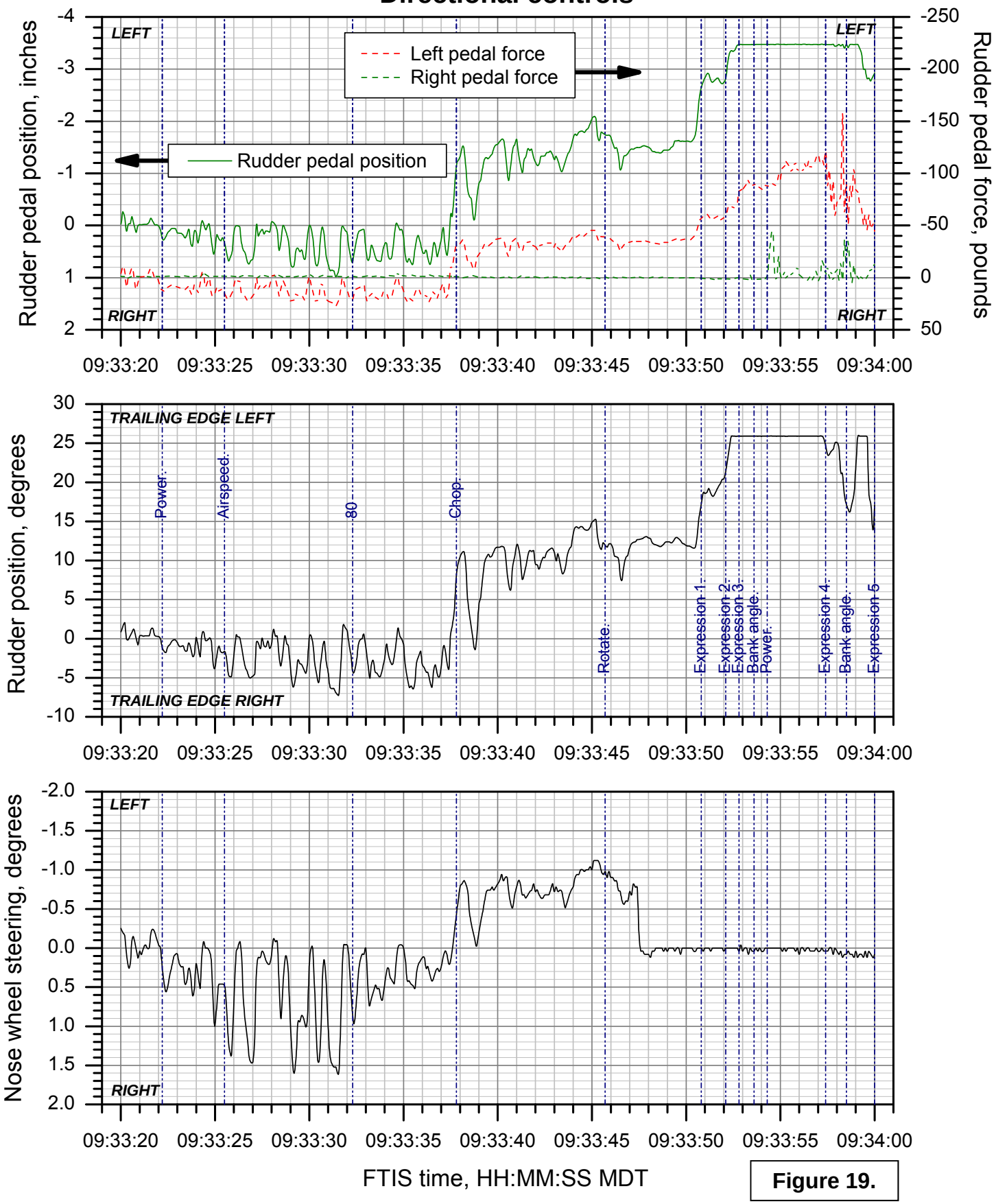

Figure 19.

Typical Baseline Simulation Logic/Data Flow.

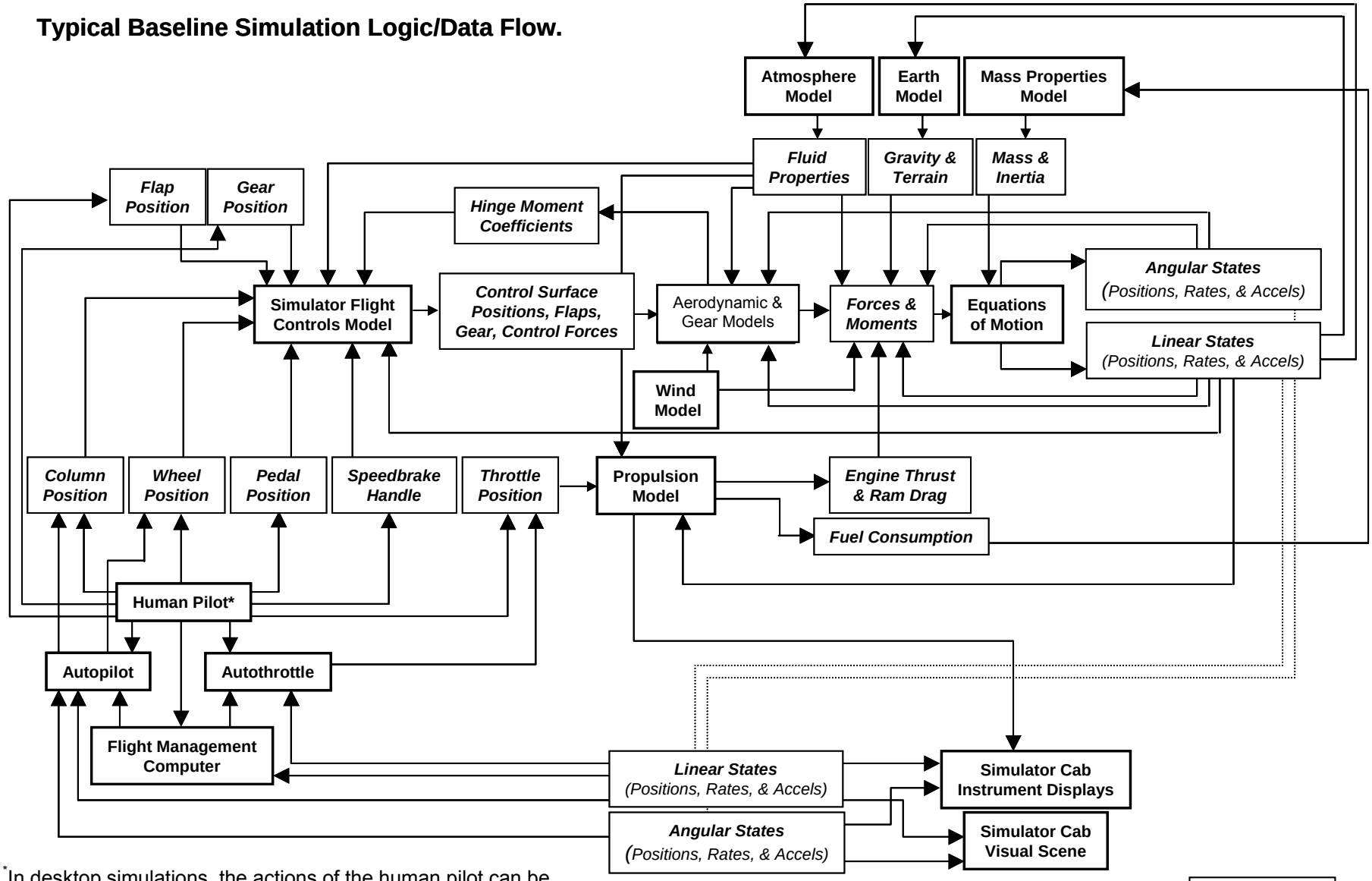

*In desktop simulations, the actions of the human pilot can be replaced by computer-based instructions.

Figure 20.

DCA11MA076: GAC G650, N652GD, Roswell, NM, 04/02/201
GAC simulation residual analysis results

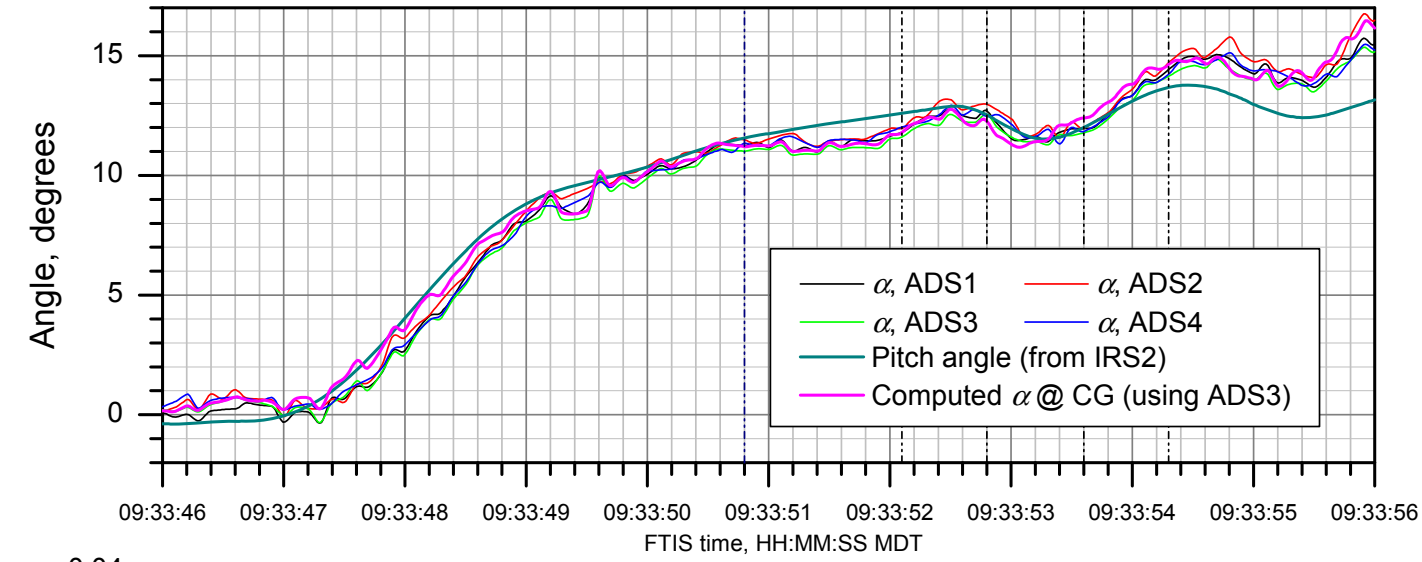

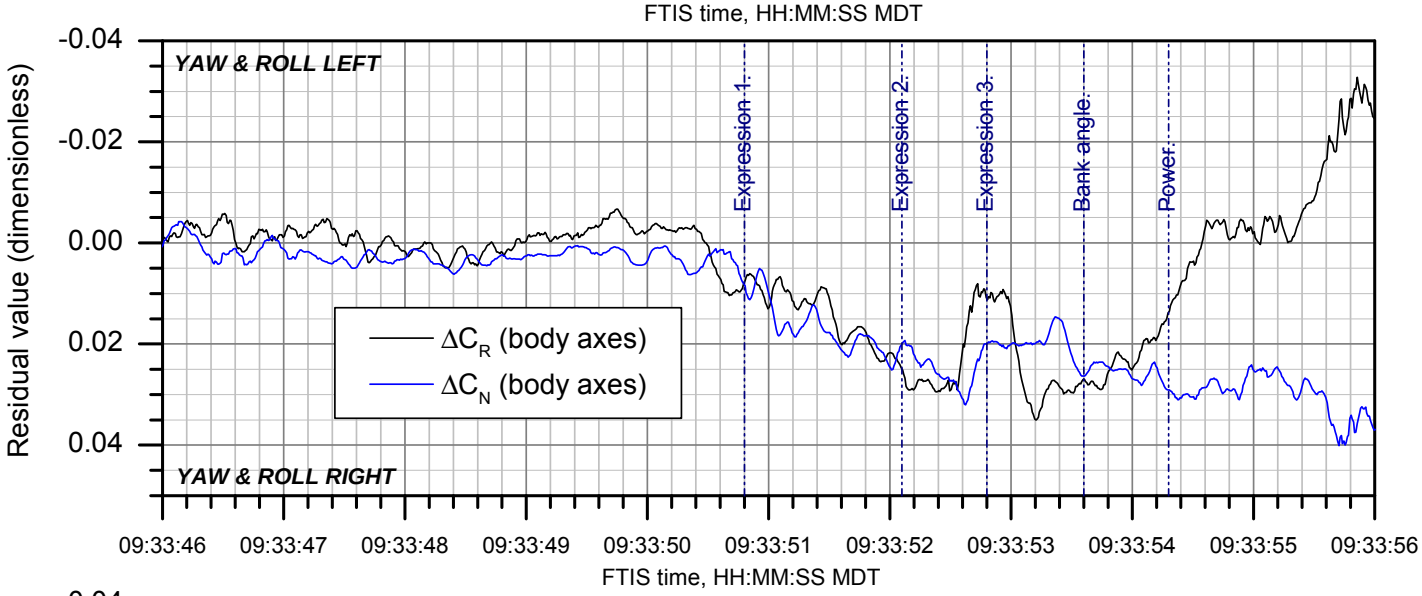

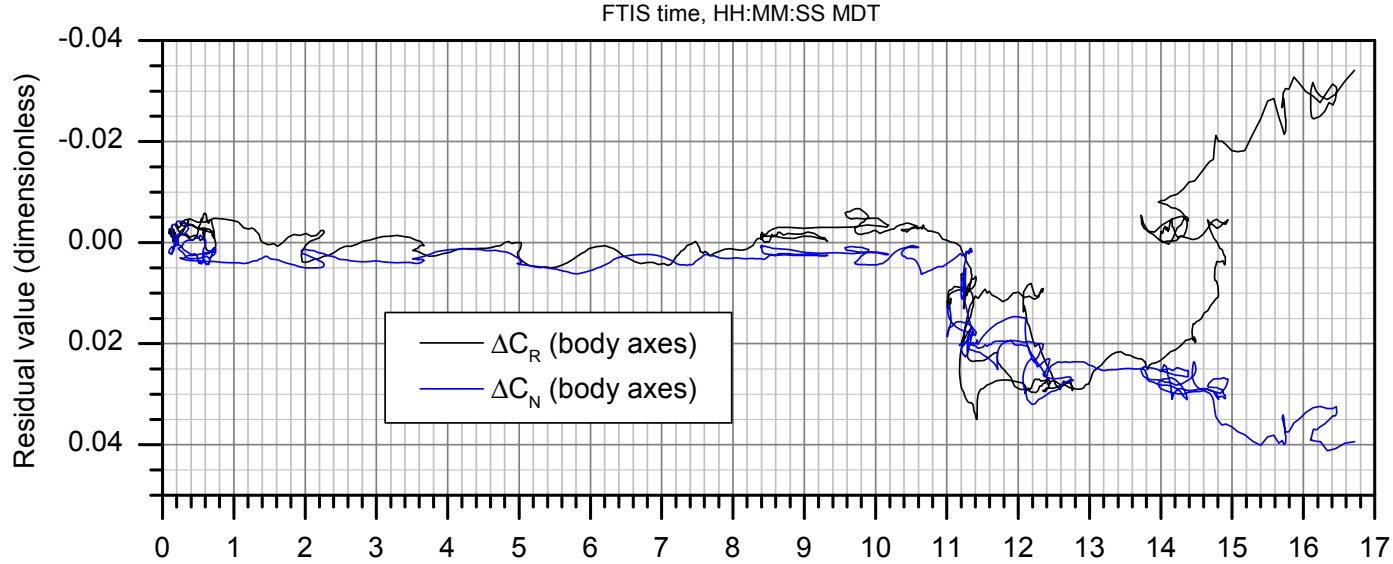

Figure 21.

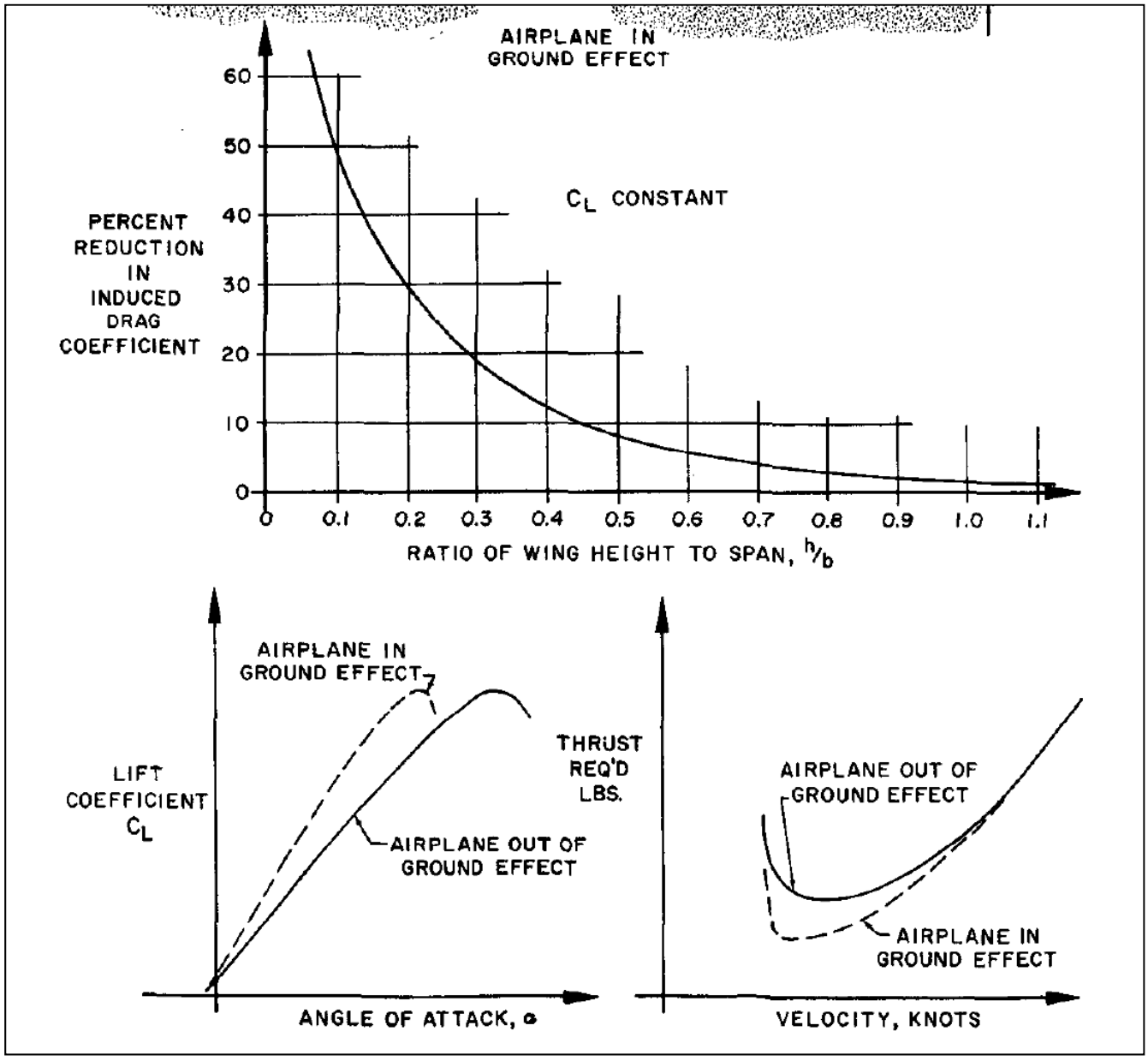

Figure 22. Ground effects on airplane aerodynamics (from Reference 15)

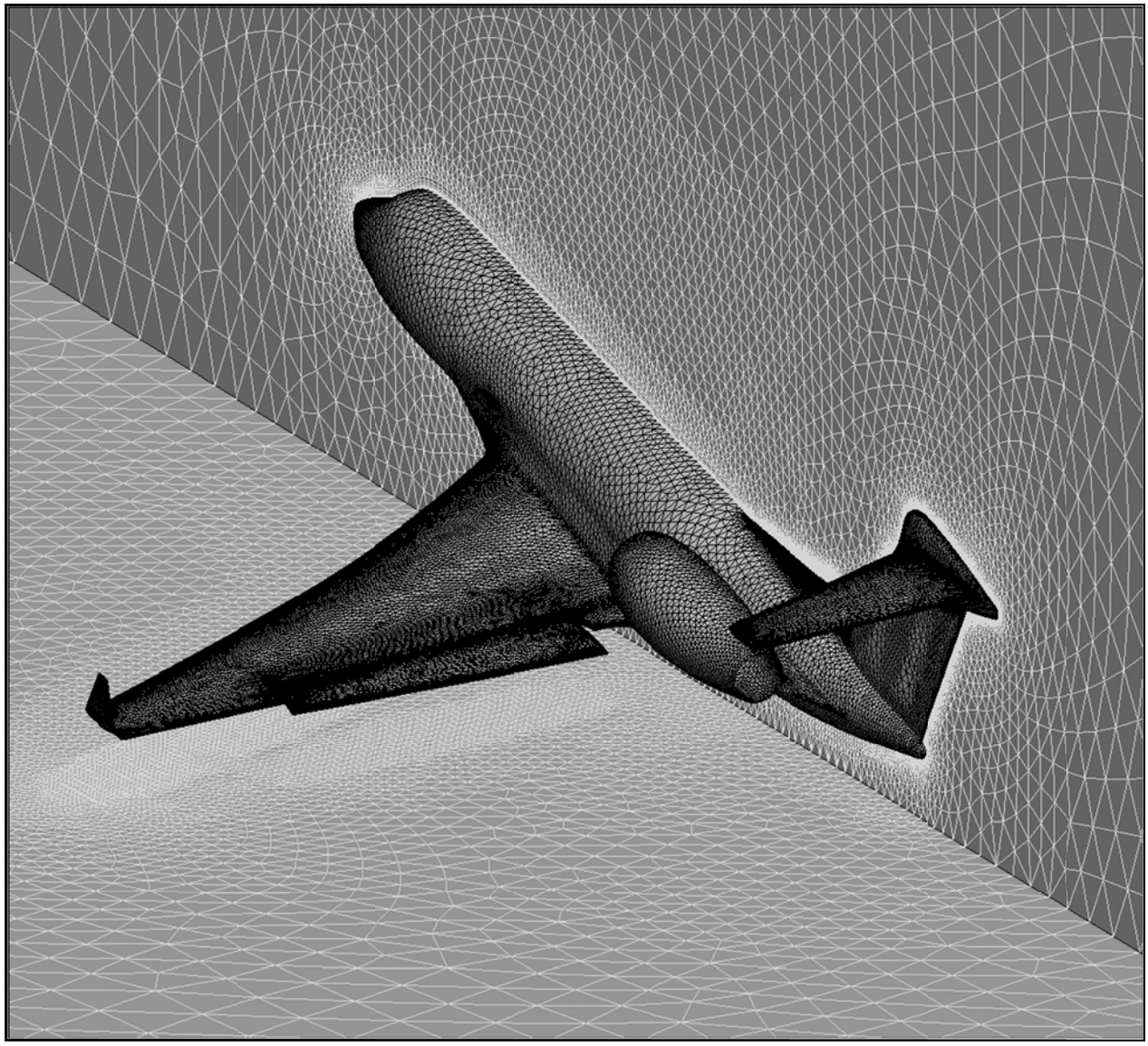

Figure 23. CFD surface grid used by GAC to define the G650 at flaps 10 and β = 0° with the gear on the ground and fully compressed (from Reference 20).

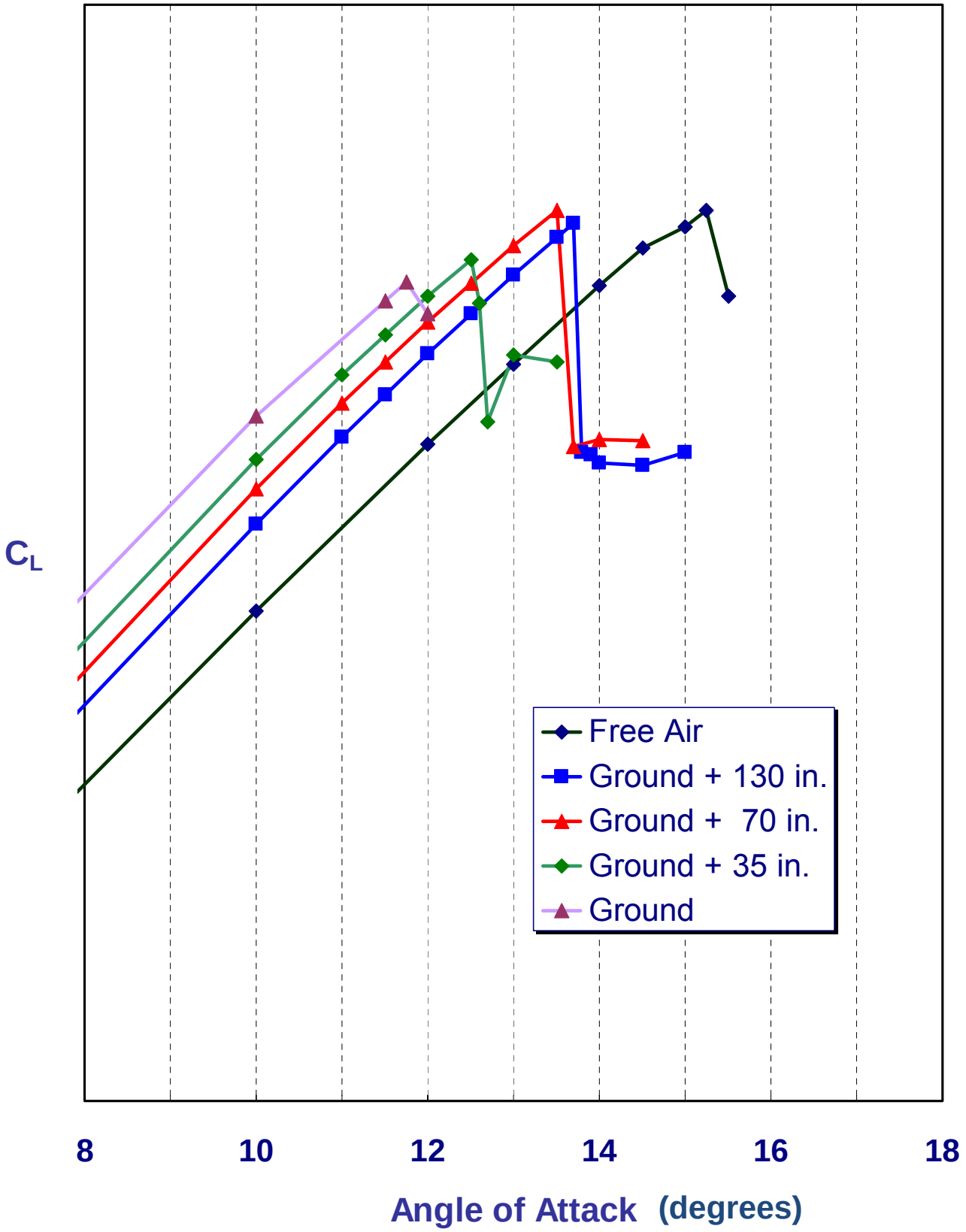

Figure 24. CFD solutions for flaps 10 C_L vs. α at various wheel heights (from Reference 20).

DCA11MA076: GAC G650, N652GD, Roswell, NM, 04/02/201
GAC CFD analysis results

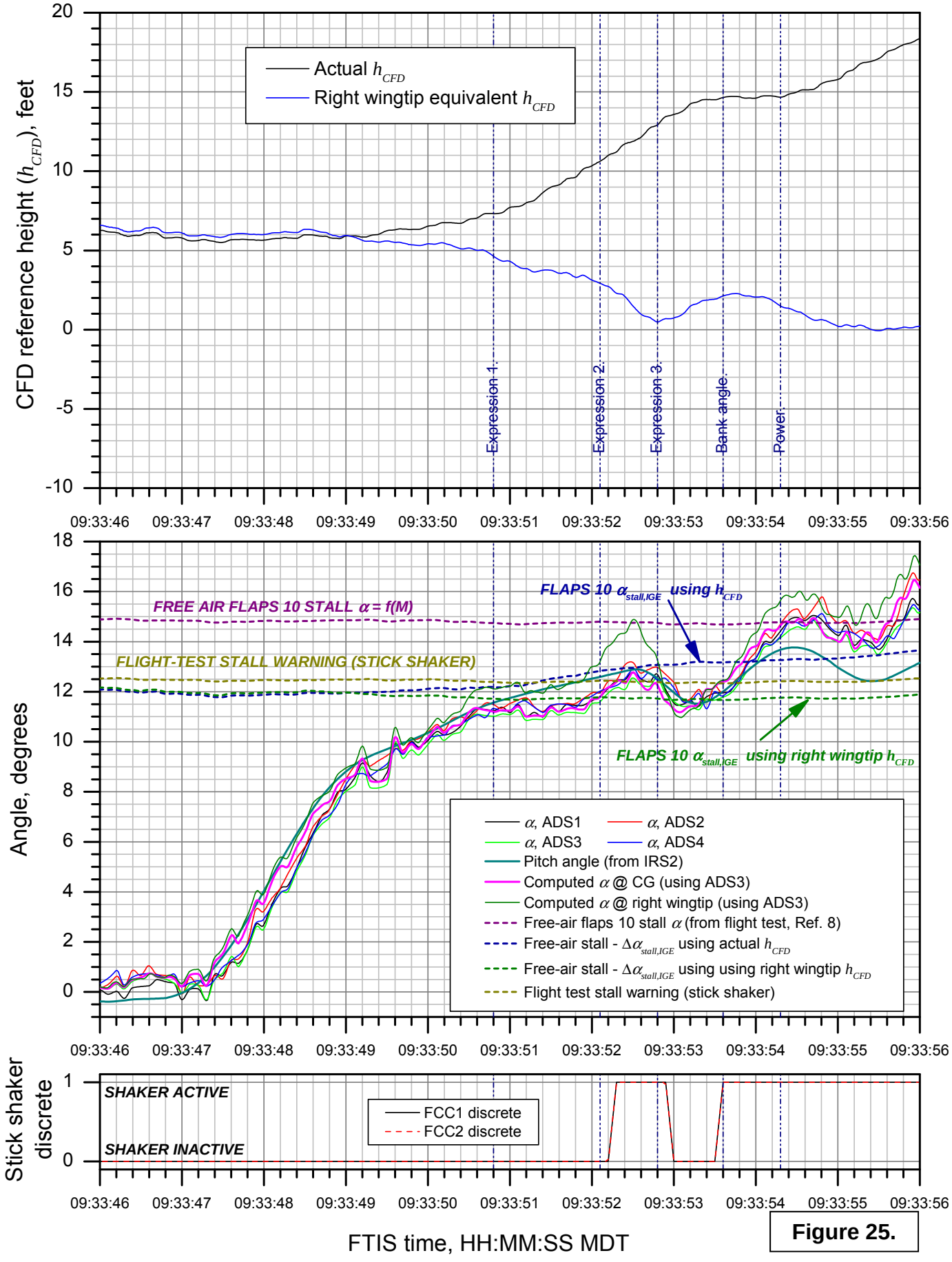

Figure 25.

$\delta_{Flap} = 10^{o}$: $\beta = 4^{o}$: On Ground (IGE)

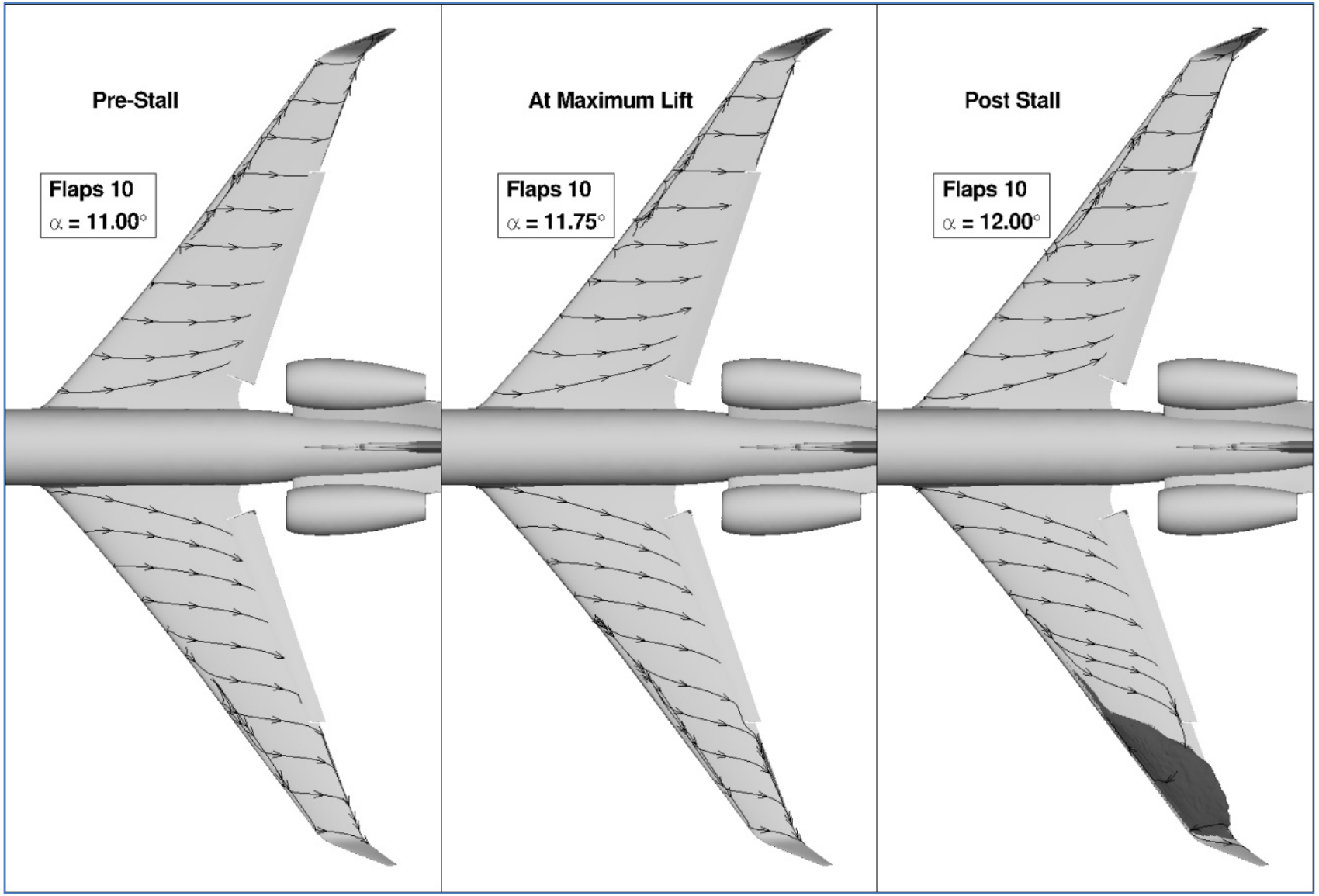

Figure 26. Visualization of the CFD flow solution at flaps 10, $\beta = 4°$ (crosswind from right) in-ground-effect. The dark coloring on the left wingtip indicates areas of flow separation (from Reference 20).